論文 / 著書情報
Article / Book Information

題目(和文)	
Title(English)	Development of a Swimming Humanoid Robot for Research of Human Swimming
著者(和文)	CHUNGCHANG HYUN
Author(English)	Changhyun Chung
出典(和文)	学位:博士（工学）, 学位授与機関:東京工業大学, 報告番号:甲第9331号, 授与年月日:2013年9月25日, 学位の種別:課程博士, 審査員:中島 求,木村 康治,宮崎 祐介,伊能 教夫,塚越 秀行,福島 E 文彦
Citation(English)	Degree:Doctor (Engineering), Conferring organization: Tokyo Institute of Technology, Report number:甲第9331号, Conferred date:2013/9/25, Degree Type:Course doctor, Examiner:,,,,,
学位種別(和文)	博士論文
Type(English)	Doctoral Thesis

Ph. D. Dissertation

Development of a Swimming Humanoid Robot for Research of Human Swimming

CHANGHYUN CHUNG

A Dissertation Submitted in Partial Fulfillment of Requirements
For the Degree of Doctor of Engineering

August 2013

Department of Mechanical and Environmental Informatics
Tokyo Institute of Technology

Supervisor Associate Prof. MOTOMU NAKASHIMA

Contents

List of Figures

List of Tables

Abstract

The objective of this study was to develop a humanoid robot for research of human swimming. In order to replace a swimmer as a subject, a humanoid robot was developed imitating the details of human such as appearance and body properties. To realize the swimming motion based on that of an actual swimmer, a joint imitating the human's scapular retraction was installed and the methodology to realize the swimming motion with that joint was established. The performance of the robot was validated by two experiments. First, the stroke motion of the crawl was observed in the water tank supported by four struts. Next, the actual movement such as body roll and swimming speed by the joint motion was confirmed by free swimming experiment.

Chapter 1

Introduction

1.1. Research Background

From the sparse descriptions on record, early attempts at swimming probably consisted of random arm and leg movements with no specific techniques; otherwise, we know little of the early history of human swimming. Before organized competitive swimming started in England, about 170 years ago, there was little need to develop methods beyond those that came naturally to each individual.

The technical development of swimming didn't start until the mid 19th century with the building of swimming pools, the invention of the stopwatch, and the beginning of competitive swimming as a formal sport.

During the first 30 years of the 20th century, a synthesis of crawl stroke fundamentals gradually emerged, the process greatly aided by coaches Louis de B. Handley, William Bachrach, and Frank Sullivan, and swimmers such as Charles Daniels, Duke Kahanamoku, Johnny Weissmuller, and many others. They developed the first great exponents of the stroke, and their techniques became examples for others to follow. These coach-swimmer teams laid the foundations of modern American swimming, and as the 20th century progressed, their better understanding of fundamentals led to the invention of two new strokes, the back crawl and the butterfly, as well as the modernizing of the centuries-old breaststroke [1].

In spite of such a long history of competitive swimming, still, its mechanics have not been fully clarified yet since it is an extremely complicated phenomenon in which a complex human body moves unsteadily with many degrees-of-freedom in the three-dimensional water flow. For example, the hand path in the crawl stroke depicts a distorted ellipse when viewed from the side in the absolute space [2],

showing that the hand does not push the water straight at a constant depth. Furthermore, the kinematics of arm and hand during the insweep and outsweep is highly unsteady [3]. From this viewpoint, many attempts were made recently to quantify the unsteady fluid forces acting on a swimmer in swimming.

The first approach was an experiment involving a human subject. However, this method has problems with insufficient repeatability, physical fatigue of the subject, and difficulty in installing sensors in the subject. Recent advances in computers have stimulated simulation study using computational fluid dynamics (CFD). However, making accurate models of swimming is still difficult because of the unsteady three-dimensional fluid dynamics involved so, they usually analyze the hand only and treat it as an isolated object, not being affected by the forearm or any other part of the anatomy [4]. In addition, the fluid simulation still needs experiments for validation. For all those reasons, some researchers have conducted experiments using physical models such as a robot instead of human subjects. A lot of measuring experiments using physical models have been conducted to date, but there is no full-body experimental platform which can consider interactions between the many segments involved in normal swimming motions. Therefore, the analysis using physical models has been performed on an isolated segment and misleading conclusions could be developed. This is discussed in more detail in the following sections.

1.1.1. Measurement of fluid forces involving human subjects

The first approach to measure the fluid forces acting on a swimmer was an experiment involving a human subject.

With respect to the hand stroke, which is the majority of propulsive force, there have been several studies in which the fluid force was discussed for given hand motion after obtaining experimentally the steady drag/lift acting on the hand [5][6] [7][8]. They use 3D-video analysis techniques but this method required much time to digitize points on the hand to determine the orientation of the hand with respect to the direction of motion of the hand and with respect to the external reference frame. In addition, the accuracy of this method has not been established yet [9][10]. Some researchers have measured a particular point of pressure on the hand surface using a

pressure transducer and discussed about a pressure profile during stroking [11][12][13][14][15][16][17]. However, these studies did not evaluate whether the location of pressure transducers on the hand accurately reflected the overall pressure distribution. Takagi et al. [16] attached pressure sensors to a swimmer's hand, as shown in Figure 1.1, and estimated the fluid forces acting on the hand in swimming motion from the relationship between the fluid forces and the pressure distribution which were obtained in advance by an experiment using a wind tunnel. Although this was an excellent idea, it still seems controversial whether the relationship between the pressure sensors and the fluid forces is also valid for the strongly unsteady swimming motion, since that relationship was obtained in a wind tunnel a steady flow.

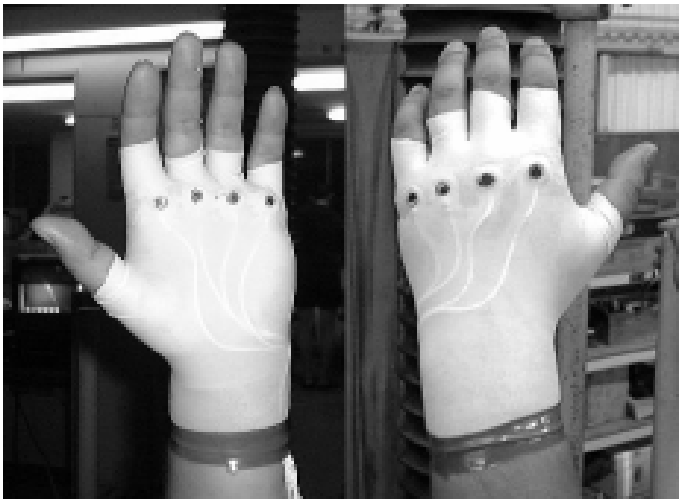

Figure 1.1 Pressure sensors attached on the metacarpophalangeal joint [17]

Meanwhile, with respect to the dynamics of the swimmer whole body, several studies have measured the drag. In the early stage, the stationary drag acting on a swimmer who takes the gliding position was investigated. This drag was called 'passive drag.' Both Amar [18] and Karpovich [19] used measurement techniques determining the resistance of swimmers gliding passively through the water. However, the body is of course never in a stable prone position when swimming, since propulsive forces need to be generated. It was conjectured that the movements necessary to create propulsion could additional resistance [20][21][22]. This led to attempts to determine the drag of an active swimming person. This drag has been

called ‘active drag.’ To date, the various attempts to measure active drag have been made. Toussaint et al. [23][24] utilized the ‘MAD system’ as shown in Figure 1.2 for measuring active drag, in which pushed the fixed paddles in water to propel instead of stroking. The technique relies on the direct measurement of the push-off forces while swimming the front crawl.

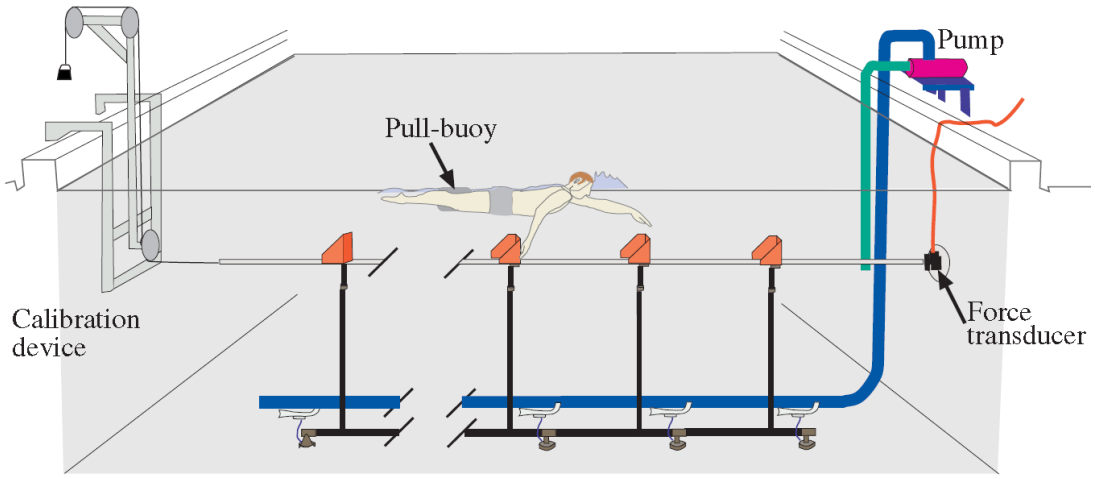

Figure 1.2 Schematic drawing of the MAD-system mounted in a 25 meter pool [25].

Kolmogorov and Duplishcheva [26] designed yet another method to determine the active drag. They estimated it by an experiment in which an additional hydrodynamic body was towed by a swimmer. In their so-called velocity perturbation method subjects are asked to swim a 30m lap twice at maximal effort: once swimming free, and once swimming with a hydrodynamic body attached that created additional resistance. For both trials the average velocity is calculated. Under the assumption that in both swims the power output is maximal and constant, active drag can be calculated since power equals force times speed. The interesting aspect of this approach is that it can be applied to measure active drag in all four competitive strokes, while the MAD system and indirect methods are applicable only to front crawl. However, the approach will yield only one drag estimate at maximal speed.

To measure active drag, Takagi et al. [27] developed an innovative method in which a swimmer fixed to a circulating tank by a harness swam at various flow speeds. In these experimental methods, the subjects of actual swimmers were basically employed. In such experiments, the dispersion due to individuals and the

bias due to the physical limitations of the subjects sometimes caused problems.

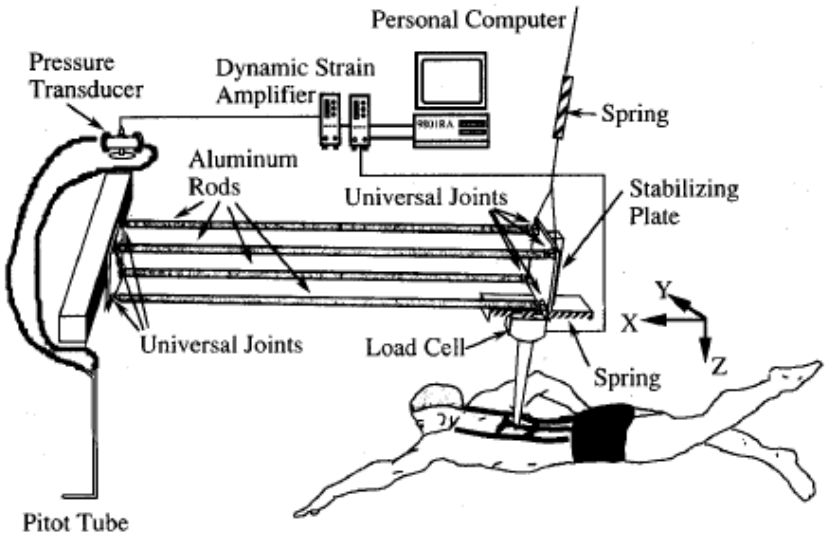

Figure 1.3 Measurement apparatus of Takagi et al. [27]

With respect to a method to measure the drag by attaching a towing device to a swimmer, it became a problem that the situation in the experiment was different from actual free swimming, since the swimmer towed some additional device. In addition to these, it is impossible, both technically and ethically, to implant a force sensor such as a load cell into a swimmer. Therefore, it has been concluded to be difficult to measure directly the unsteady fluid forces acting on limbs in the present situation.

1.1.2. Simulation study in human swimming

The second approach was using CFD (Computational Fluid Dynamics). Bixler et al. [28], Rouboa et al. [29], Sato et al. [30], and Alberto E. Minetti et al. [31] constructed computational models of a hand and forearm, and calculated the fluid forces by CFD. Keys et al. [32] constructed a whole body model and conducted an analysis of the dolphin kick. Such approaches are greatly effective to clarify the mechanism of thrust generation since it has a great advantage of displaying the whole flow field due to solving the flow around the swimmer. Nakashima et al. have developed the swimming human simulation model ‘SWUM’ [33] and various analyses using SWUM have been conducted and its validity has been confirmed as

well [34][35][36][37][38][39][40]. However, this approach still needs experimental validation of the obtained unsteady fluid force, since it is only a simulation.

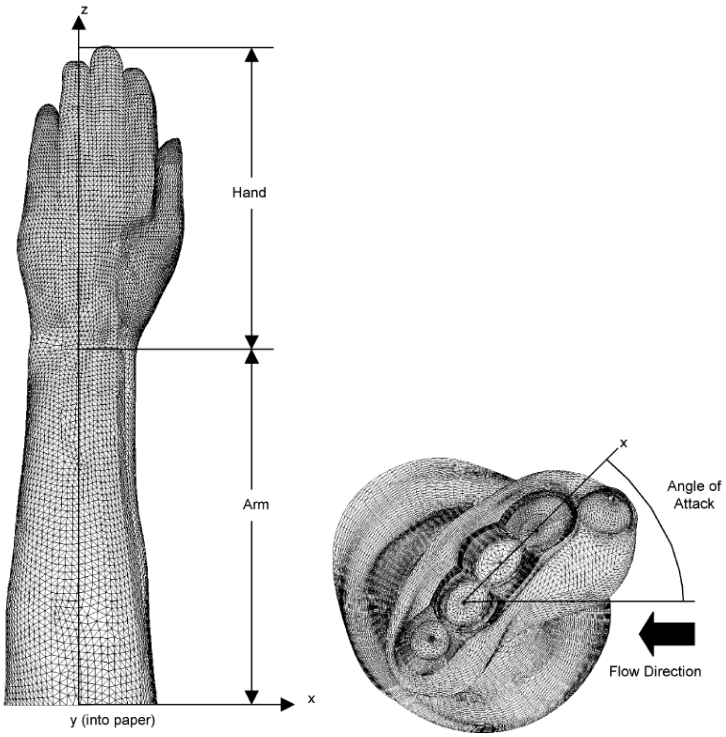

Figure 1.4 Simulation model of hand and arm (Bixler et al.[28])

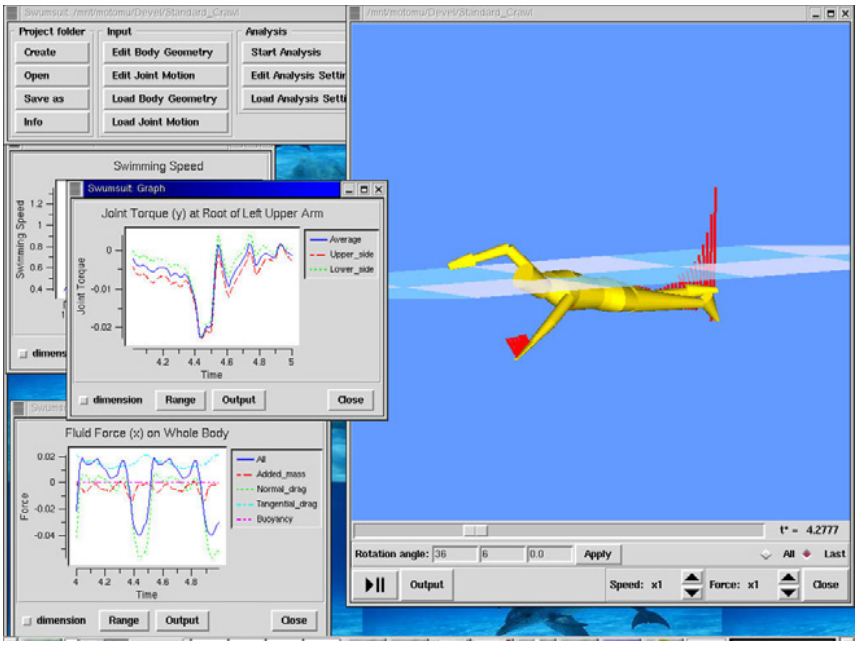

Figure 1.5 Screenshot of the free software 'SWUM' (Nakashima et al. [41])

1.1.3. Utilization of physical models in human swimming

The third approach was an experiment using a physical model instead of a swimmer. It is generally possible to attach sensors to a model and even implant them into the model. It is also easy to have the model perform the same motion repeatedly if the model is mechanically driven like a robot. In previous studies, Berger, M.A.M et al. [42] measured drag and lift forces on two models of a human hand and forearm when towed in a towing tank as shown in Figure 1.6. The orientation of the model with respect to the line of motion was varied by rotating the models around three axes, and quantified using the angle of pitch and the sweep-back angle. Influence of the orientation of the model with respect to the flow, velocity, size of the model and the relative contribution of the hand and forearm on drag and lift coefficient were studied.

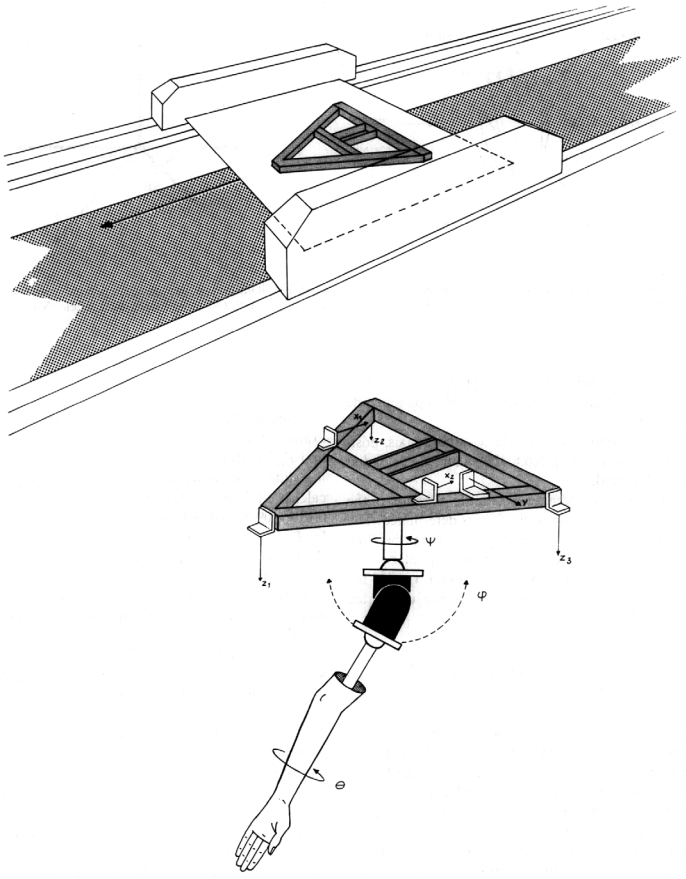

Figure 1.6 Upper part: schematic drawing of the towing carriage across the basin. Lower part: model fixed at a six-component dynamometer. The orientation of the model with respect to the flow could be adjusted (Berger, M.A.M et al. [42])

Pai [43] and Kudo et al. [44] respectively had a cylinder and a model imitating a hand and forearm perform a 1 DOF (degree-of-freedom) rotating motion, and measured the unsteady fluid forces acting on them. Lauder and Dabnichki [45] developed a full-scale mechanical arm to estimate propulsive forces as shown in Figure 1.7 (a). It had 1 DOF at the shoulder and was used to simulate a single plane underwater rotation at four elbow configurations. Nakashima et al. also measured the unsteady forces for a limb model which performed a model in the proposition of the swimming human simulation model SWUM [33][34].

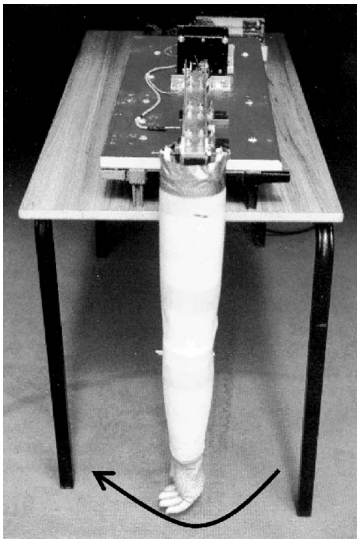

(a) Full-scale mechanical arm model and driving mechanism (Lauder and Dabnichki [45])

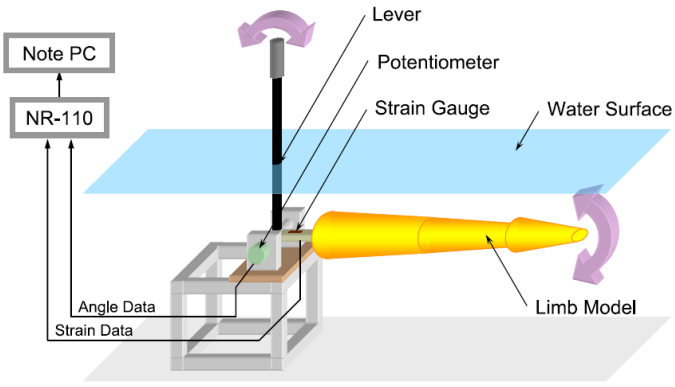

(b) Schematic view of experimental setup (Nakashima et al. [33])

Figure 1.7 Experimental models of 1 DOF

Sidelnik et al. [46] made a motor-driven arm model which could perform 2 DOF motion as shown in Figure 1.8, and measured the fluid forces in the unsteady condition.

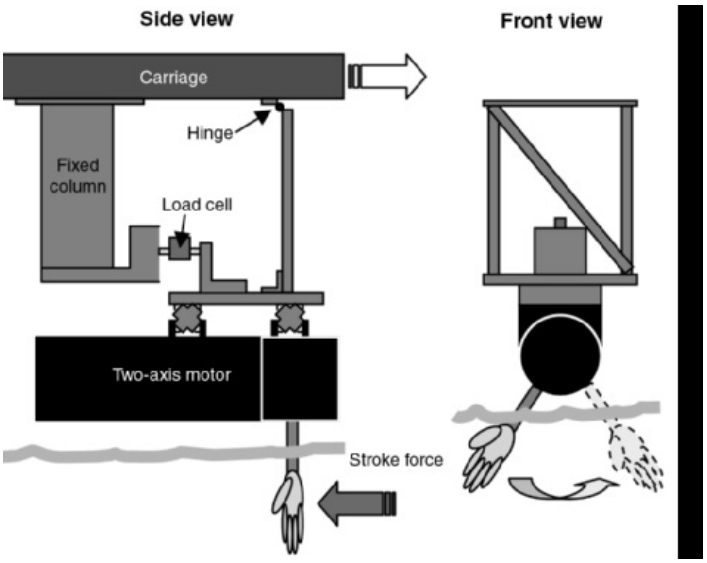

Figure 1.8 Conceptual drawing of 2 DOF test model (Sidlenik et al. [46])

Nakashima and Takahashi [47][48] conducted experiments using an underwater robot arm which had 5-DOF as shown in Figure 1.9 and could perform a swimming motion which was much more similar to that of a human than in previous studies.

Figure 1.9 Photograph of 5 DOF robot arm model (Nakashima et al. [47])

However, the above-mentioned robots have a single limb and there was no example to measure the dynamic drag acting on the whole body including the trunk using a robot.

Nakashima and Ejiri [49] measured the unsteady fluid forces acting on the trunk of a swimmer using the 'swimmer mannequin robot.' This robot consisted of a swimmer mannequin and its driving mechanism which could move the mannequin in the pitching, heaving and rolling motions as shown in Figure 1.10.

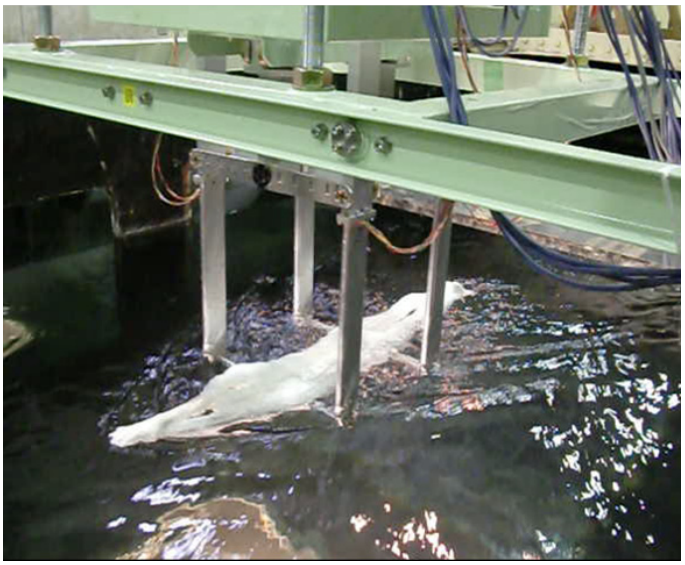

Figure 1.10 Measurement system using a swimmer mannequin and driving mechanism

As mentioned above, so far, various attempts have been made and diverse measurement systems were proposed to measure fluid forces acting on a swimmer. However, detailed discussion in which both all the fluid force acting on all parts of the body and the whole body dynamics are considered, has yet to be done. Also, to date there have not been any tools for analysis relating to such discussion.

1.1.4. Applications of a humanoid robot in research of swimming

As discussed above, current analyses of fluid forces using human subjects or computer simulation are limited. The experiments using a physical model to date were also not sufficient in order to clarify the fluid forces acting on a swimmer.

On the other hand, a swimming humanoid robot can provide more realistic environmental conditions. Also, the autonomous platform leads to a possible various experiments which have been impossible with the previous models.

A prime example is study of rolling motion in swimming. The rolling motion is one of important subjects in human swimming researches. The rolling motion of the trunk during front crawl and backstroke swimming has been of increasing interest in recent years.

Counsilman [50] was one of the first authors to emphasize the potential importance of body roll in swimming. He suggested that body roll could: make the recovery of the arm easier and permit a shorter radius of rotation of the recovery arm; place the strongest part of the arm pull more directly under the center of mass; and place the hips in such a position that the feet can be thrust partially side-wards, thus cancelling the side-wards sway of the torso possibly created by the forward swing of the recovery arm. Other authors have suggested that body roll has functions such as facilitating the breathing action in front crawl swimming [51], increasing propulsion or decreasing the drag forces [52], and reducing the risk of developing shoulder injuries [53][54][55].

Since then, researchers have defined and examined body roll in two different ways. First, in some studies the roll of the whole trunk was calculated based on the assumption that the trunk rolls as a rigid segment while swimming. Researchers have estimated trunk roll with simulation methods [56][57] or measured trunk roll using two-dimensional (2D) techniques [58][59][60][61][62]. The trunk roll angle was defined as the angle between the pool-fixed axis and the trunk fixed axis as shown in Figure 1.11.

Second, the shoulder roll and hip roll of swimmers have been measured separately with the use of three-dimensional (3D) methods [63][64][65][66][67][68][69] or simulation method [70], while in some of these studies the roll of the entire body (rather than just the trunk) around its longitudinal axis was also considered [67][68].

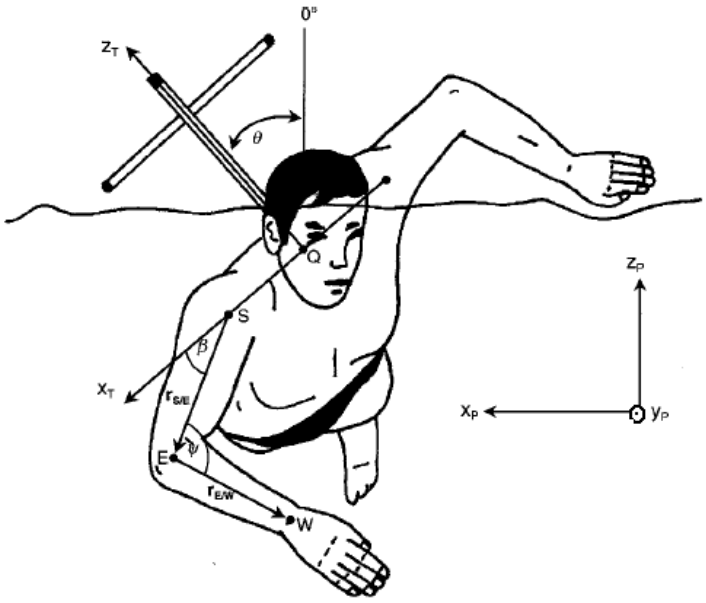

Figure 1.11 Reference system used to define the trunk roll angle (θ) as the angle between the pool fixed z-axis (z_P) and the trunk fixed z-axis (z_T). A wood fin strapped on the swimmer's back served as the fixed z-axis of the trunk. The midpoint of the shoulders (Q) was the origin of the local reference system (x_T, y_T, z_T). (Payton et al. [61])

These researches have improved our understanding of the functions of body roll and its link to front crawl swimming. However, the previous researches investigated human swimming so, the results were different according to the subjects or subject group. It's difficult to clarify such differences in human swimming because it is impossible to adjust detail motion and consider every individual difference. A swimming humanoid robot is the only thing that will clarify through experiments.

Furthermore, a humanoid robot for underwater use can be utilized for investigating the mechanism of human swimming just the same as the humanoid robots on land have been utilized for investing the mechanism of human's on land motion and the studies about human using a humanoid robot are becoming more diverse [71][72][73]. The findings obtained by such investigations will be useful for the performance enhancement of competitive swimmers, as well as the development of instruments in the water, such as functional swimwear, fin attached to a swimmer, prosthesis for underwater use, and so on.

1.1.5. Studies about humanoid robots for underwater use

In spite of such applicability of a humanoid robot for underwater use, development examples are few. Actually, a humanoid robot has been studied for several decades. In initial stage, a major concern of the researches was how a humanoid robot walks like a human but currently a humanoid robot can run, go up and down the stairs and even dance [74][75][76]. Recently some researchers develop a humanoid robot to use not only for indoor work but also under real environment contacting dust and water [77]. In a further study, researchers have studied to widen humanoid robot's application field such as space [78]. However, still, the researches about a humanoid robot for underwater use are not activated considering potentials for utilization of a robot in the water. One of the reasons why few researchers have developed a humanoid robot for underwater use is difficulty of making waterproof body of a humanoid robot which is consist of complex joints. The other one is difficulty of making robot locomotion in the water.

Only a few researchers developed humanoid robots for underwater use. Figure 1.12 shows examples. Oya and Suzuki proposed a diver-type small humanoid robot to estimate water depth by the robot's behavior [79]. Li et al. developed a swimming humanoid robot with a flutter kick [80]. Nakashima and Kobayashi developed a small swimming humanoid robot for research of human swimming [81]. They developed waterproof robot platforms and proposed locomotion in the water. However, there is still much room for improvement. The previous robots were remodeled from land-based robots for underwater use and had waterproof clothes such as a diving suit on to make a waterproof body. However, such thick clothes restricted the movement of a robot and made it difficult to do the appropriate movement. They moved in the water with either their legs or arms. The former two models moved only by the flutter kick motion. However, it is known that the flutter kick does not generate much propulsive force and is not efficient in human swimming [34]. Although the latter model realized arm movement, it was unnatural due to the limitation of the degree of freedom and the range of the joint angles.

(a) Oya et al. [79] (b) Li et al. [80] (c) Nakashima et al. [81]

Figure 1.12 Research about humanoid robots for underwater use

1.2. Research Objective

The primary objective of this research is to develop a full-body swimming humanoid robot which is available to be used as an experimental platform in various experiments for research of human swimming. To achieve this aim, the platform features as follows:

1. Imitating the details of human such as appearance and body properties.
   To determine the dimensions of the robot based on the body geometry of a real human is important because they affect fluid forces during swimming. In addition, body properties such as center of mass and specific gravity are considered to keep body balance in the water and to investigate correct locomotion of the robot by the swimming motions.

2. Realization of the swimming motion based on that of an actual swimmer.
   The robot has enough DOF to reproduce the complicated swimming motions with high fidelity. The swimming motion of an actual swimmer can be realized by the joint angles of the robot.

3. Validation of swimming performance through experiment.
   The robot is validated swimming performance and usefulness as an experimental platform. Experiment is conducted not only in conventional

experimental conditions of quasi-steady state but also in more realistic experimental conditions. For example, the realization of the free swimming will be useful particularly for the research of human swimming related to control strategy of the body motion during swimming.

4. Connectivity with a simulation tool for future research.
   For better understanding of the characteristics, modeling based on a formulation is necessary. The robot can be modeled in simulation and the swimming motion of the robot can be analyzed in simulation, as well. Analysis of the hydrodynamic force in human swimming using both the experimental platform and simulator has the advantage. Each analysis can be validated mutually and it will be very powerful tools to clarify the mechanics of human swimming.

1.3. Thesis Organization

The paper is organized as follows:

"Chapter 2 Design of the Robot" presents design features of the developed humanoid robot. Design concepts as to be experimental subject and configuration of degrees of freedom are discussed. Also, efforts to imitate human body geometry and waterproofing methods for each part are explained. Followed by explain about electrical parts and conclusion.

"Chapter 3 Methodology to Realize Swimming Motions" describes the methodology to realize swimming motions using the scapular joint. First, the process to make swimming stroke motions of the developed robot from human swimming is discussed briefly. The installed scapular joint to realize the swimming arm stroke is explained. Inverse kinematic of the arm accompanying the scapular joint is analyzed and the methodology to realize the swimming motion is established. The efficiency of the design is discussed through simulation result.

"Chapter 4 Stroke Motion Experiment in Fixed State" describes underwater experiments to validate the created swimming stroke motions by the proposed methodology. The measurement system which is constructed to measure fluid forces during the swimming of the humanoid robot is discussed. A major part of the system

such as a driving mechanism and a circulating water tank are explained. Finally, the experimental method and results using the measurement system are discussed.

“Chapter 5 Free Swimming Experiment” describes a series of process to realize free swimming in the crawl stroke. Remodeling of the upper body to fit a free swimming is discussed. Accompanied simulation study to raise feasibility is discussed. The established two improved models in the simulation are described. The experiment using the swimming humanoid robot fitted to the two simulation models is explained.

“Chapter 6 Conclusion” concludes with a summary of the research and future works is discussed.

Additionally, in the Appendices, the transformation matrixes of the robot arm are presented (Appendix A), the position and orientation of the hand and elbow of simulation model during the model swimming are calculated (Appendix B), and finally the formulation of fluid forces in SWUM is presented (Appendix C)

Chapter 2

Design of the Robot

2.1. Introduction

This chapter deals with the design of full-body swimming humanoid robot for research of human swimming. The developed robot is named SWUMANOID (SWimming hUMANOID). It is developed to be used in experimental platform for research of human swimming. Therefore, it has a detailed human's body shape and 21-DOF for the joints in order to reproduce the complicated swimming motions with high fidelity. Already several humanoid robots were built for underwater use [79][80][81]. However, their thick waterproof clothes and insufficient DOF are not suitable for the experimental platform. Unlike the previously developed humanoid robot for underwater, SWUMANOID is developed with waterproof body and had sufficient DOF as well as the range of motion to generate swimming stroke motion of human.

2.2. Design Concepts

The design concepts of SWUMANOID are as follows:

a) Waterproof design
b) Imitation of human body geometry
: Appearance, body proportions, center of mass and specific gravity
c) Realization of swimming motions
d) Half the size of a real human

Since SWUMANOID is the swimming experimental platform substituting a human subject, the design concepts a)-c) are obvious. The robot size was determined to be half the size of a real human in order to make development easier and to be more convenient when it is operated in experiments. The ratio of the lengths of each segment is about the same as that of a human. So the fluid forces can be calculated proportionally according to the size factor.

On the other hand, the different size can affect the fluid force characteristics as the difference of the Reynolds number *Re* in the water. If the half size model swims at the same stroke cycle, the Reynolds number becomes one fourth. Therefore, to make the same Reynolds number, the robot should swim at the four times faster stroke cycle and it's practically difficult to realize. However, *Re* was 6×10^3 to 9×10^4 in the present study and 2.4×10^4 to 3.6×10^5 in the full-size human swimming. It is generally known that, in these ranges of *Re*, the flow field around a body similar to the human limb, such as a cylinder and plate accompanying a large separated region, does not change significantly according to the change in *Re*, and therefore the fluid force characteristics also do not change much [47][82]. Therefore, it will not become a serious problem to apply the fluid force characteristics obtained in the experiment.

Figure 2.1 shows SWUMANOID which was developed based on the design concepts a) to d). As shown in Table 2.1, SWUMANOID is 890 [mm] in height and 5.5 [kg] in weight including the battery. The height was determined by the design concept d) and the weight was determined by the design concept b), which considered human's specific gravity. To realize the design concept c),

SWUMANOID has a total of 21-DOF but the leg doesn't have sufficient degrees of freedom to perform the breaststroke kick, so in this study, realization of the breaststroke is excluded.

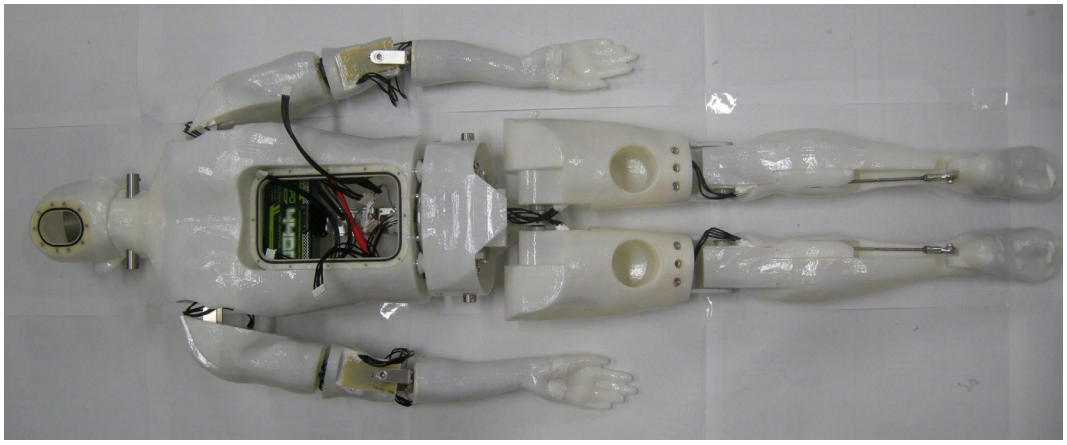

(a) Rear view of the robot

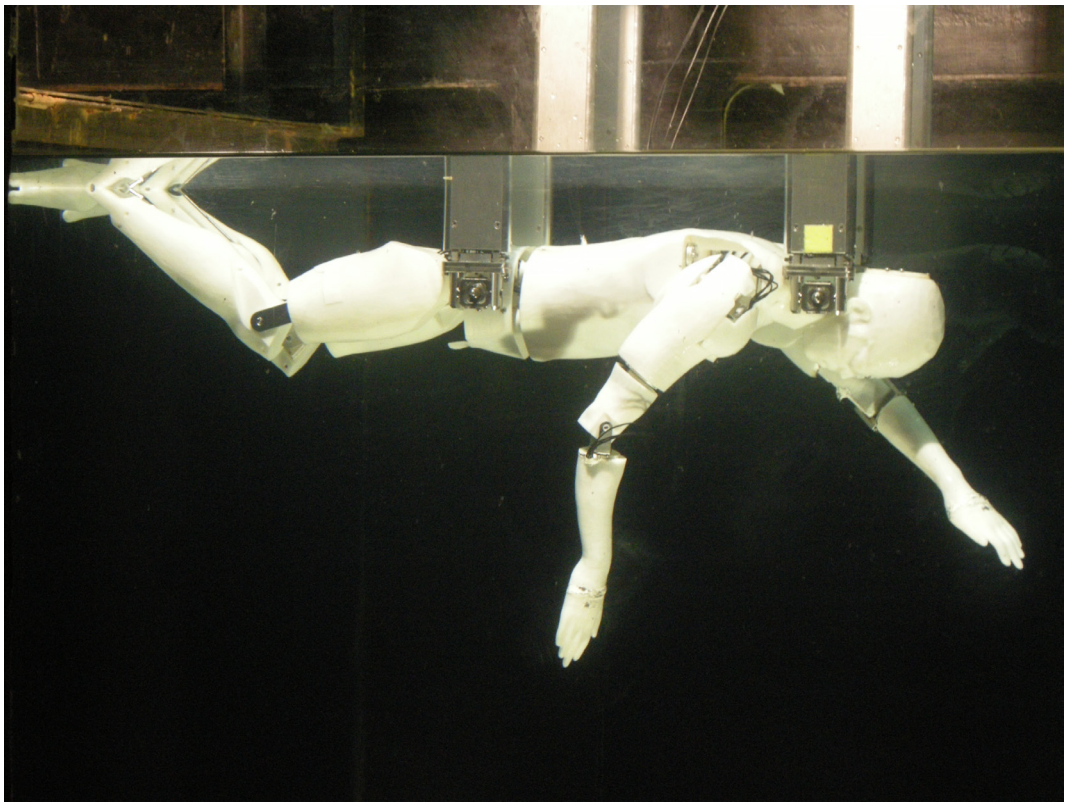

(b) Side view of the robot in the water tank

Figure 2.1 The developed swimming humanoid robot

Table 2.1 Specifications of SWUMANOID

Items	Specifications
Dimensions	Height: 890 mm Width: 270 mm Depth: 100 mm
Weight inc. battery	5.5 kg
Degree of freedom	Total: 21 DOF Head (Free joint): 1 DOF Arm: 6 DOF x 2 Arms Waist: 2 DOF Leg: 3 DOF x 2 Legs
Microprocessor	ATmega 2561 (Atmel Corp.)
Battery	Li-Po 11.1V 4400 mhA

2.3. Configuration of Degrees of Freedom

The robot has 21 degrees of freedom; 14 are for the upper body and 7 are for the lower body. Figure 2.3 shows the positions of the actuators and joints. All actuators are connected to the joints directly except for the head and ankle joints. The head joint is a free joint in order to keep the head down during swimming motions. The ankle joint is actuated using a four-bar linkage because there is no space for the installation of an actuator in the ankle. Each arm has 6-DOF. The elbow has 2-DOF and the shoulder has 4-DOF. The position of the shoulder joint was determined considering the elevation motion as shown in Figure 2.2. The shoulder joint of human moves and the position is different depends on arm's posture. So, the position of the shoulder was determined in the middle of the range of motion of the shoulder during swimming. Three of the shoulder joints are for the roll-pitch-yaw motion and one is for the scapular retraction as shown in Figure 2.4 (scapular joint in Figure 2.3).

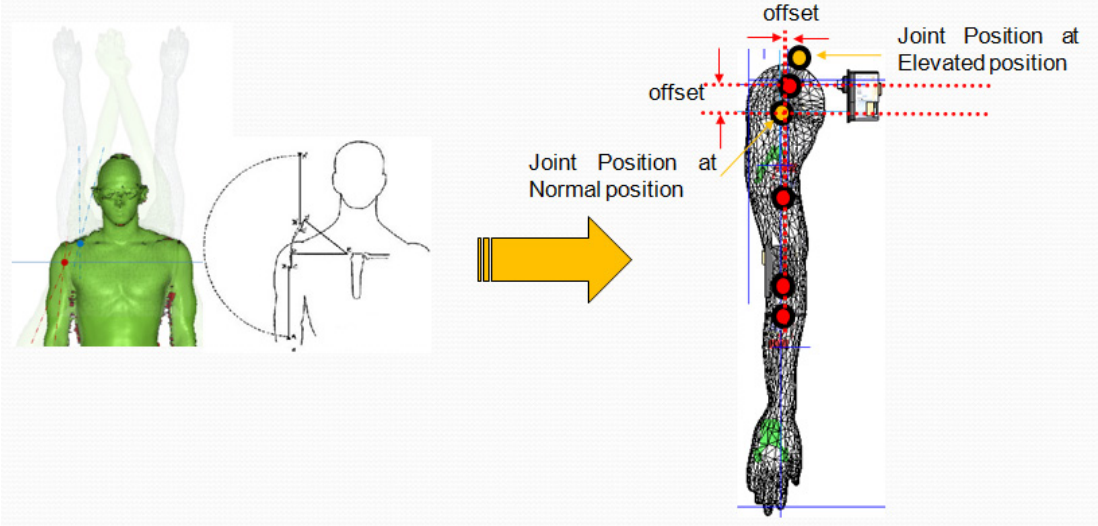

Figure 2.2 Determination of the position of the shoulder joint

Using this retraction motion of the scapular joint, the robot can realize swimming stroke motion continuously. The reason for installation of the scapular joint and application methodology are described in Chapter 3. Each leg had 3-DOF for extension and flexion of the hip, knee and ankle joints.

The swimming humanoid robot has 2 DOF in the waist. One is assembled in the upper body and the other one is assembled in the lower body. The upper body and lower body are connected by assembling of these two waist joints. Figure 2.5 shows the connection between a waist joint in the upper body and a bracket of waist joint in the lower body. It has roller guide parts to support lower body.

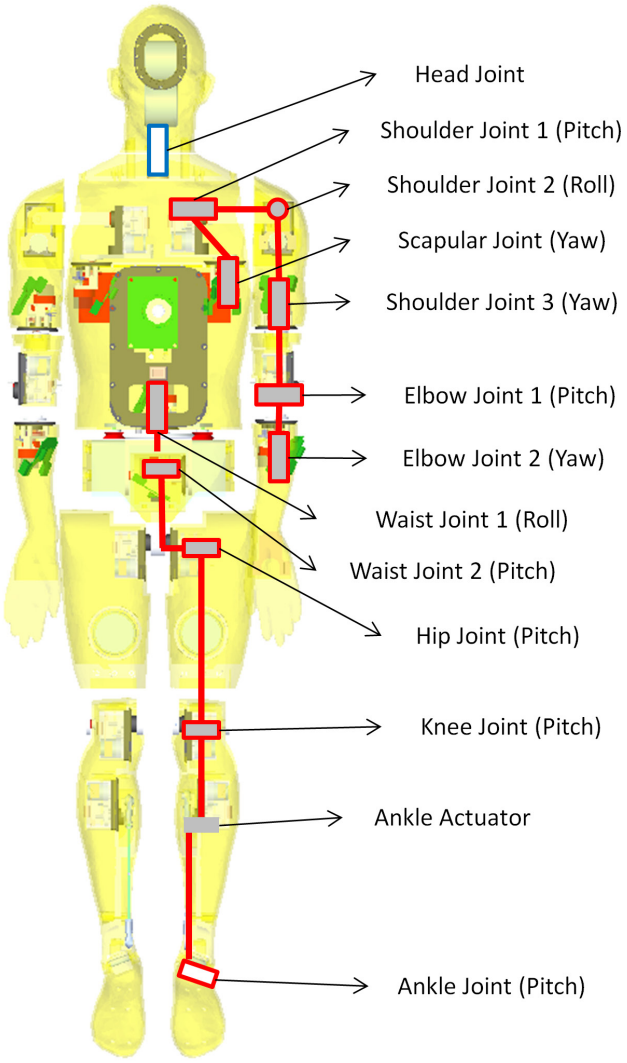

Figure 2.3 DOF configuration of the developed humanoid robot

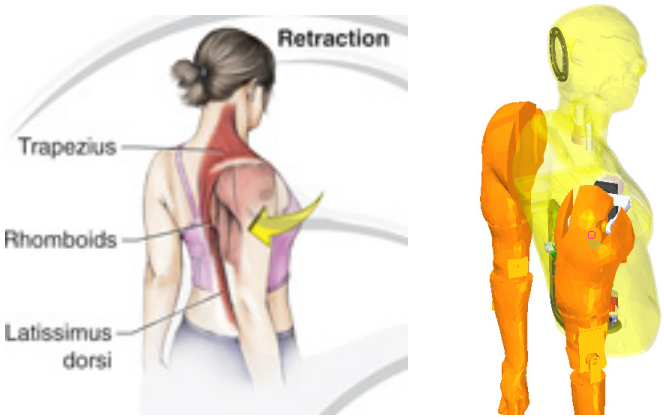

Figure 2.4 Scapular retraction of human and that of a swimming humanoid robot

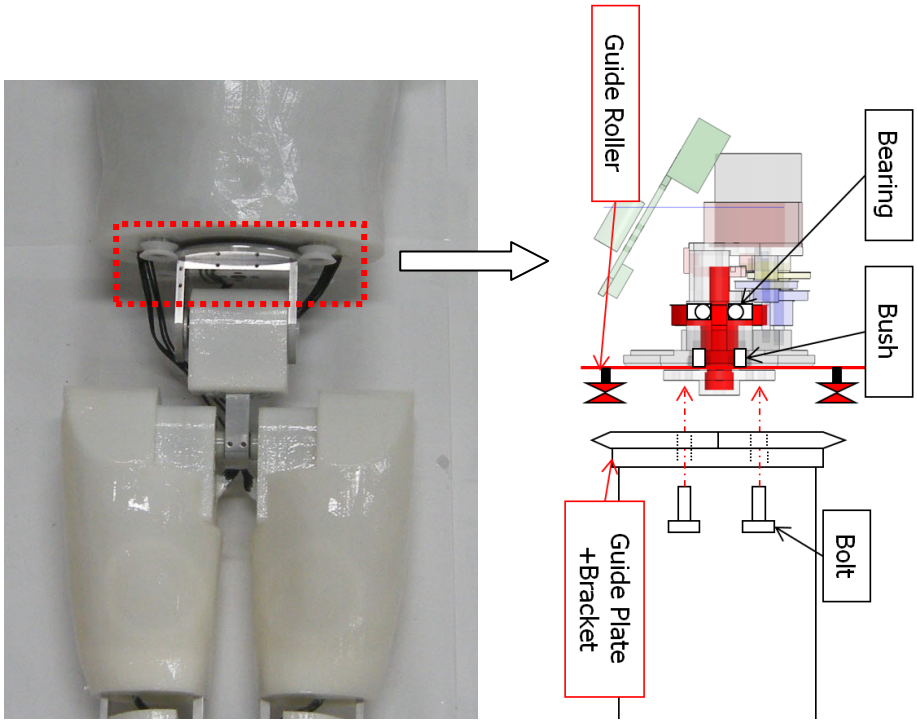

Figure 2.5 Assembling of the upper body and the lower body with roller guide

2.4. Imitation of Human Body Geometry

2.4.1. 3D scanning and 3D printing

Appearance, body proportions, center of mass, and specific gravity were considered to imitate a human subject. To mimic the real human body, the outer cases of the humanoid robot were made based on the scanned body data of a world-class elite male swimmer. To begin with, the 3D shape of a swimmer was measured. The subject swimmer was a top-ranking Japanese male swimmer. His stature and weight were 1.79m and 72 kg, respectively. The swimmer took several positions and his body was scanned by a Whole Body 3D Scanner (WB4 Scanner, Cyberware Inc., USA). Difficult positions in the air such as gliding were scanned in twice. His upper and lower halves of his body were scanned respectively and these data were composed into one whole body. Using the obtained body data, robot cases were designed. Each case had a half length of real body parts and a 2~3 mm thickness. They were built by a rapid prototyping (RP) machine with ABS material. Figure 2.6 shows the scanned body data and developed robot cases.

(a) 3D scanned body data of an elite swimmer

(b) Modified data file

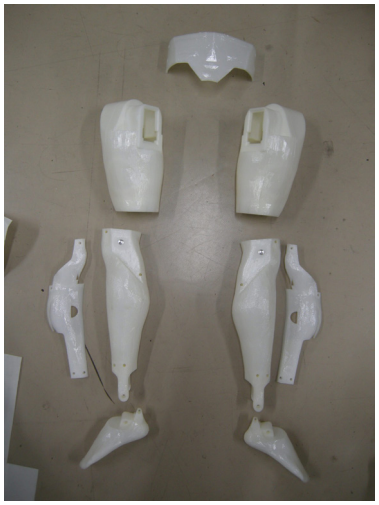

(c) Printed robot cases by a rapid prototype machine

Figure 2.6 Development of body cases based on real human data

2.4.2. Remodeling of actuators

The robot was driven by 20 servo actuators called 'DYNAMIXEL' (RX-24F, Robotis Co.). They were linked by a daisy chain, so wiring was simple and we saved many steps in waterproofing the wires compared to normal RC servo motors. However, the motor was too large to be installed inside of the robot cases as shown in Figure 2.7 (a). Therefore, a motor case and gear housing were newly designed to be compact and waterproof. Figure 2.7 (b) shows the modified motor. The one-sided output axis was centered, and unnecessary cases were removed. The modified motors were successfully installed in narrow parts, such as the longitudinal axis of the forearm as shown in Figure 2.7 (c).

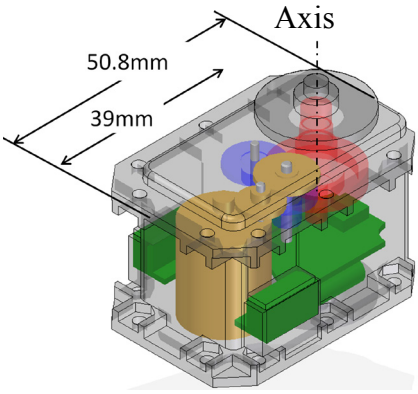

(a) DYNAMIXEL RX-24F

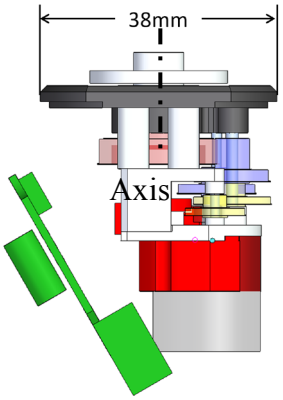

(b) Modified motor

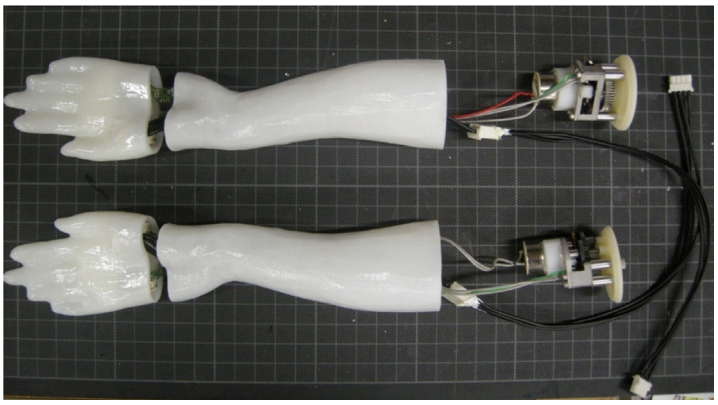

(c) Forearm assembly with a modified motor

Figure 2.7 The features of a developed compact waterproof motor

2.4.3. Weight and volume

Every driving part of the robot was installed inside to keep the scanned body shape. Actuators were redesigned compactly to be installed inside. The controller and battery were also inside of the robot, so that the humanoid robot obtained a similar appearance to a human and could swim without any connection from the ground. The weight and volume of each segment of the robot are listed in Table 2.2. Basically the weight and volume of each segment are proportional to that of human. Therefore, specific gravity is also about the same as that of human. We expect that the overall center of weight and buoyancy correspond well with that of human, as well. The total weight of the robot is approximately 5.5 kg and the specific gravity is about 0.82. In the experiment, the initial conditions, the center of gravity and the total weight of the robot was adjusted by adding more weights inside the robot. The robot could maintain proper buoyancy and balance without any other buoyancy equipments in the water, suggesting a possibility of an autonomous underwater humanoid robot.

In this humanoid robot, modified motors are used for longitudinal axes and the other motors are removed original covers to reduce weight and save space. The front cover was modified to contain O-ring and quad-ring. We could reduce motor's weight from about 20g to 10g per one motor. Original commercial model's weight is 67g but modified motor is 50g and cover changed motor is 55g as shown in Figure 2.8.

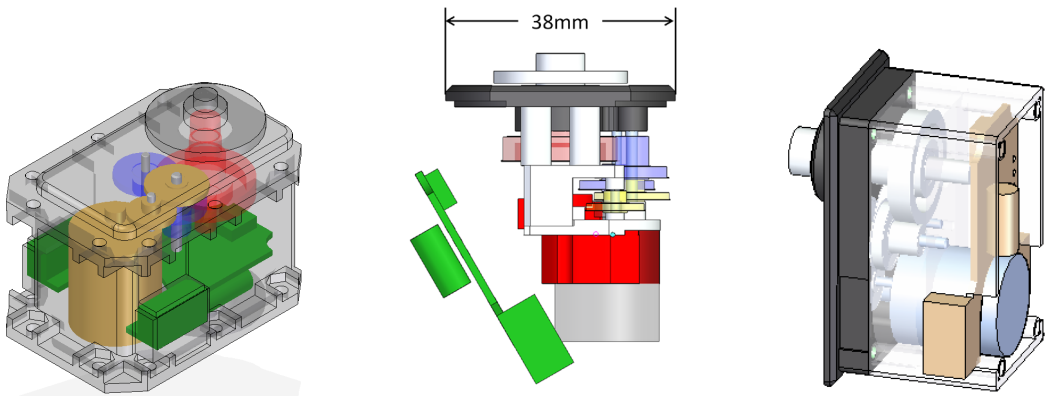

(a) RX-24F:67g (b) Motor for longitudinal axis:50g (c) Cover changed motor:55g

Figure 2.8 Weight of motors

Table 2.2 Volume and weight of the developed swimming humanoid robot

Parts	Weight(g)	Added weight(g)	Volume (cm^3)	Specific gravity
Head & Neck	264	590	1000	0.85
Upper arm*2	570		720	0.79
Forearm*2	250		280	0.89
Breast	1050	370	2100	0.68
Waist	360		353	1.02
Thigh*2	560	682	1400	0.89
Shank*2	670		700	0.96
Foot*2	82	60	200	0.71
Total	3806	1702	6753	0.82

2.5. Waterproofing

2.5.1. Actuators

Making waterproof body is one of the most important and essential work to develop an underwater robot. In the previous research of an underwater humanoid robot, most robots wore waterproofing clothes and were sealed by silicone for the waterproofing [79][80][81]. It is an easy and simple method to waterproof a robot body, but this method is not suitable for our research objective. First, it is difficult to keep a uniform body shape and it would exert a bad effect on the measurement of fluid force. Second, it makes it difficult to measure body volume and density. In this study, keeping a constant specific gravity is important not only for measurement of

fluid force but also for a free swimming experiment in the future. In order to maintain a uniform body shape and similar specific gravity with that of a human, we utilized three types of waterproof methods as follows: First, we modified motor cases for the waterproofing. The rotational axis of the motor was sealed by a quad-ring and O-ring as shown in Figure 2.9 (a) and the control board of the motor was sealed by silicon as shown in Figure 2.9 (b), in case of leakage from the outer case. Second, the motors and electric wires were fixed and sealed by silicone and epoxy bond because there were not enough space to install the O-ring and screws.

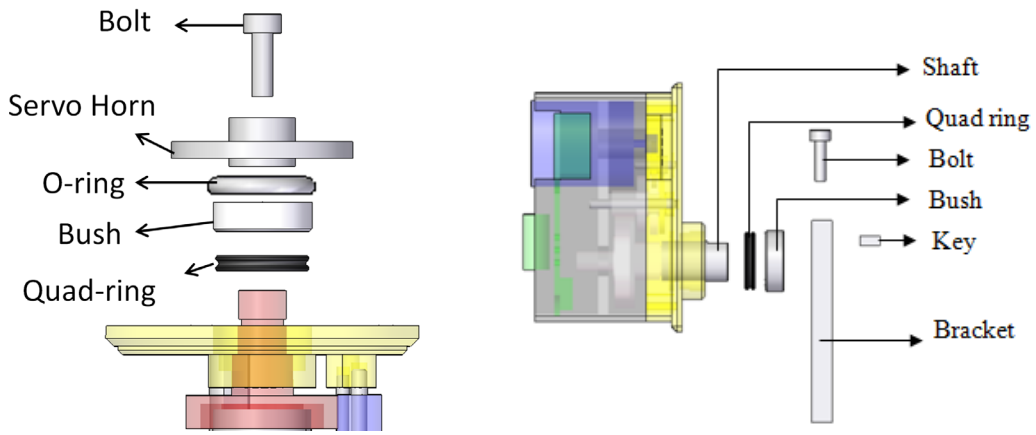

(a) Waterproofing of the axis

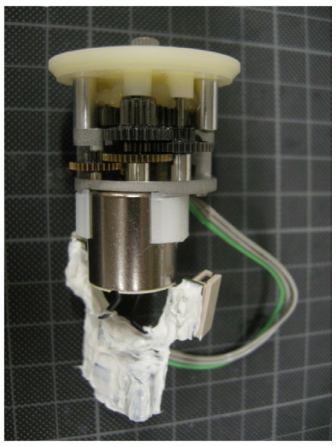

(c) Waterproofing of the board

Figure 2.9 Waterproofing of the motor

2.5.2. Body cases

Actuators were inserted in the case and the contact area was sealed by silicone as shown in Figure 2.10. Assembled parts also can be waterproofed with O-ring but there is not enough space for combine two different parts. On the other hand, if we use silicone, we can save space because silicone does double duty as sealing and glue.

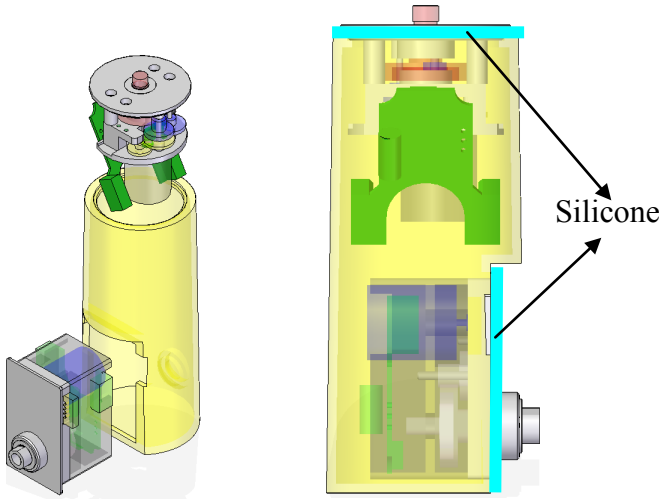

Figure 2.10 Waterproofing of the assembling parts

The body cases produced by the rapid prototyping (RP) machine were coated with a waterproofing chemical to protect electrical components inside such as a motor and control board from water leak. Also, it is necessary to maintain constant specific gravity of the robot. The outer cover of the developed humanoid robot was made by RP machine but the built cases are not waterproofed because robot cases were produced stacking ABS material up and water leaks out from the gaps between the layers. For the waterproofing function, cases were coated with waterproofing chemical on the surface. Figure 2.11 shows the selected waterproofing chemical. It is commercial chemical for waterproofing of plastic water pipe and it works well for constructed parts by RP machine because material of the constructed part is engineering plastic. It was well matched with the chemical's usage. It was very powerful and dried quickly. Figure 2.12 shows photos of the robot hand before and after applying the waterproofing chemical.

Figure 2.11 Waterproofing chemical for RP cases

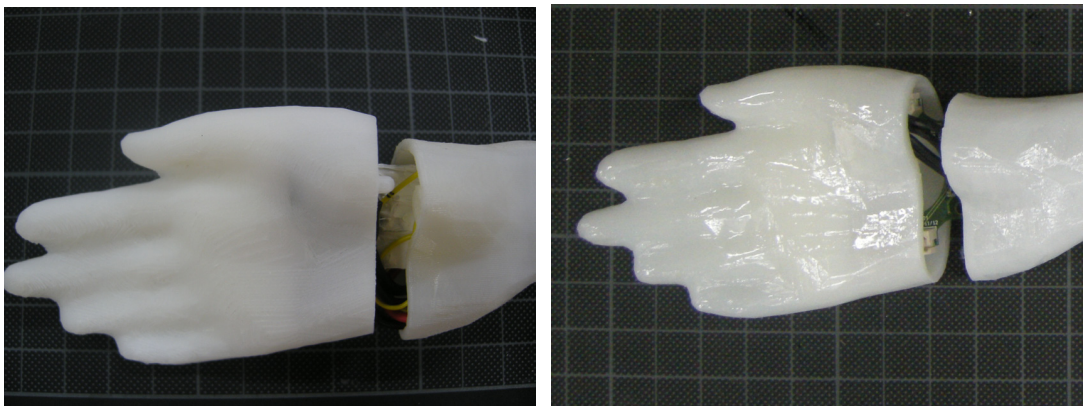

(a) Before application of chemical (b) After application of chemical

Figure 2.12 Application of waterproofing chemical for RP cases

2.6. Electrical Parts

Every electrical part except actuators was installed in the back of the robot and sealed by O-ring and cover. The robot was driven by 20 servo actuators called 'DYNAMIXEL' (RX-24F, Robotis Co.) and the hardware specifications were shown in Table 2.3. The motor can transmit status such as position, temperature, load, and input voltage. The installed motors were controlled by a robot controller (CM-700, Robotis Co.) as shown in Figure 2.13 and hardware specifications were shown in Table 2.4.Power source was Li-Po 4400mhA battery and it also installed in the back of the robot considering weight balance.

Table 2.3 Hardware specifications of actuator [83]

Product name	RX-24F (Robotis co.)
Weight	67g
Dimension	35.5mm x 50.8mm x 41.8mm
Gear Ratio	193:1
Operation Voltage (V)	12
Stall Torque (N.m)	2.6 (12V)
Stall Current (A)	2.4
No Load Speed (RPM)	126 (12V)
Motor	Coreless Motor
Minimum Control Angle	About 0.29° x 1024
Operating Range	Actuator Mode : 300°
	Wheel Mode : Endless turn
Operating Voltage	9~12V (Recommended voltage : 11.1V)
Operating Temperature	-5°C ~ 70°C
Command Signal	Digital Packet
Protocol	Half duplex Asynchronous Serial Communication (8bit, 1 stop, No parity)
Link (physical)	RS485 Multi Drop Bus
ID	254 ID (0~253)
Baud Rate	7843bps ~ 1Mbps
Feedback Functions	Position, Temperature, Load, Input Voltage, etc.
Material	Case: Engineering Plastic
	Gear: Full Metal
Position Sensor	Potentiometer
Default Setting	ID #1 (1 Mbps)

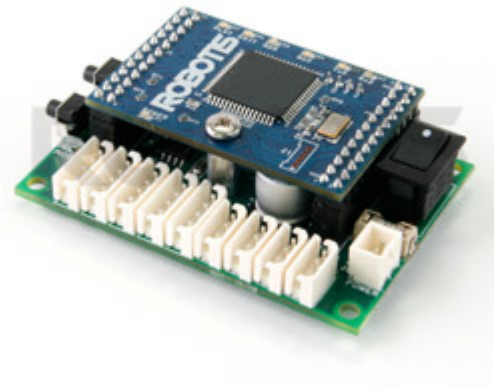

Figure 2.13 Main controller of the robot ‘CM-700’ [83]

Table 2.4 Hardware specifications of controller [83]

Product name	CM-700 (Robotis co.)
Weight	37.3g
Size	66mm x 46mm x 17mm
CPU	ATMega2561
Operation Voltage	Tolerance Range : 7V ~ 35V
Current Consumption	When IDLE : 40mA
	Internal I/O max current : 0.9A
	Overall max current : 10A (Fuse)
Operating Temperature	-5°C ~ 70°C
Internal I/O device	Button : 2 (Reset 1; Start 1)
	Temperature Sensor : 1
	Voltage Sensor : 1
External I/O device	OLLO compatible I/O 5 pin port : 6
	(TTL) 3 pin connector : 4
	(RS-485) 5 pin connector : 5

2.7. Conclusion

In this chapter, the swimming humanoid robot, named SWUMANOID, was developed. In order to use it as an experimental platform for research of human swimming, the appearance and body properties were fitted to those of human. To preserve the shape of human body, compact waterproofing motor was developed. The developed robot was driven by 20 motors. In order to realize swimming stroke motions, each arm has 6 DOF, and each leg has 3 DOF.

Chapter 3

Methodology to Realize Swimming Motions

3.1. Introduction

Most swimming strokes involve swing motions of arms in wide arcs to keep the stroke motions continuously. General robot arm, which is constructed of a three rotation sequence of roll, pitch and yaw, has singular points during swimming motions. One approach to solve the problem was to develop a new mechanism. Okada and Nakamura proposed Cybernetic Shoulder which has no singular point on simple mechanism [84]. However, the analytical solution of the forward and/or inverse kinematics of the cybernetic shoulder is difficult to obtain and the strict analysis of the singularity is difficult. Another approach is to modify the trajectory (limit angular velocities) [85][86] but the generated motion by this method is somewhat different from the real movement.

This chapter the swimming motion of the robot is presented. Swimming motions were determined based on human swimming movements. To realize the swimming arm stroke, a joint imitating the human's scapular retraction was installed and the methodology to realize the swimming motion with that joint was established. Finally, the efficiency of the design was validated by simulation

3.2. Overview of Swimming Motion Generation

The method of swimming motion generation is schematically shown in Figure 3.1. First, we analyzed movies of model swimming by a human subject [87] and determined joint angles of a simulation model using a swimming human simulator, SWUM [39]. Using SWUM, we could check the fluid forces acting on the robot as well as the joint torques when the robot performed swimming motions. In SWUM, the model of the swimmer's body was divided into 21 cylindrical segments, and one stroke cycle was divided into 18 motion frames. We calculated the desired positions and orientations of the robot arm, solving forward kinematics at each motion frame. Also, the joint angles of the robot arm were determined by applying the coordinate transformation and solving the inverse kinematics. On the other hand, leg motions were simply realized because the flutter kick and butterfly kick were expressed by two dimensional motions. The determined joint angles were simulated with a robot model and finally performed by the developed humanoid robot.

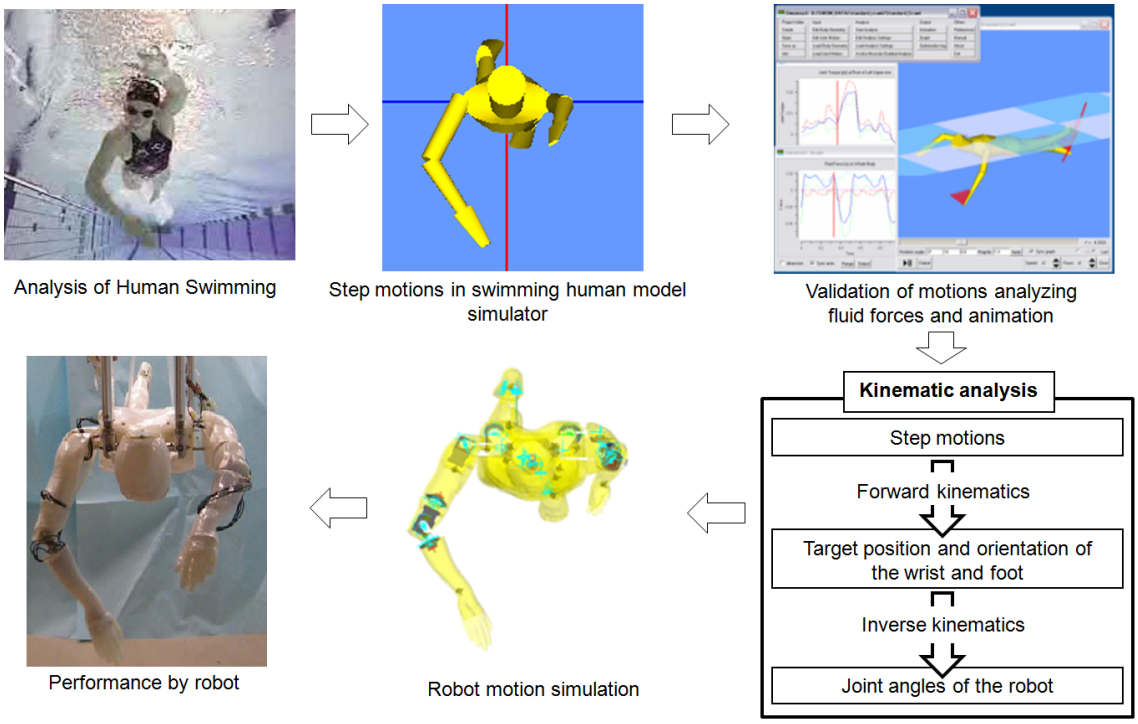

Figure 3.1 Overview of swimming motion generation

3.3. Usage of Scapular Joint

Arm motions during swimming are composed of the underwater stroke and recovery stroke. Swimmers perform these two strokes continuously. However, such a continuous stroke motion cannot be realized with a general robot arm which is constructed of a three-rotation sequence of pitch, yaw and roll. This problem is schematically explained in Figure 3.2. Stroke motion is mainly generated by the pitch joint (shoulder joint 1 in Figure 2). It can be generated by a 360 degree rotation motor, as shown in Figure 3.2 (a). However, the endless rotation by the pitch joint is an impossible motion for humans and it is difficult to realize with the robot arm as well, because, usually, the range of motion of a servo motor is limited, and wires will become tangled. The stroke motion of a general robot arm which has a 3-DOF shoulder joint can be generated, as shown in Figure 3.2 (b). The angle of shoulder joint 1 is increased from 0 to 180 degrees for the underwater stroke. Then, it returns to 0 degrees in order to perform the recovery stroke. The hand position can be constant during this return by changing the angle of shoulder joint 2 from 0 to 180 degrees. However, such a 'switching' motion of shoulder joint 1 and 2 makes it difficult to generate continuous stroke motions. Therefore, in this study, the scapular joint was installed on the robot arm based on the idea that the human scapular retraction motion makes it easy to perform an over arm motion. As shown in Figure 3.2 (c), shoulder joint 1 moves from 0 to 180 degrees for the underwater stroke. Then, the retraction motion is created by the scapular joint and the angle of shoulder joint 1 returns to 0 degrees during the retraction. In order to use the scapular joint systematically, we limited the range of the retraction motion to the over arm motions, such as the recovery motion in the crawl stroke. It was reasonable considering the motion of humans. Figure 3.2 (d) shows the usefulness of the scapular joint comparing the recovery strokes with retraction motion and without that. The robot could realize the over arm motion in the recovery stroke using the scapular joint. Afterwards, we re-calculate the position and orientation of the elbow coordinate considering the moved position of the shoulder joint by the scapular joint. From the re-calculated goal position of the elbow, we could calculate the rest motor angles through the inverse kinematics. The details are described in the following sections.

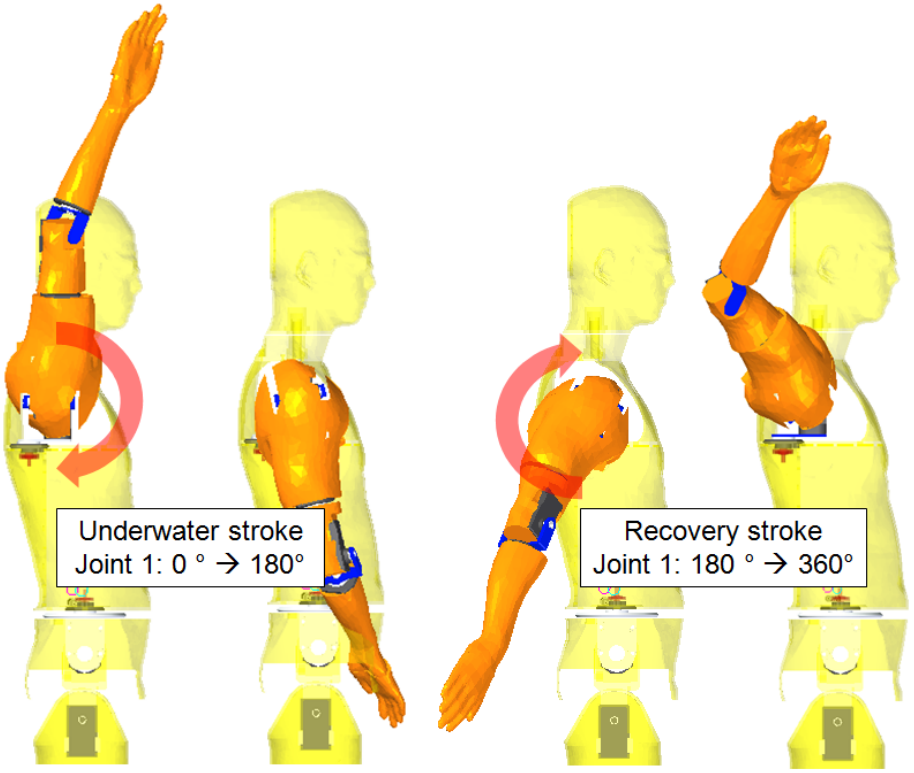

(a) 360-degree rotation without scapular joint

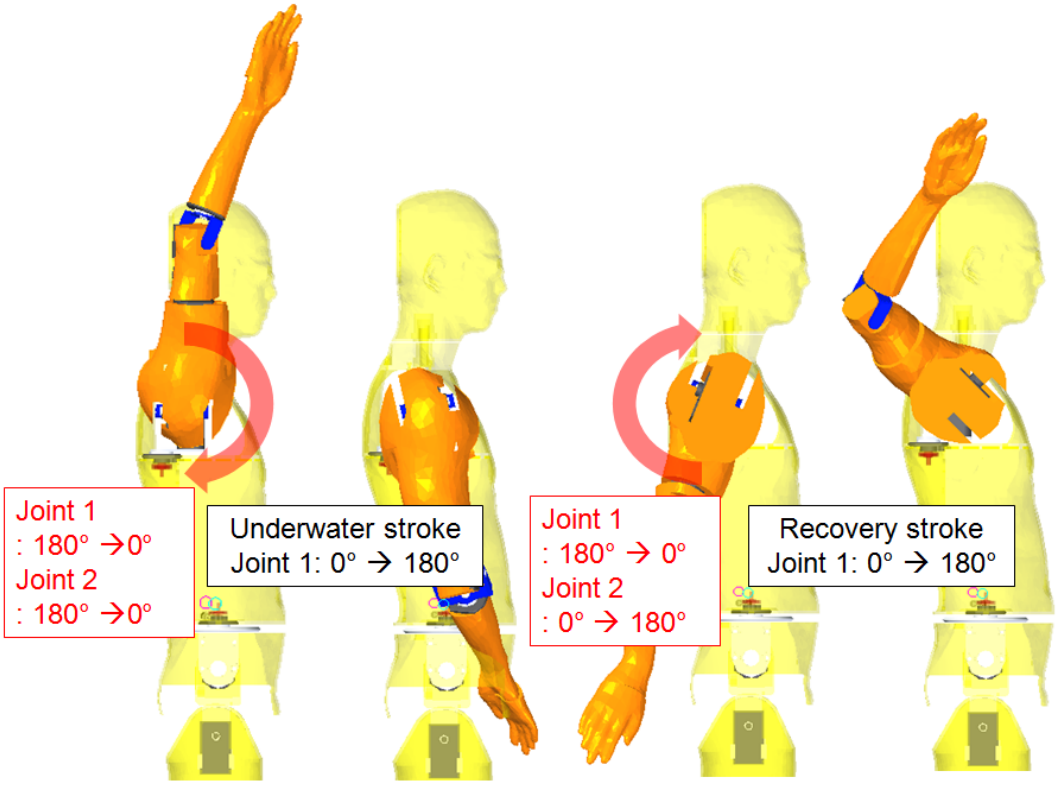

(b) 180-degree rotation without scapular joint

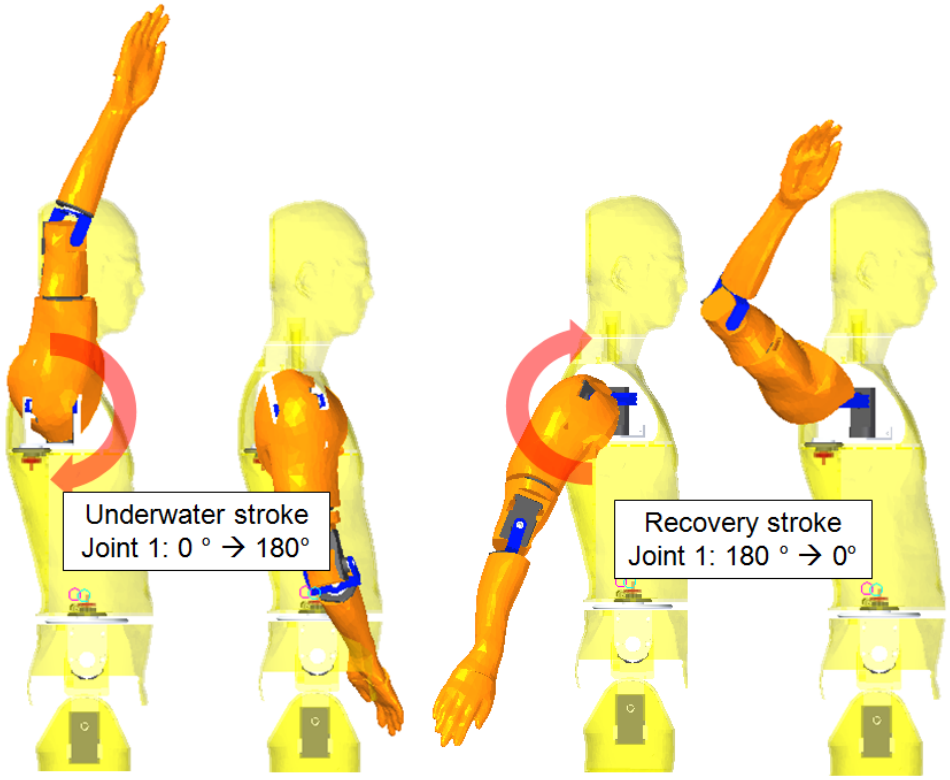

(c) 180-degree rotation with scapular joint

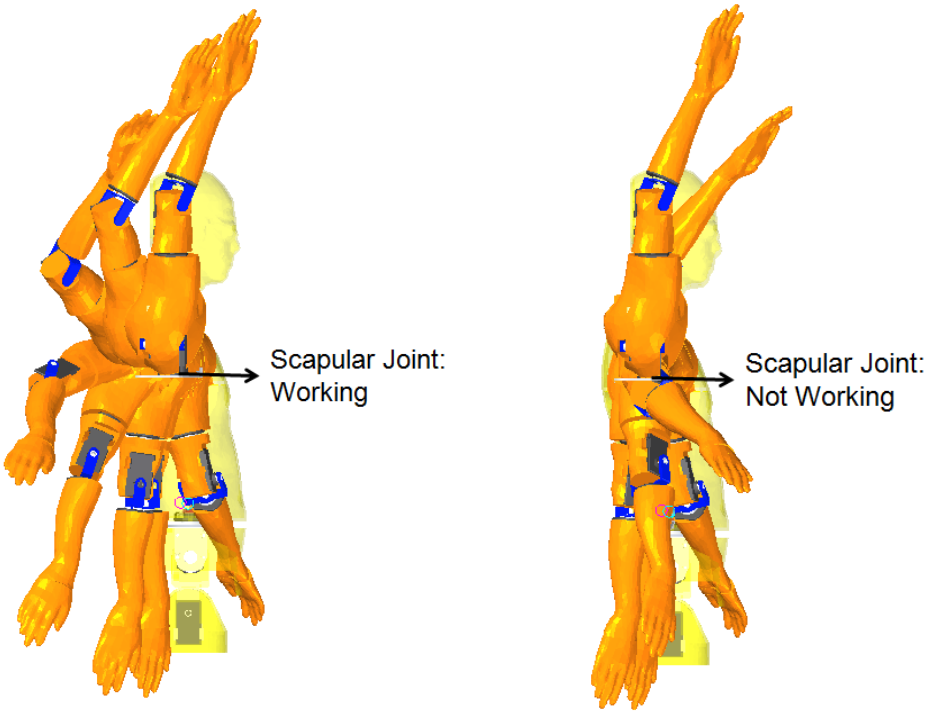

(d) Comparison of recovery stroke with scapular joint and without scapular joint

Figure 3.2 Stroke motions of the robot

3.4. Inverse Kinematics Accompanying Scapular Joint

3.4.1. The kinematics model of the arm

The joint motion in the present study was determined based on standard six-beat crawl stroke of SWUM. Figure 3.3 shows the reference and link coordinate systems of the 6-DOF robot arm using the Denavit-Hartenberg convention. The values of the kinematic parameters are listed in Table 3.1, where *a*, *b* and *c* are the lengths between the shoulder joints, and l_1, l_2 and l_3 are the arm's lengths. They correspond to the home position pictured in the link coordinate diagram of Figure 3.3.

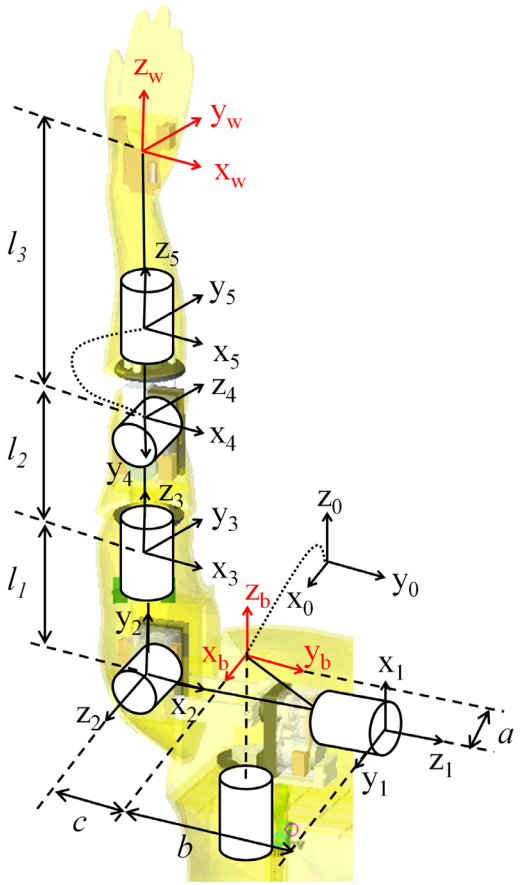

Figure 3.3 Coordinate system of the 6-DOF robot arm

Table 3.1 Denavit-Hartenberge parameters of the arm

i	α_{i-1}	a_{i-1}	d_i	θ_i
0	0	0	0	θ_0
1	-90°	a	b	$\theta_{1\text{-}90°}$
2	-90°	c	0	$\theta_{2\text{-}90°}$
3	-90°	0	l_1	θ_3
4	-90°	0	l_2	θ_4
5	90°	0	0	θ_5
6	0°	0	l_3	0

a_i = the distance from Z_i to Z_{i+1} measured along Xi;

α_i = the angle from Z_i to Z_{i+1} measured about Xi;

d_i = the distance from X_{i-1} to X_i measured along Zi; and

θ_i = the angle from X_{i-1} to X_i measured about Zi.

The position and orientation of the wrist with respect to the base frame is expressed as:

$$T_{wrist} = {}^{b}_{0}T \cdot {}^{0}_{1}T \cdot {}^{1}_{2}T \cdot {}^{2}_{3}T \cdot {}^{3}_{4}T \cdot {}^{4}_{5}T \cdot {}^{5}_{w}T = \begin{bmatrix} r_{11} & r_{12} & r_{13} & p_x \\ r_{21} & r_{22} & r_{23} & p_y \\ r_{31} & r_{32} & r_{33} & p_z \\ 0 & 0 & 0 & 1 \end{bmatrix} \quad (1)$$

where ${}^{b}_{0}T$, ${}^{0}_{1}T$, ${}^{1}_{2}T$, ${}^{2}_{3}T$, ${}^{3}_{4}T$, and ${}^{4}_{5}T$ are transformation matrix and represented as a function of joint displacements, θ_0, θ_1, θ_2, θ_3, θ_4 and θ_5, respectively. Each matrix is represented in Appendix A. $[r_{11}\ r_{21}\ r_{31}]^T$, $[r_{12}\ r_{22}\ r_{32}]^T$ and $[r_{13}\ r_{23}\ r_{33}]^T$ are the unit vectors of the frame attached to the wrist, and$[p_x\ p_y\ p_z]^T$ is the position vector of the origin of this frame with respect to the origin of the base frame ($x_b\ y_b\ z_b$) (Figure 3.3).

3.4.2. Determination of the angle of scapular joint

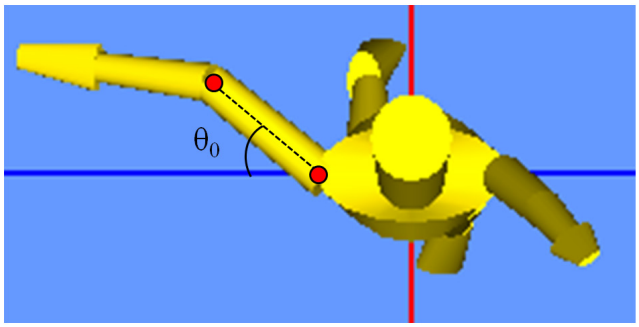

(a) Determination of the angle of scapular joint from SWUM

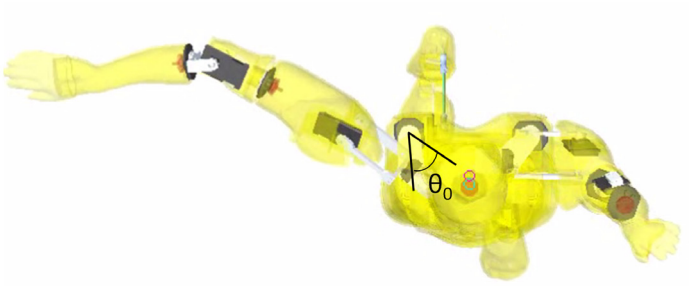

(b) Application of the angle of scapular joint in the robot model

Figure 3.4 Determination of the angle of scapular joint (θ_0) of the robot from the simulation model

The angle of the scapular joint in the over arm motion was determined as the upper arm angle with respect to the horizontal line θ_0, which is shown in Figure 3.4 (a). This angle can be calculated from the elbow transformation matrix. The transformation matrix is expressed as:

$$T_{elbow\_SWUM} = \begin{bmatrix} r'_{11} & r'_{12} & r'_{13} & p'_x \\ r'_{21} & r'_{22} & r'_{23} & p'_y \\ r'_{31} & r'_{32} & r'_{33} & p'_z \\ 0 & 0 & 0 & 1 \end{bmatrix} \quad (2)$$

where $[r'_{13}\ r'_{23}\ r'_{33}]^T$ is the unit vector of z_3 in Figure 9 and it represents the upper arm's direction. Therefore, the angle of the upper arm with respect to the horizontal line or with respect to axis y_{sb} in Figure 3.5 is obtained by followed equation:

$$\theta_0 = \arctan\left(\frac{r'_{13}}{r'_{23}}\right) \quad (3)$$

Also, around the beginning and end of the over arm motion, we set the angle of scapular joint θ_0 so that it varied gradually.

3.4.3. Determination of the elbow position and orientation

As shown in Figure 3.5, the base frame of the simulation model {sb} and the base frame of the robot model {b} are different. The frame {sb} is located at the end of the shoulder and the frame {b} is located in the scapular joint because there is no scapular joint in the simulation model. Therefore, the original desired frame of the wrist, which was calculated from the simulation model, was derived from frame {sb}.

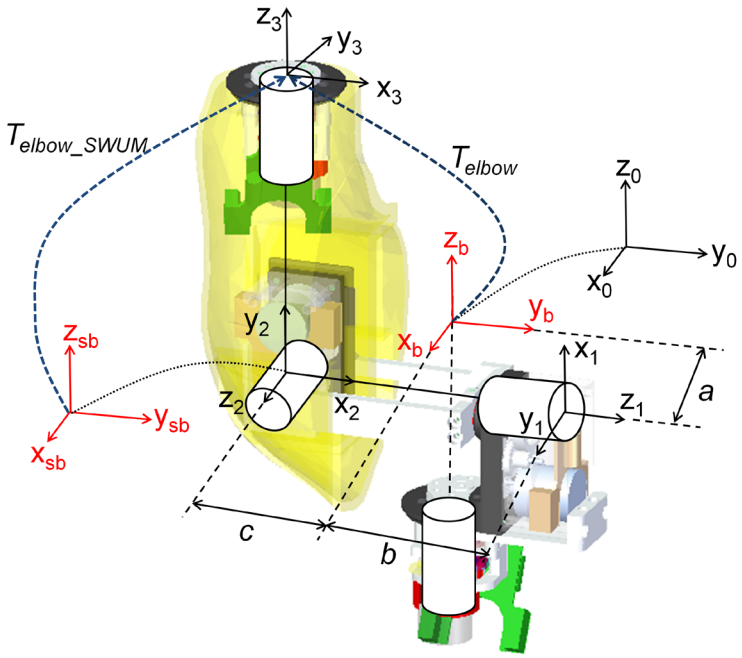

Figure 3.5 Relationship of SWUM's base frame and the robot's base

For the robot, the origin of the base frame of the simulation model is the same as initial position of robot frame {2} in Figure 3.5, but the frame {2} moves depending

on movement of θ_0 at each motion frame. The difference between frame {sb} and frame {2} is given by equation (4). To simplify the notation, s_i, c_i, s_{i-90} and c_{i-90} are $\sin\theta_i$, $\cos\theta_i$, $\sin(\theta_i\text{-}90°)$, and $\cos(\theta_i\text{-}90°)$ respectively.

$$ {}^{b}_{0}T \cdot {}^{0}_{1}T \cdot {}^{1}_{2}T = \begin{bmatrix} c_0c_{1-90}c_{2-90} + s_0s_{2-90} & -c_0c_{1-90}s_{2-90} + s_0c_{2-90} & -c_0s_{1-90} & cs_0 + ac_0 \\ s_0c_{1-90}c_{2-90} - c_0s_{2-90} & -s_0c_{1-90}s_{2-90} - c_0c_{2-90} & -s_0s_{1-90} & -cc_0 + as_0 \\ -s_{1-90}c_{2-90} & s_{1-90}s_{2-90} & -c_{1-90} & 0 \\ 0 & 0 & 0 & 1 \end{bmatrix} \quad (4) $$

We could not calculate the joint angles of the robot arm because the origin of frame {2} was not consistent with the origin of frame {sb} but if we moved the origin of frame {sb} to the origin of frame {2}, we could calculate the joint angles using the motion data of the simulation. Considering the difference, the desired position and orientation were modified as follows in equation (5):

$$ \begin{aligned} T_{elbow} &= {}^{b}_{0}T \cdot {}^{0}_{1}T \cdot {}^{1}_{2}T \cdot {}^{2}_{3}T \\ &= T_{elbow\_SWUM} + \begin{bmatrix} 0 & 0 & 0 & cs_0 + ac_0 \\ 0 & 0 & 0 & -cc_0 + as_0 \\ 0 & 0 & 0 & 0 \\ 0 & 0 & 0 & 1 \end{bmatrix} \\ &= \begin{bmatrix} r''_{11} & r''_{12} & r''_{13} & p''_x \\ r''_{21} & r''_{22} & r''_{23} & p''_y \\ r''_{31} & r''_{32} & r''_{33} & p''_z \\ 0 & 0 & 0 & 1 \end{bmatrix} \end{aligned} \quad (5) $$

As a result, the shoulder's position would have a small error because of the difference of the base frames. However, we could calculate the joint angles of the robot from the motion data of simulation, as described in the following section.

3.4.4. Solution of the inverse kinematics problem

To determine the arm joint angles for a given position and orientation of the wrist, we solved the inverse kinematics problems. The relationship between the elbow and the reference base frame is given by equation (5). The target matrix of the robot arm, T_{elbow_SWUM} and T_{wrist_SWUM} are obtained from swimming motion data of SWUM. The calculation is explained in Appendix B. With the target matrixes, the solution starts from the matrix equation (6):

$$\underbrace{{}^{b}_{0}T^{-1} \cdot T_{elbow}}_{\text{L1}} = \underbrace{{}^{0}_{1}T \cdot {}^{1}_{2}T \cdot {}^{2}_{3}T}_{\text{R1}} \tag{6}$$

The equations L1(1,3)=R1(1,3) and L1(3,3)=R1(3,3) of the elements of the matrices L1 and R1 can be used to solve for θ_1. This yields:

$$\theta_1 - 90^\circ = \tan^{-1}\left(\frac{-r''_{33}}{c_0 r''_{13} + s_0 r''_{23}}\right) \tag{7}$$

The equations L1(2,2)=R1(2,2) and L1(2,1)=R1(2,1) of the matrices L1 and R1 provide the solution for θ_3:

$$\theta_3 = \tan^{-1}\left(\frac{s_0 r''_{12} - c_0 r_{22}}{-s_0 r''_{11} + c_0 r''_{22}}\right) \tag{8}$$

The equation L1(2,1)=R1(2,1) and L1(2,3)=R1(2,3) of the matrices L1 and R1 provide the solution for θ_2:

$$\theta_2 - 90^\circ = \tan^{-1}\left(\frac{s_0 r''_{11} - c_0 r''_{21}}{(s_0 r''_{13} - c_0 r''_{23})c_3}\right) \tag{9}$$

$$T''' = {}^{1}_{2}T^{-1} \cdot {}^{0}_{1}T^{-1} \cdot {}^{b}_{0}T^{-1} \cdot T_{wrist}$$
$$= {}^{2}_{3}T \cdot {}^{3}_{4}T \cdot {}^{4}_{5}T \cdot {}^{5}_{w}T = \begin{bmatrix} r'''_{11} & r'''_{12} & r'''_{13} & p'''_{x} \\ r'''_{21} & r'''_{22} & r'''_{23} & p'''_{y} \\ r'''_{31} & r'''_{32} & r'''_{33} & p'''_{z} \\ 0 & 0 & 0 & 1 \end{bmatrix} \quad (10)$$

$$\underbrace{{}^{2}_{3}T^{-1} \cdot T'''}_{\text{L2}} = \underbrace{{}^{3}_{4}T \cdot {}^{4}_{5}T \cdot {}^{5}_{w}T}_{\text{R2}} \quad (11)$$

The equations L2(1,3)=R2(1,3), L2(3,3)=R2(1,3) and L2(2,1)=R2(2,1)), L2(2,2)=R2(2,2) of the matrices L2 and R2 provide the solution for θ_4, and θ_5:

$$\theta_4 = \tan^{-1}\left(\frac{c_3 r'''_{13} - s_3 r'''_{33}}{r'''_{23}}\right) \quad (12)$$

$$\theta_5 = \tan^{-1}\left(\frac{-s_3 r'''_{11} - c_3 r'''_{31}}{-s_3 r'''_{12} - c_3 r'''_{32}}\right) \quad (13)$$

If multiple values were obtained as solutions, we determined the value considering the range of motion and natural pose of a real human.

3.5. Validation of the Scapular Joint for Swimming Motions

The joint angles of the shoulder were simulated in the crawl stroke, backstroke and butterfly stroke. In order to validate and confirm the efficiency of the scapular joint for the retraction motion (θ_0), we simulated two conditions. First, we did not use the scapular joint and performed stroke motions with a 5-DOF robot arm, according to the results of the conventional inverse kinematics. It corresponds to the situation of Figure 3.2 (b). Next, we used the scapular joint as explained above, corresponding to Figure 3.2 (c). Figure 3.6 shows the joint angles of the shoulder. The graphs in Figure 3.6 (a), (c), and (e) are without the scapular joint, while those in Figure 3.6 (b), (d), and (f) are with the scapular joint. As shown in Figure 3.6 (a), (c), and (e), when there is no scapular joint, the shoulder joints 1 and 2 switch their positions (time

frame 0 to 1 and 6 to 7 in crawl, 17 to 0 and 9 to 10 in back, and 9 to 10 and 17 to 0 in butterfly). On the other hand, as shown in Figure 3.6 (b), (d), and (f), when the scapular joint moves, the motion of shoulder joint 1 was continuous and the range of motion of the joint 2 became significantly smaller.

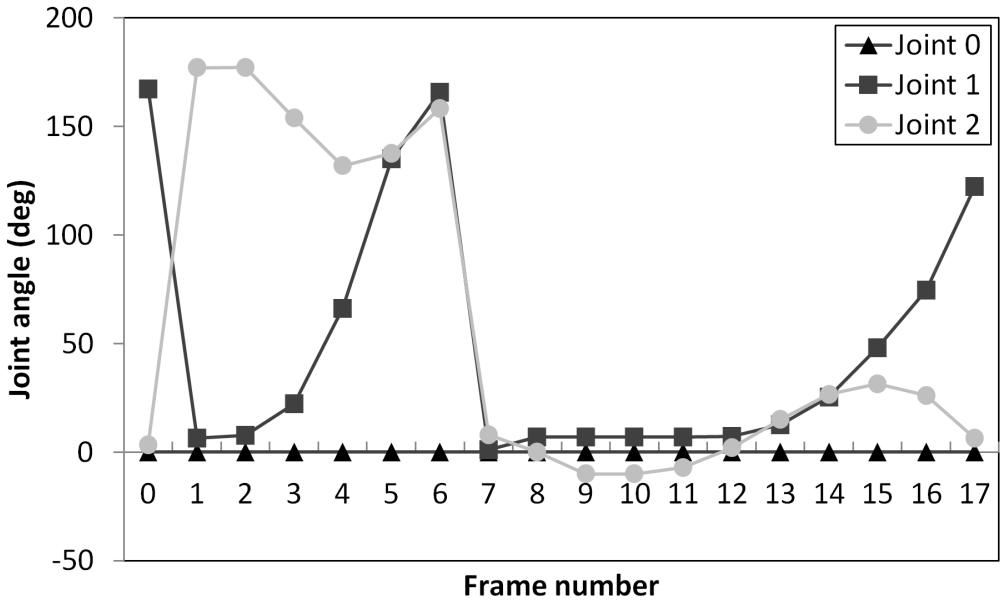

(a) Crawl stoke without scapular joint

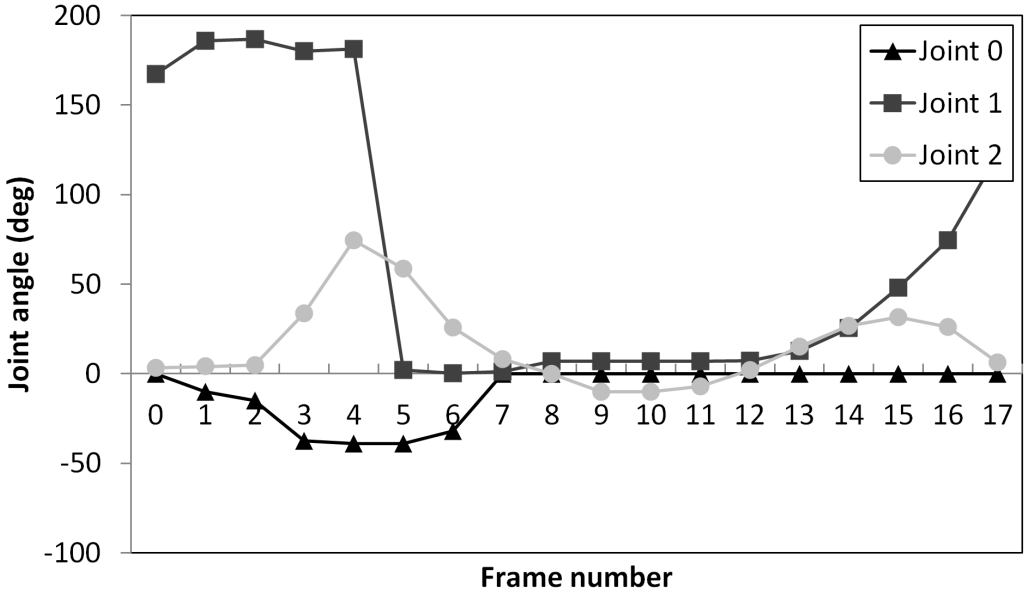

(b) Crawl stroke with scapular joint

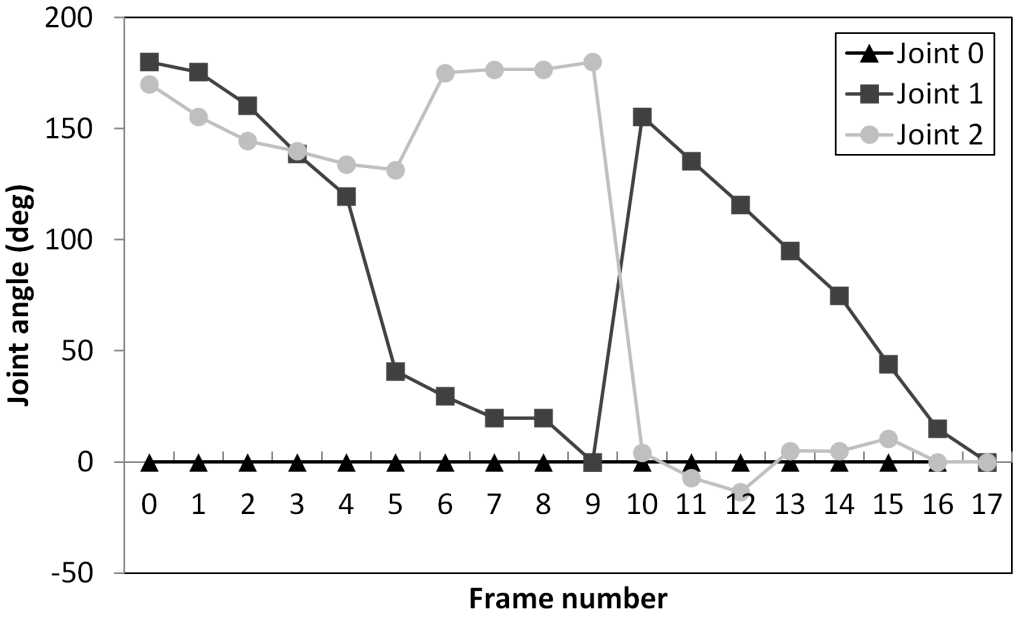

(c) Back stroke without scapular joint scapular joint

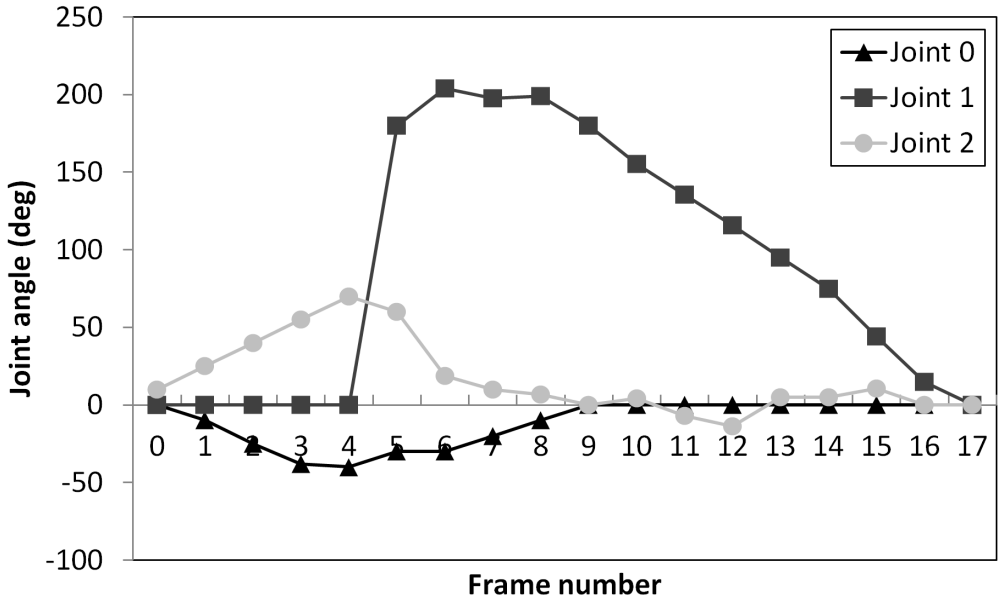

(d) Back stroke with scapular joint

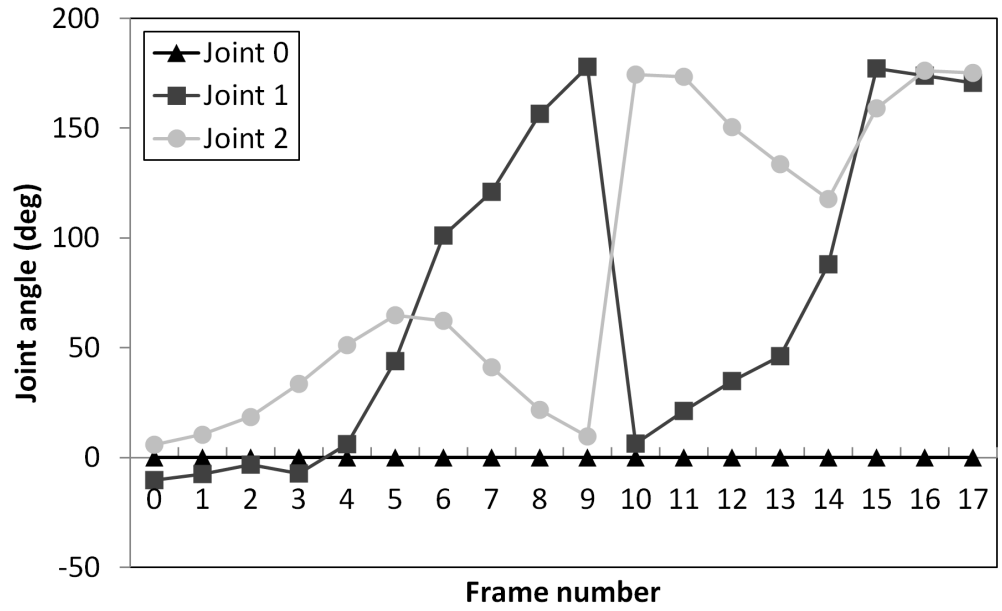

(e) Butterfly without scapular joint

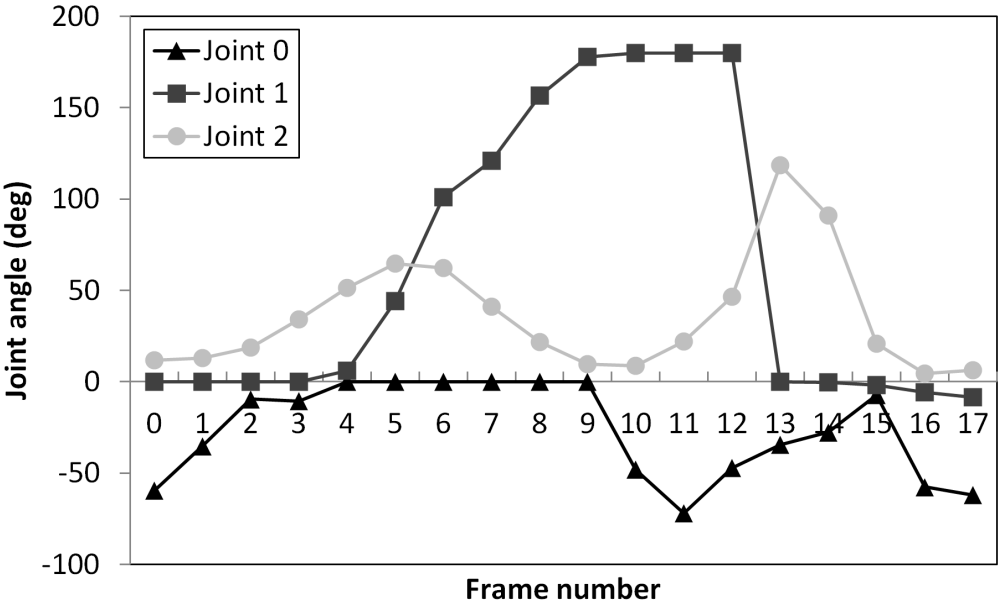

(f) Butterfly with scapular joint

Figure 3.6 Joint angles of the right shoulder

3.6. Conclusion

To realize the human swimming motion, we added a scapular joint for the retraction motion and also developed an inverse kinematics model to determine the angle of the scapular joint. The efficiency of the scapular joint was validated by simulation of the crawl, back and butterfly strokes. In the simulation, it was confirmed that the robot can rotate its shoulder continuously.

Chapter 4

Stroke Motion Experiment in Fixed State

4.1. Introduction

In chapter 3, we established methodology to generate swimming motions of the robot. In this chapter, representatively, the stroke motion of the crawl was observed in the circulating water tank supported by four struts. The rolling motion during the crawl stroke was generated by the driving mechanism which was connected by the struts. In addition, the measurement system involving the swimming humanoid robot is discussed. On a trial basis, the propulsive forces during several experiments were measured using the measurement system.

4.2. Configuration of the Measurement system

4.2.1. Driving mechanism

A driving mechanism was developed for the experiment of a swimmer mannequin [49] and remodeled for the present study. The photographed driving mechanism and its drawing are shown in Figure 4.1 and Figure 4.2. In previous research, the swimmer mannequin and the driving machine were connected by four struts and two shafts. Rolling, heaving and pitching motions of the mannequin were driven by the driving mechanism. In this study, the driving mechanism was used to generate rolling, heaving and pitching motions of the humanoid robot in the same manner.

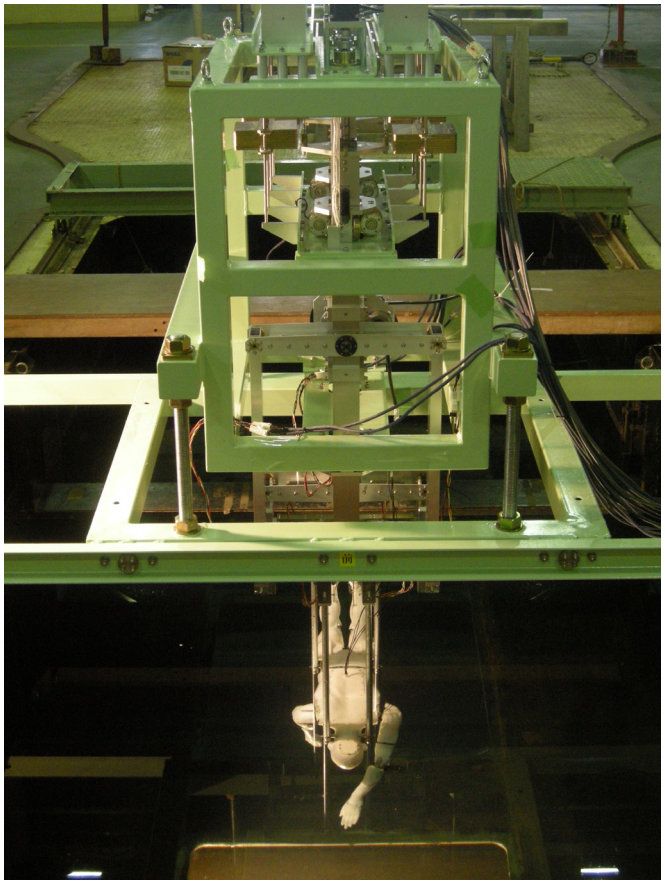

Figure 4.1 Photographed driving mechanism [49]

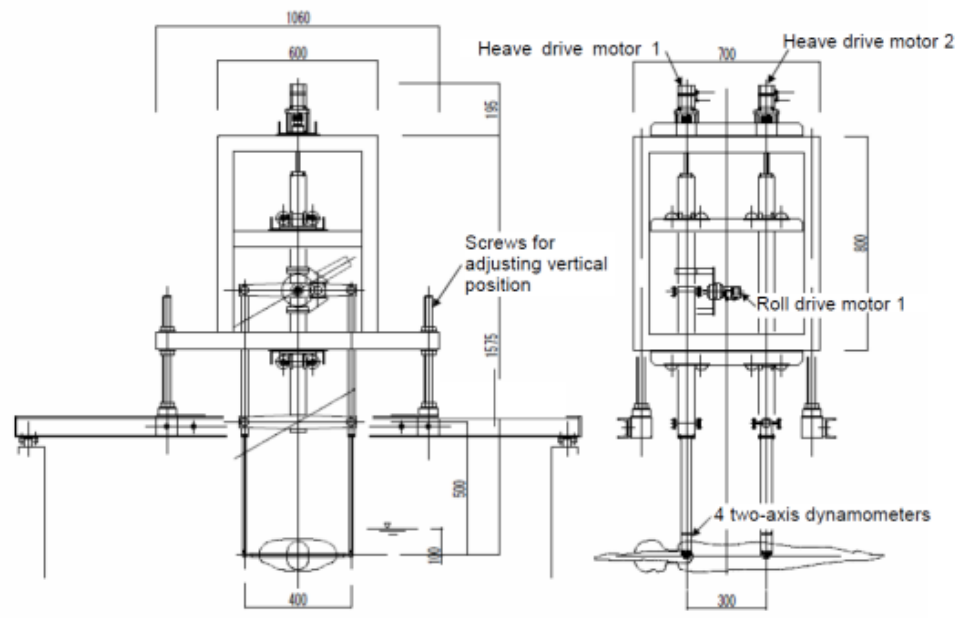

Figure 4.2 Drawing of the driving mechanism [49]

However, the connecting position and length of shafts were modified to avoid interference during performing swimming motions. The front shaft was connected on the neck and the rear shaft was connected on the waist as shown in Figure 4.3 (b) and link mechanism was added between the driving mechanism and struts to adjust interval of struts and to parallelize the motion of the driving mechanism and that of the humanoid robot.

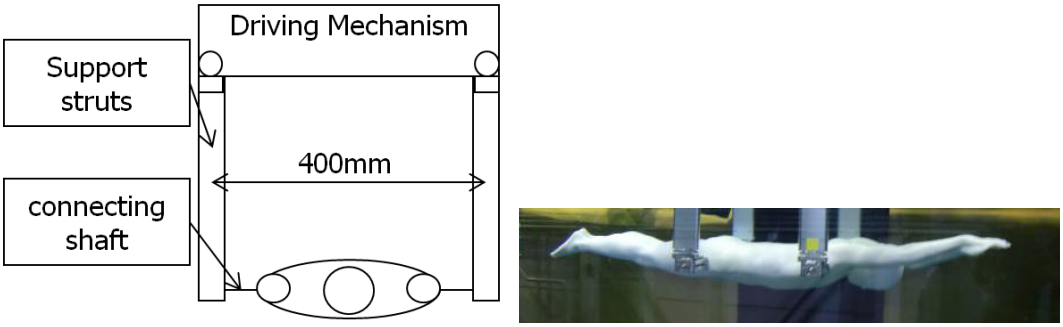

(a) Connecting of the mannequin and the driving mechanism

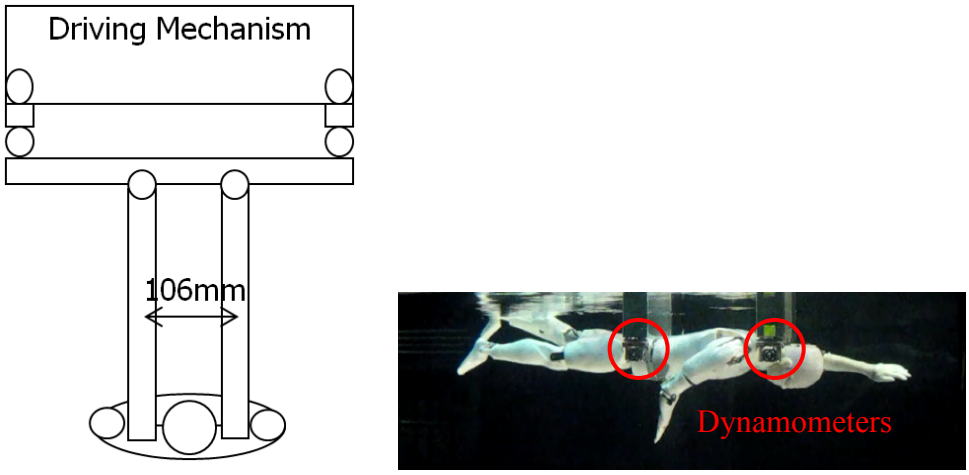

(b) Connecting of the swimming humanoid robot and the driving mechanism

Figure 4.3 Connection of the driving mechanism and subjects

When the humanoid robot performed the rolling motion, the right two (anterior and posterior) struts and left ones move upward and downward in opposite phase.

Also, the combination motion of heaving and pitching can be generated by moving the anterior two (right and left) struts and posterior ones move upward and downward in different phases. These motions were driven by three AC servo motors. The minimum/maximum angle of the rolling was ± 30 degrees. The minimum/maximum heave (up and down) displacement is ± 100 mm. The time curves for these angle and displacements can be fully programmable at a sampling frequency 200Hz. In order to measure the forces acting on the robot, four dynamometers were embedded at the tip of the struts, as shown in Figure 4.3 (b). Each dynamometer detected the forces in the x (flow) and z (vertical) directions. The maximum ranges of the forces were ± 9.8N for x and ± 98N for z.

4.2.2. Circulating water tank

The experiment was carried out using a vertically circulating water tank for a ship experiment in Mitsuizosen Akishima Laboratory. Figure 4.4 shows the view from above and a general drawing of the tank. The size of the measurement area was 5.5m in length, 2.0m in width and 1.2m in depth. The flow velocity was changeable in the range from 0.2m/s to 1.7m/s.

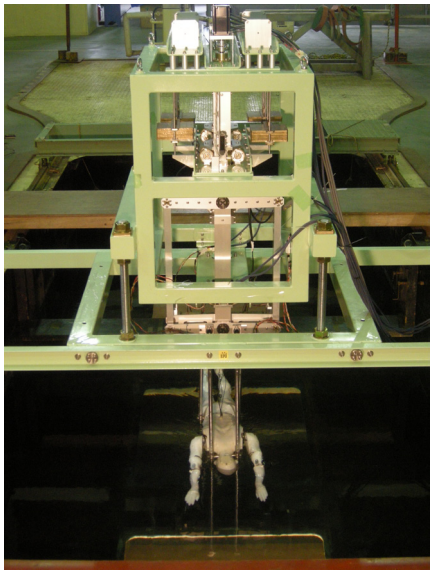

(a) View from above

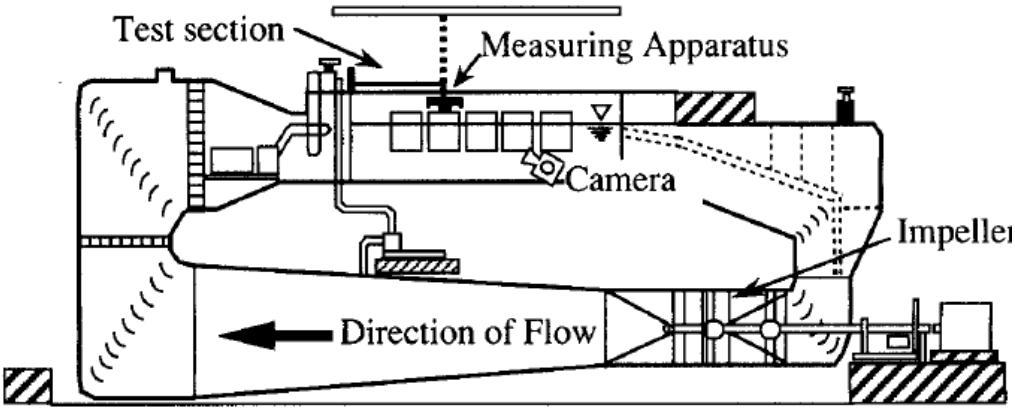

(b) Schematic side view of the circulating water channel

Figure 4.4 Circulating water tank

4.2.3. Measurement and control system

The setup of the measurement and control system is shown in Figure 4.5. The sampling frequency for the measurement was 200Hz. The swimming motion of the humanoid robot was arbitrarily programmable due to the computer control. If the roll angle of the driving mechanism for a one stroke cycle as input data is given in the CSV format, the system automatically creates the reference angle data for the control, by crating the motion data for the start and stop, and conducting interpolation with time to adjust data to the sampling frequency. The robot and the driving mechanism were controlled by each controller and they were connected through an interface board for synchronization of the swimming stroke motion and the rolling motion. The controller of the driving mechanism generated 5V signal during moving and the humanoid robot used the signal as start signal.

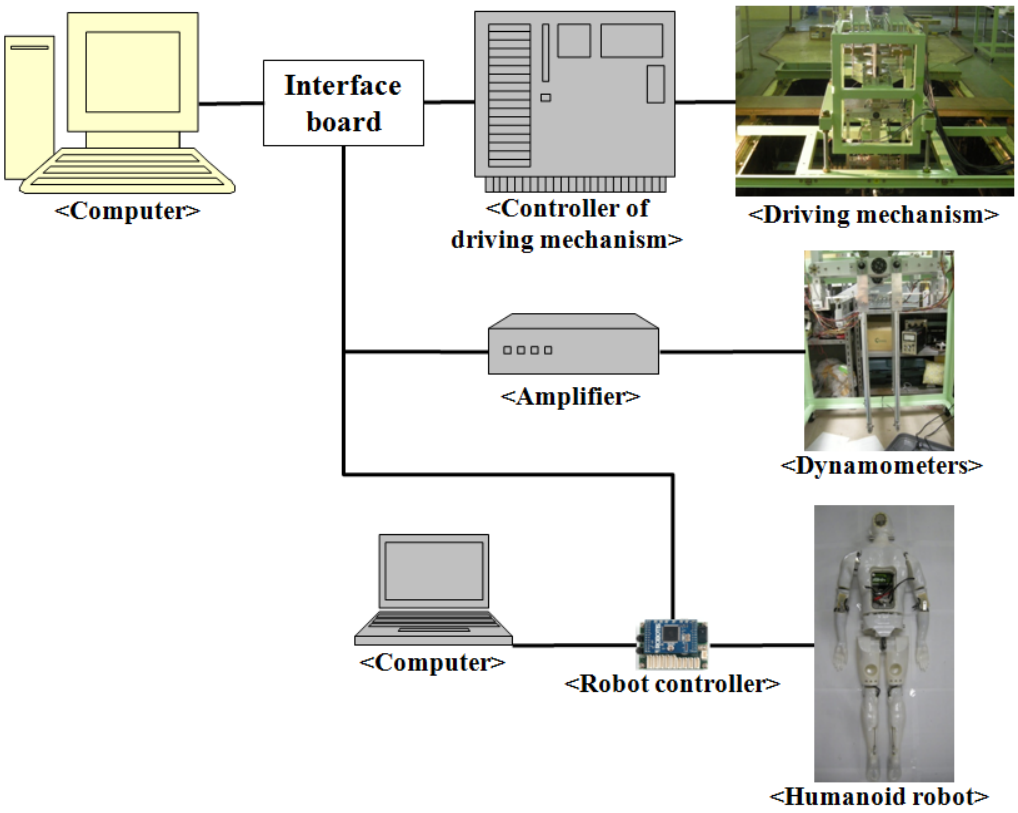

Figure 4.5 Configuration of the measurement and control system

4.3. Experiment

4.3.1. Experimental setup

By the dynamometers, forces in the directions parallel and perpendicular to the flow in the horizontal plane were measured. The coordinate of the dynamometers is shown in Figure 4.6 (a). Every data was captured by the computers and video images were recorded by two cameras.

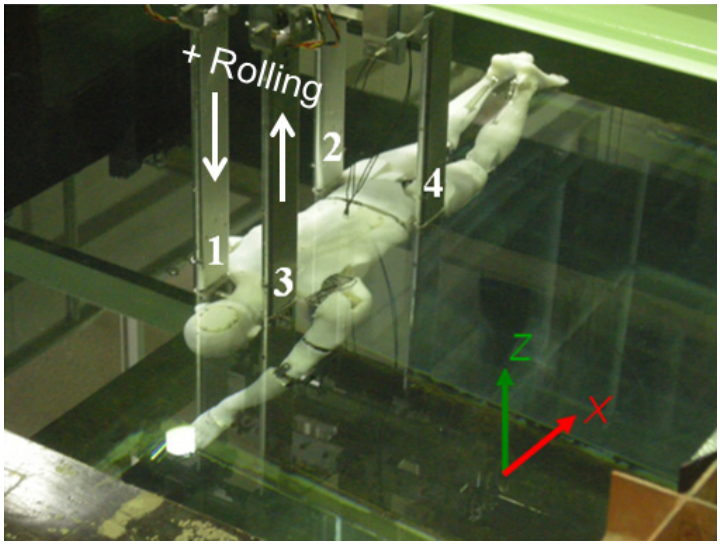

Figure 4.6 Coordinate system of the driving mechanism

4.3.2. Experimental conditions

We measured propulsive force during the front crawl stroke to verify the usefulness of this system. Joint angles of the robot, stroke cycle, mounting height of the robot, rolling amplitude, and flow velocity were given as the experimental condition for each trial. The conditions of all trials are shown in Table 4.1.

The joint angles for one stroke cycle were determined using 'SWUM' and detail parts were modified to avoid interference. The velocities of the swimming motions performed by the robot in the present study were 2 to 4 times slower than the actual movies.

The mounting heights of the robot were determined by the front offset and rear offset of the supporting struts as shown in Figure 4.8. The offset was determined by visual confirmation so that the timings of the entry into the water and out from the water were as consistent as possible with the model swimming.

For the crawl stroke, the rolling motion was performed by the driving mechanism. The input angles of these motions were created based on movies of an actual swimmer [87]. The time curves of the input roll angles for the crawl stroke is shown in Figure 4.7. The original measured angle which was calculated from the movie has an asymmetrical curve about the middle point of the time because of the breathing motion. Actually, the measured angles in the latter half became larger than those in the first half. Therefore, the amplitude I the first half (non-breathing side) was taken

for the input angles. In the experiment, the amplitudes of rolling were limited because of the limited range of motion of the driving mechanism. The 'amplitude ration' was defined so that it becomes 1.0 when the amplitude of the motion input to the driving mechanism is equal to the actual one, which was obtained by video analysis.

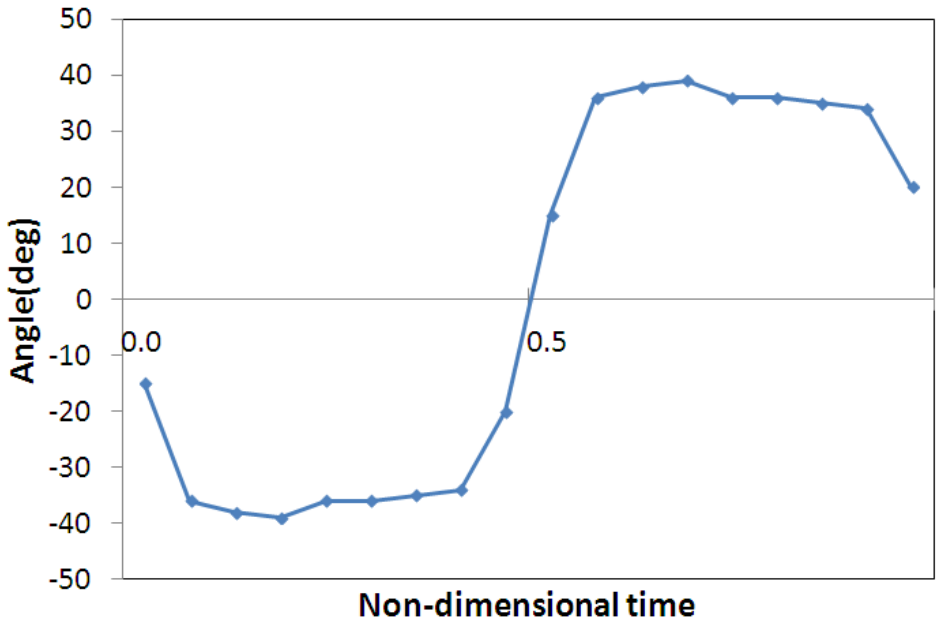

Figure 4.7 The time curves of roll angle for the crawl stroke

Before each trial, the loads were first measured in the gliding position in the flow. The loads in this condition will be deducted from those in each trial, that is, those loads will be used as 'zero points'. The flow velocities were determined half speed of the real swimmer and decreased proportionally to the stroke cycle.

Table 4.1 Experimental conditions

No.	Cycle [sec]	Flow speed [m/s]	Rolling amp. ratio	Front offset [mm]	Rear offset [mm]
1	8.874	0	0.75	30	50
2	5.328	0.2	0.7	10	40
3	5.328	0.25	0.75	10	40
4	4.104	0.32	0.75	10	40

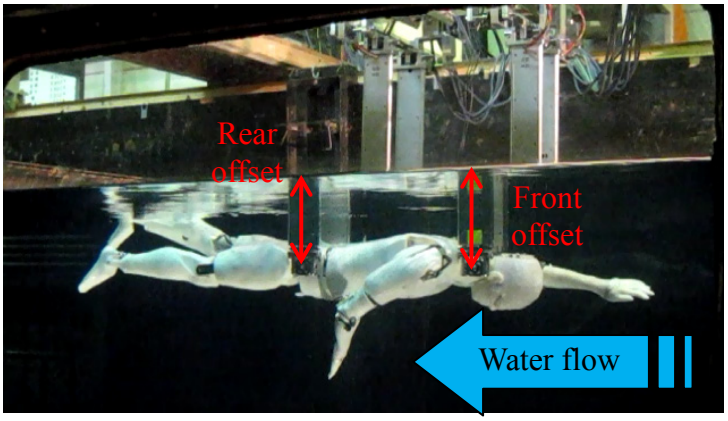

Figure 4.8 Mounting height of the front and rear

4.3.3. Experimental results

Figure 4.9 shows the desired and generated position trajectories in the Cartesian space during the execution of the crawl stroke motion. The commanded joint angles were derived from the crawl stroke data of simulation through the proposed kinematics method. The robot was controlled in open loop because it was enough to produce correct stroke motion as shown in Figure 4.9. Figure 4.10 shows a series of images during the crawl stroke. The swimming humanoid robot performed the crawl stroke naturally and the driving mechanism made roll movement harmoniously as well.

The results show the potential of the experimental system for measurement of fluid force during swimming using a swimming humanoid robot. Also, we confirmed that the robot could generate swimming motions using the proposed methodology. It means we can link the developed simulation model, ‘SWUM’ and the robot model, ‘SWUMANOID’. We could simulate various underwater motions and realize with the robot as well using the proposed kinematic methodology. It could make it easier to develop underwater locomotion of the robot and could be a base of research of humanoid robot for underwater use.

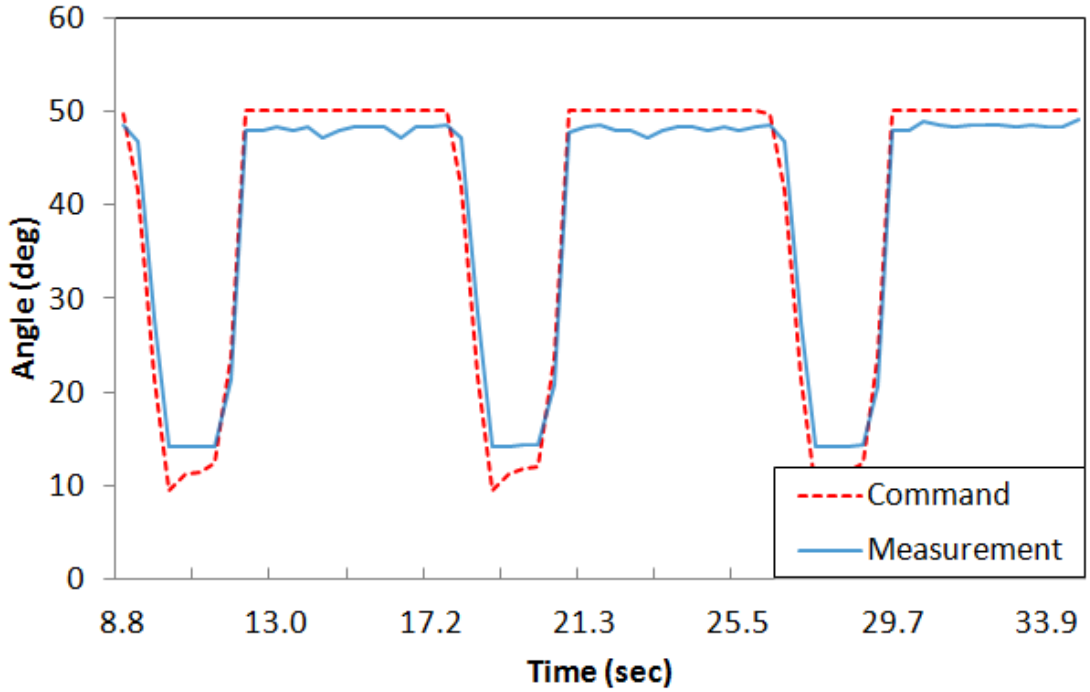

(a) Angles of scapular joint (θ_0)

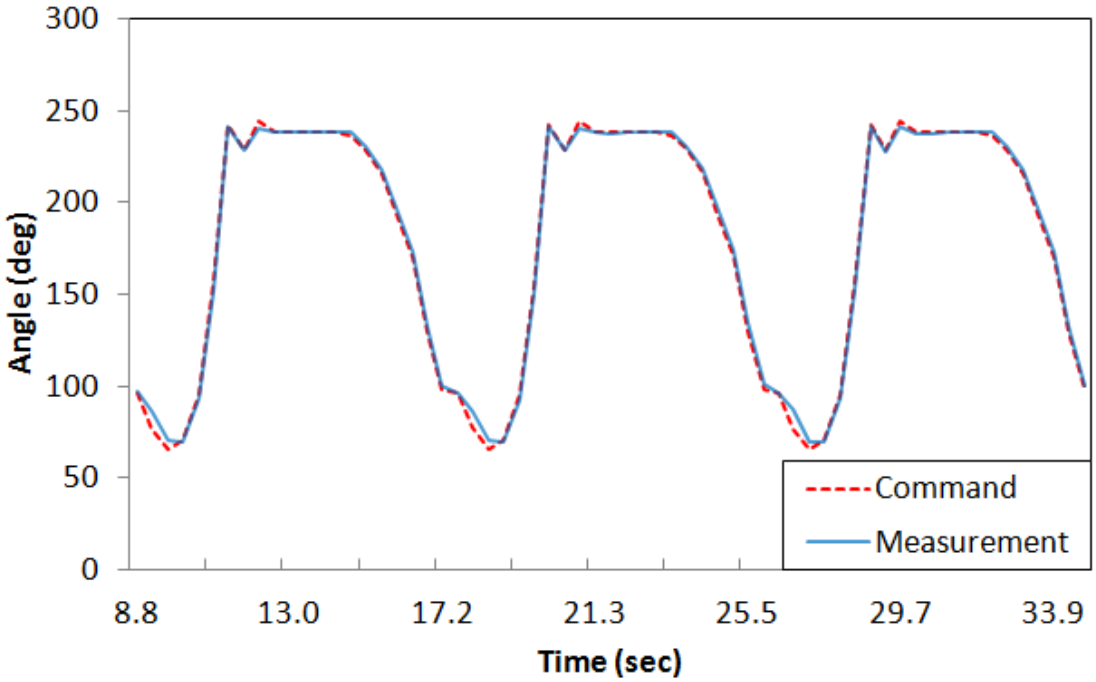

(b) Angles of shoulder joint 1 (θ_1)

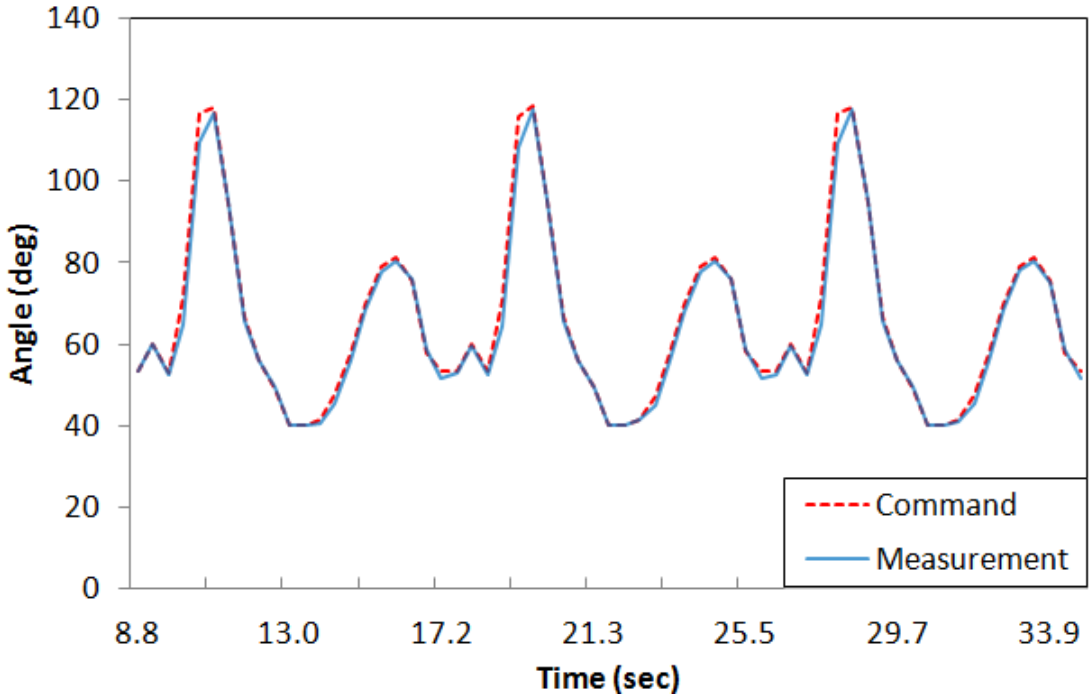

(c) Angles of shoulder joint 2 (θ_2)

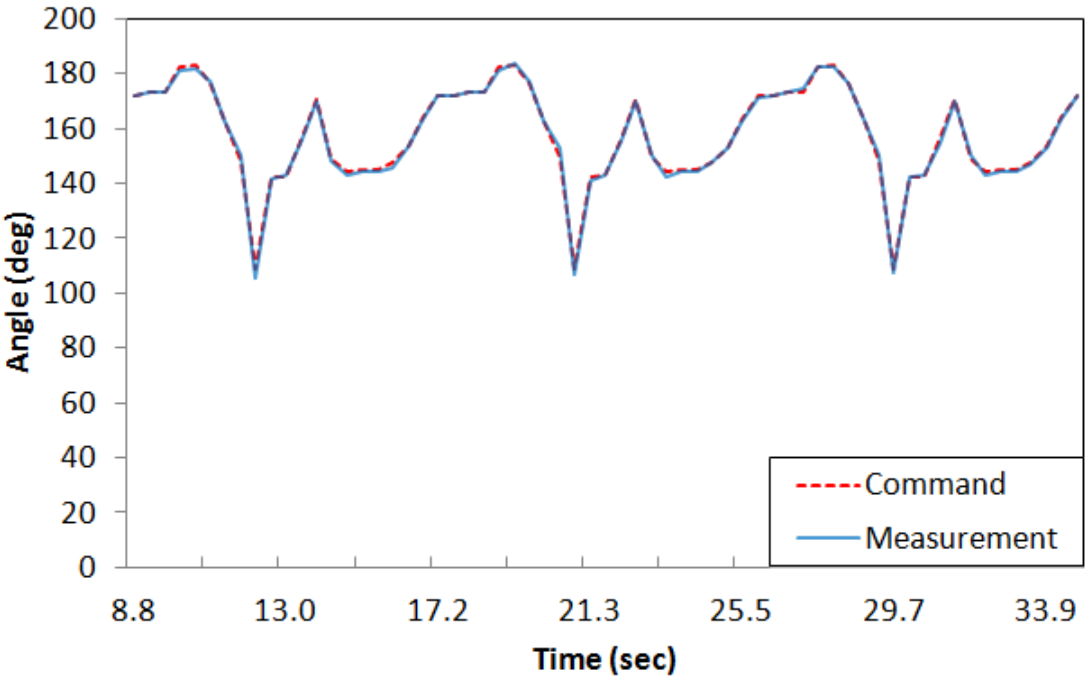

(d) Angles of shoulder joint 3 (θ_3)

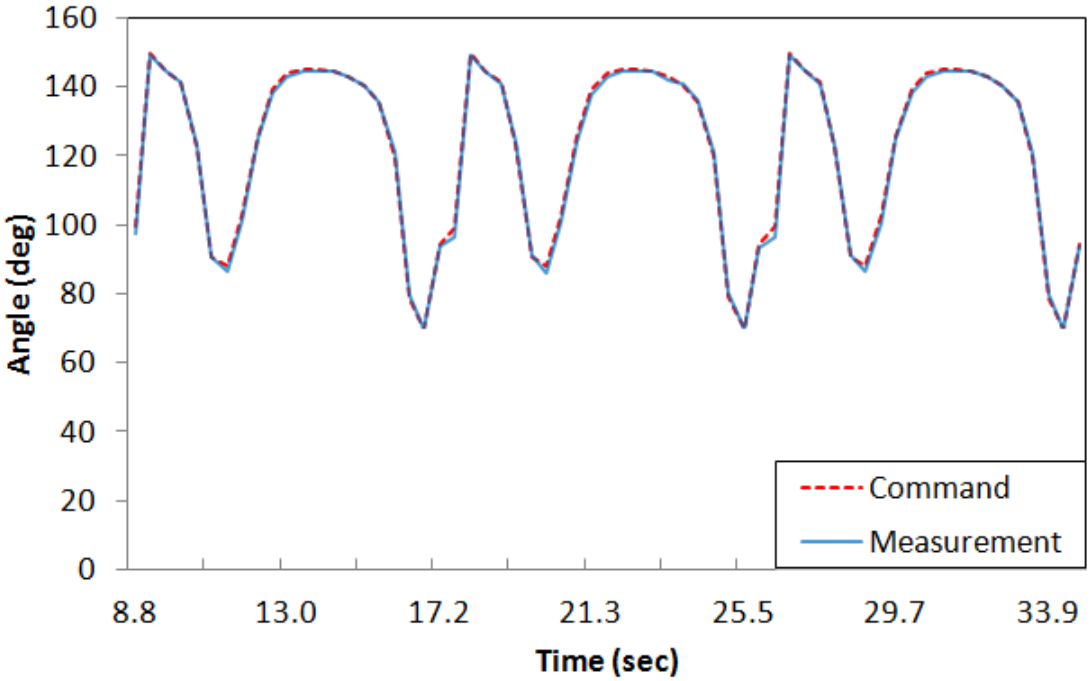

(e) Angles of elbow joint 1 (θ_4)

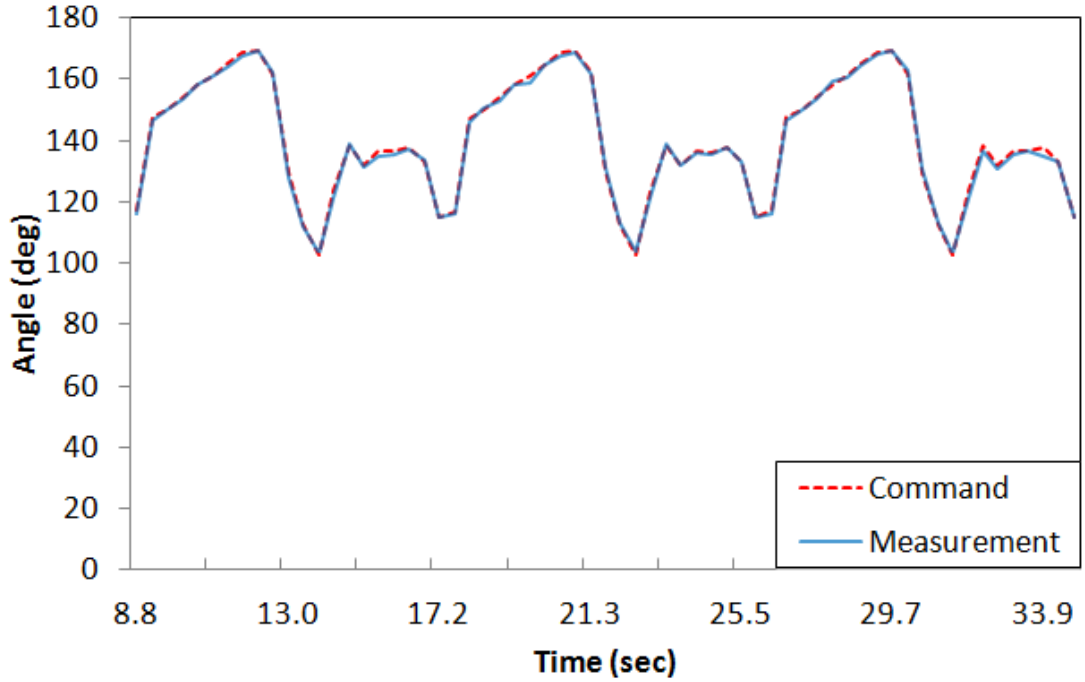

(f) Angles of elbow joint 2 (θ_5)

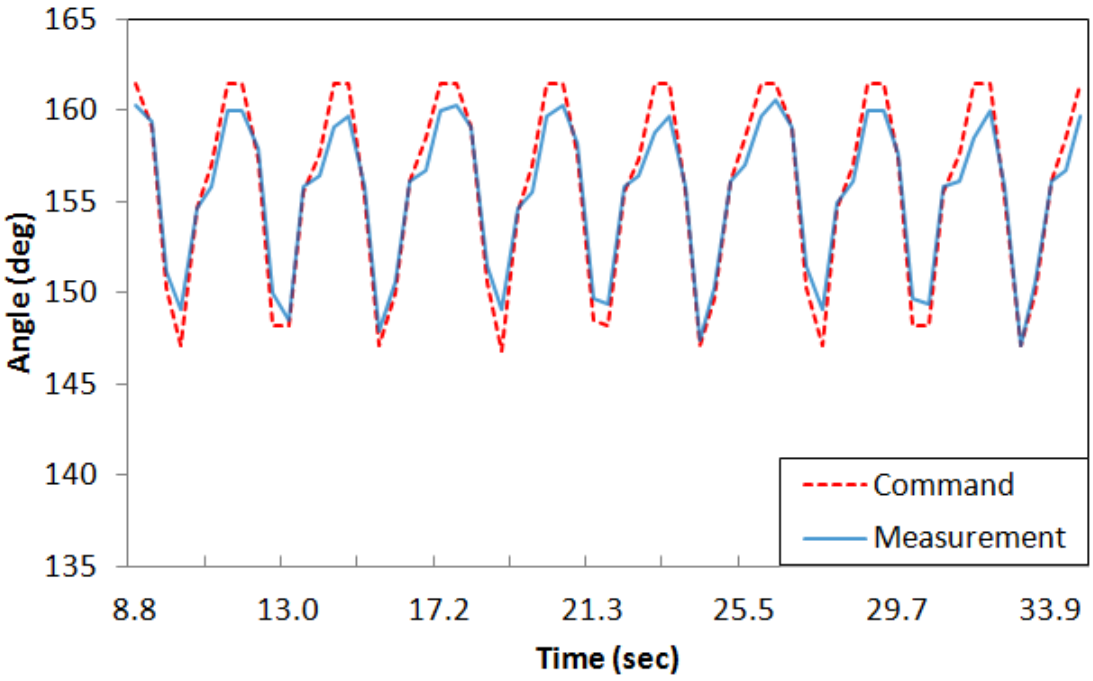

(g) Angles of hip joint

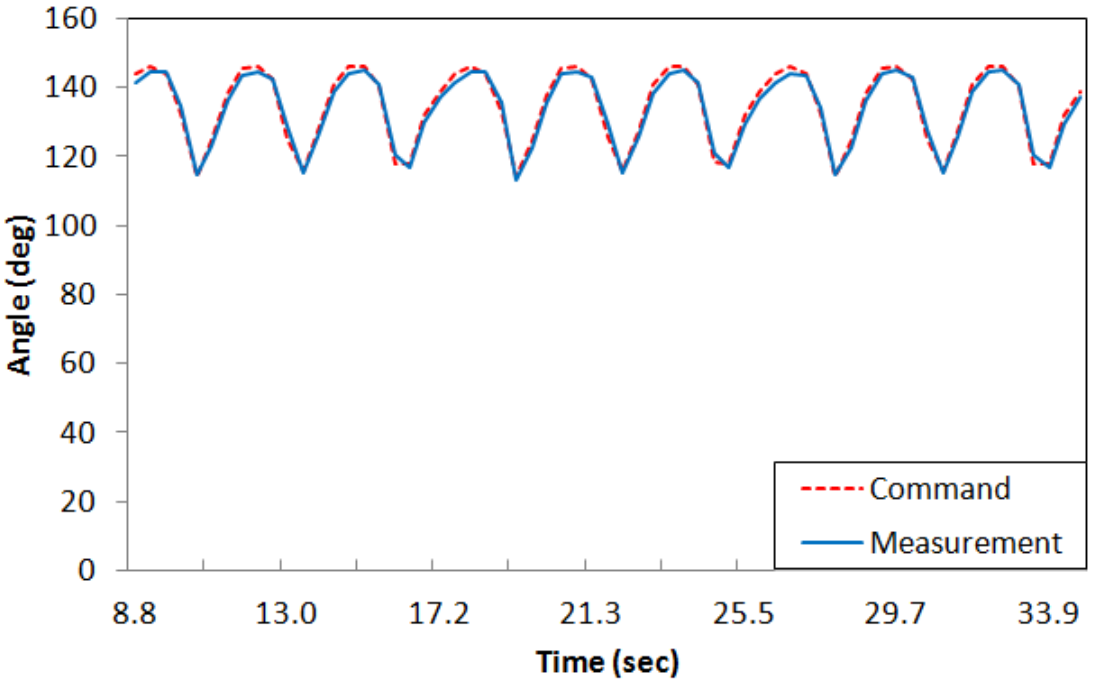

(h) Angles of knee joint

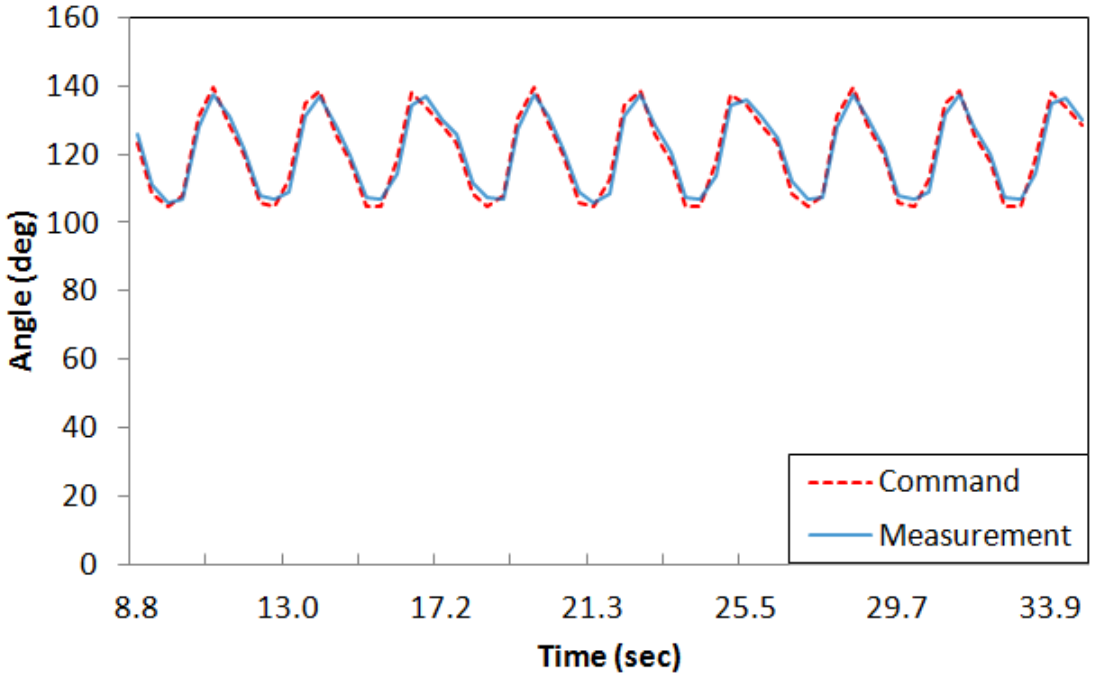

(i) Angles of ankle joint

Figure 4.9 Joint angles of the right arm and right leg

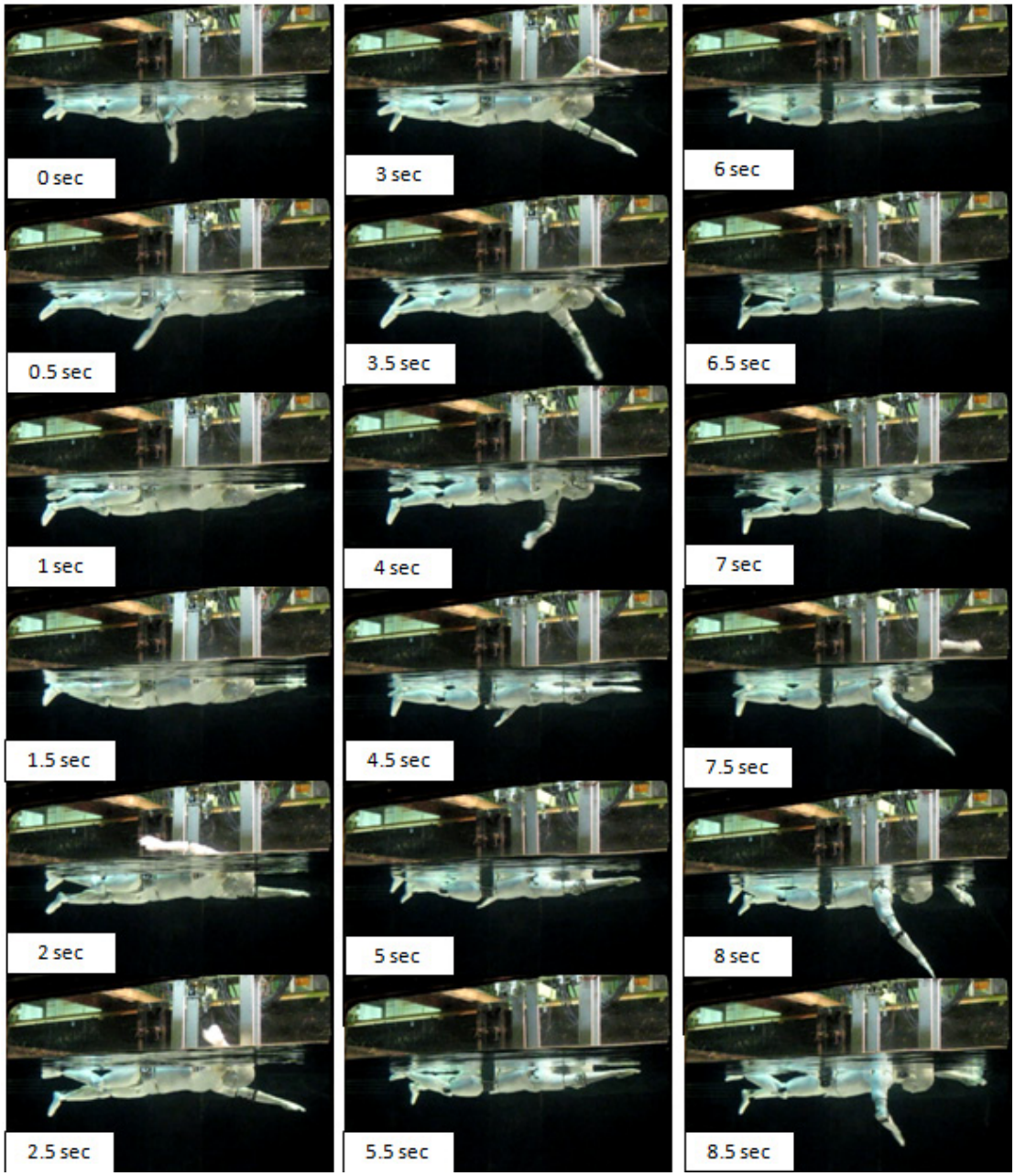

Figure 4.10 Snapshots of SWUMANOID in swimming experiments

During the stroke motion experiment, propulsive force was measured together on a trial basis. Figure 4.11 is one of the results of the experiments to measure propulsive force. Five stroke motions were conducted at each trial and we plotted one stroke cycle in the middle of the five strokes. The swimming robot performed crawl stroke at a speed of 4.10 sec per one stroke and there was a flow of the water at a speed of 0.32m/s. Figure 4.11 (a) is a series of images during one stroke. Measured fluid force is shown in Figure 4.11 (b). In order to analyze propulsive force, we plotted x-directional forces measured by the four dynamometers. A great part of generated force was measured in the front dynamometers because the kick motion didn't generate propulsive force compared to the arm motion. When the arms changed motions, magnitude of force was changed and the direction of force was changed by rolling motion. The graph is not perfect symmetry with respect to the center of rolling motion but overall trend was similar. The difference may result from the difference of initial position or setting conditions of the robot and the driving mechanism.

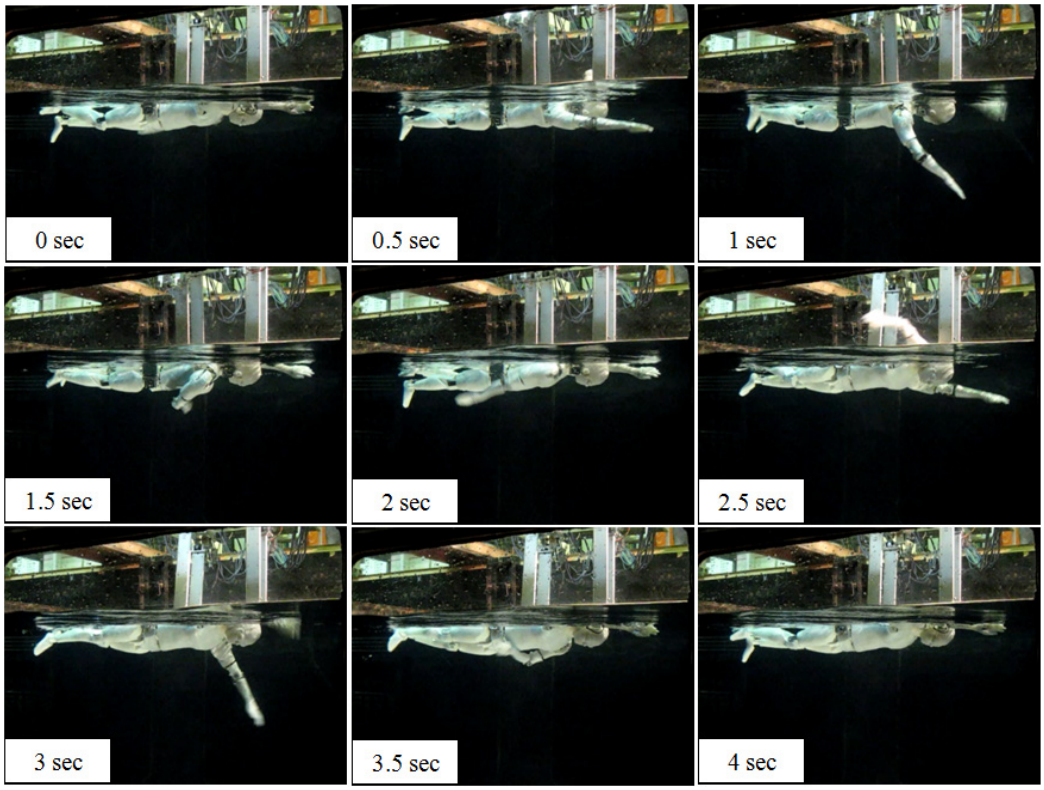

(a) Series of images during crawl stroke

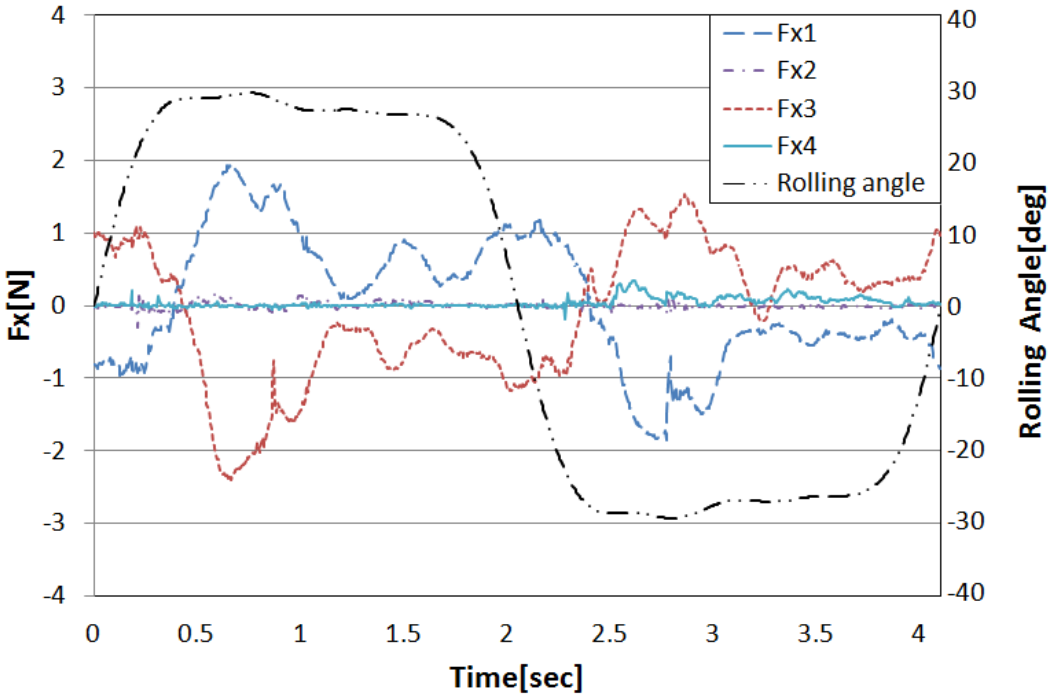

(b) Measured data

Figure 4.11 One result of experiments (stroke cycle 4.10 sec, flow speed 0.32 m/s)

To confirm that the humanoid robot generated thrust force by the stroke motion, we added the results of the front dynamometers, Fx1 and Fx3, as shown in Figure 4.12. To remove the noise of low frequency, we used moving average method. One value in this graph is an averaged value of back and forth 51 data of the result. The results in the minus range indicate that propulsive force was generated by the humanoid robot. Figure 4.12 (a) and (d) shows that the humanoid robot generated thrust force by motion of left arm and right arm but (b) and (c) shows that only right arm generated thrust force. Possible cause of the different propulsive force according to the left and right arm is the change of the initial setting. Experiment results indicate that the driving mechanism was exerted moment of rotation periodically by the swimming stroke. There is a probability that the robot's initial setting was changed by series of experiments and water current. Although the constructed measurement system left room for improvement, we confirmed that the developed swimming humanoid robot generated propulsive force by swimming stroke motion and measured it using the system. It shows the possibilities of new measurement system for research of human swimming.

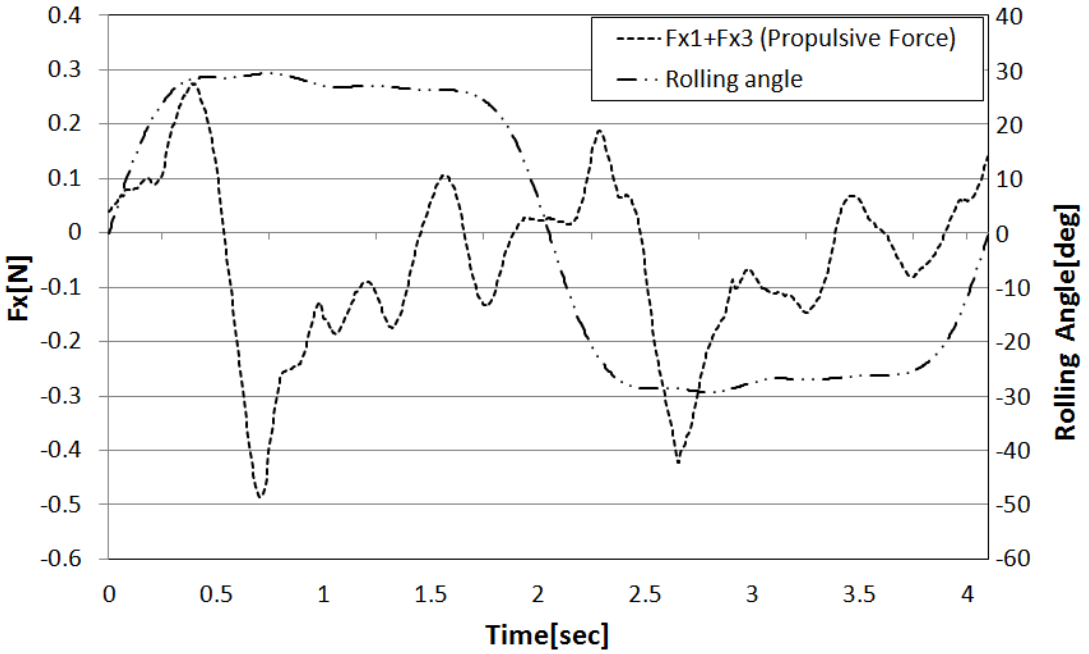

(a) Propulsive force at stroke cycle 4.104 sec, flow speed 0.32m/s

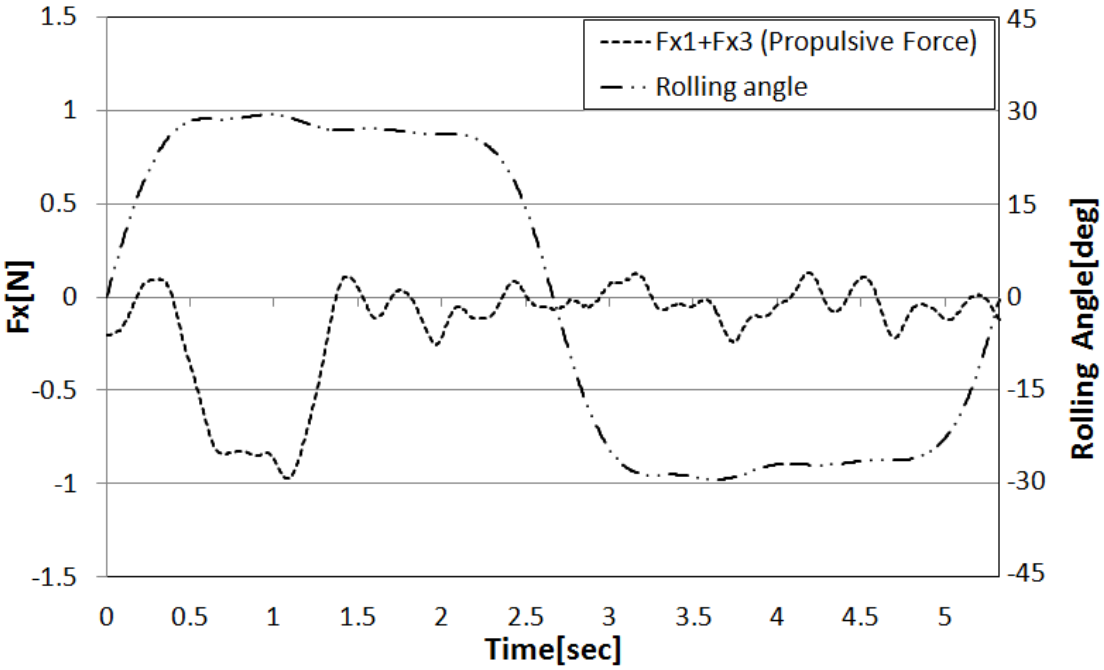

(b) Propulsive force at stroke cycle 5.328 sec, flow speed 0.2m/s

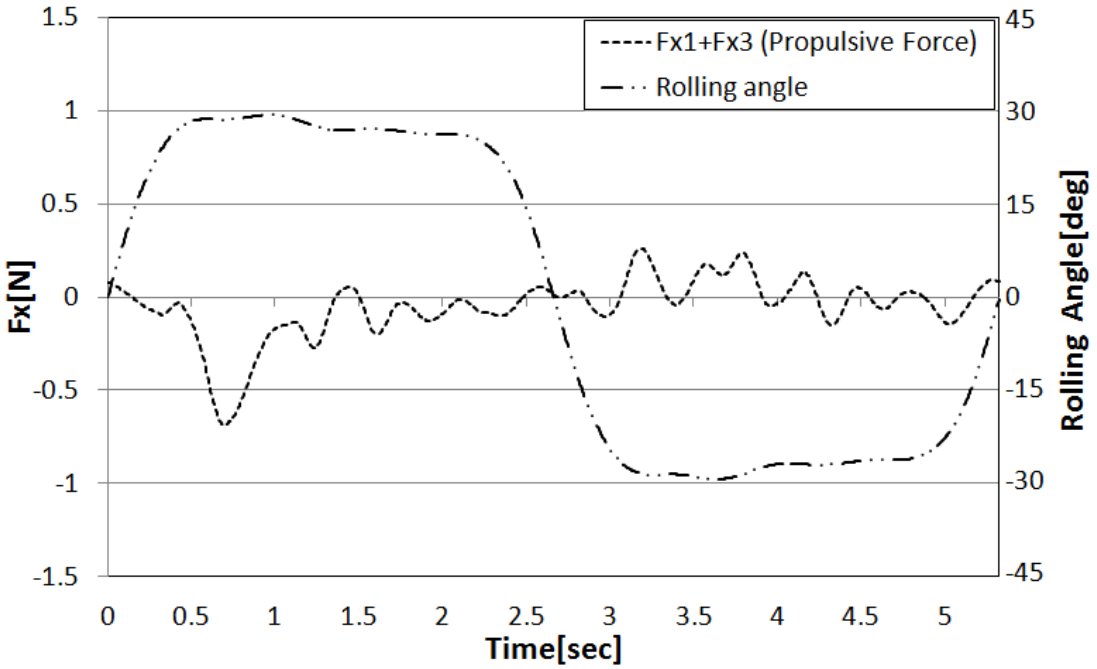

(c) Propulsive force at stroke cycle 5.328 sec, flow speed 0.25m/s

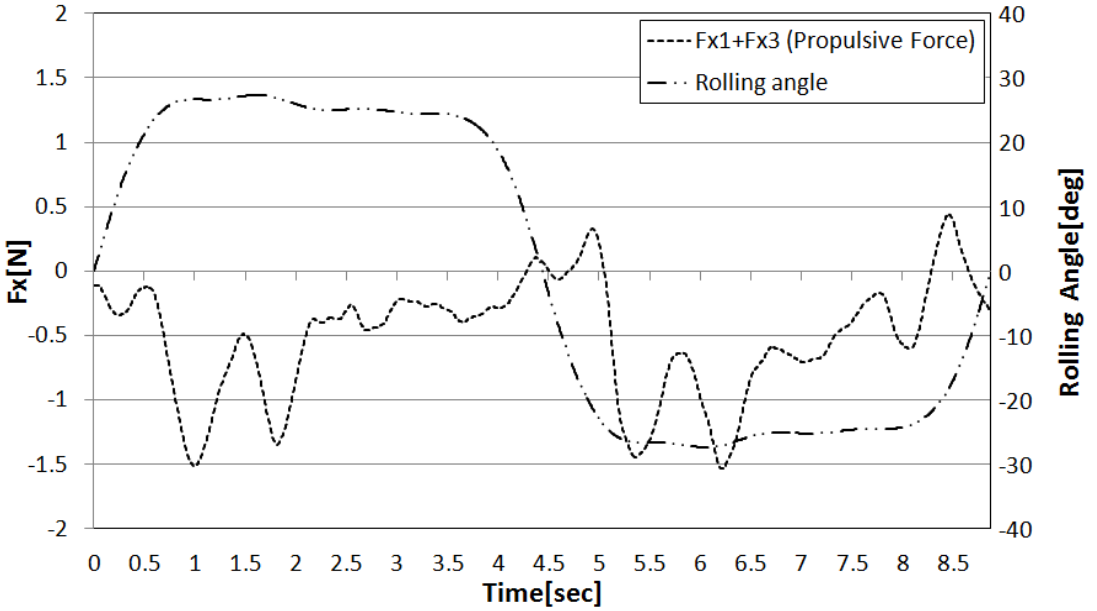

(d) Propulsive force at stroke cycle 8.874 sec, flow speed 0m/s

Figure 4.12 Summation of Fx1 and Fx3 (Propulsive force)

4.4. Conclusion

In this chapter, we confirmed that the developed humanoid robot could realize swimming motion by the methodology which was proposed in Chapter 3. Also, we constructed measurement system of fluid force using the humanoid robot. We confirmed that the developed humanoid robot could generate propulsive force and we could measure it through experiments. Even though we couldn't get consistent results from experiments, the constructed measurement system shows the possibilities as a new type of measurement system for measuring fluid force acting on a swimmer.

Chapter 5

Free Swimming Experiment

5.1. Introduction

In this chapter, free swimming performance of the robot is presented. The upper body of the developed robot is remodeled to fit a free swimming. The developed robot is simulated to raise feasibility of the crawl stroke. In the experiment, overall swimming performance is confirmed by measuring the roll angle and swimming speed. The roll movement and swimming speed are difficult to be estimated in fixed state experiment. Therefore, the robot performance which could not be estimated in the previous chapters is discussed in this chapter. The realization and measuring data from this experiment is very meaningful in research of human swimming, as well, because, so far, it was impossible to conduct with the previously established measurement systems.

5.2. Improvement of the Upper Body for Free Swimming

5.2.1. Overview

From the simulation and experiment, it was proved that the developed swimming humanoid robot can perform swimming stroke motions precisely and the propulsive force of the robot could be measured [88][89]. However, from the previous experiments, several problems were found to conduct a free swimming experiment. Such problems were compensated to achieve the free swimming. The improved points are as follows:

- Buoyancy of the breast part
- Driving torque of the shoulder
- Modularization of the parts
- Waterproofing of the cases

5.2.2. Modification of the breast part

To produce proper buoyancy on the breast part, breast cases were designed and assembled in the body case. The former model had an empty cover in the breast part to install a scapular joint as shown in Figure 5.1 (a). It could be a problem for free swimming because the water could come into the breast part and could not generated buoyancy much. On the other hand, a real human has lungs in the breast and they are the main source of buoyancy. Buoyancy plays an important role in producing roll motion [34][68]. To keep body balance, especially about the rolling motion of the crawl stroke, cases were installed at the location of lungs keeping the front shape of the breast as shown in Figure 5.1 (b). The two orange parts are the two separated cases which were newly installed. The size of the breast cases was determined by specific gravity of the human breast part.

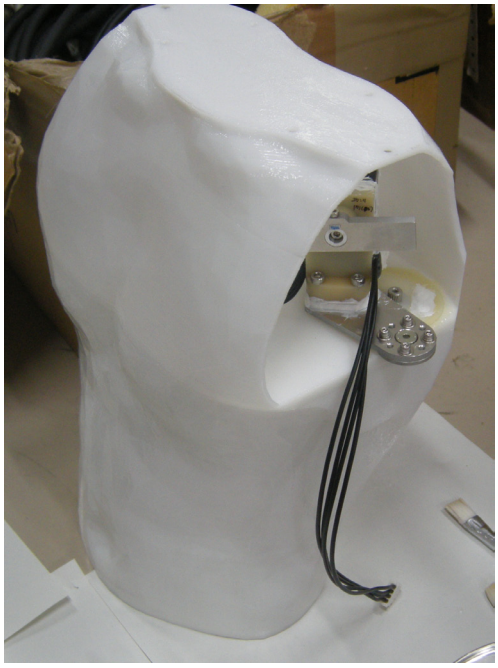

(a) Body case of the former model

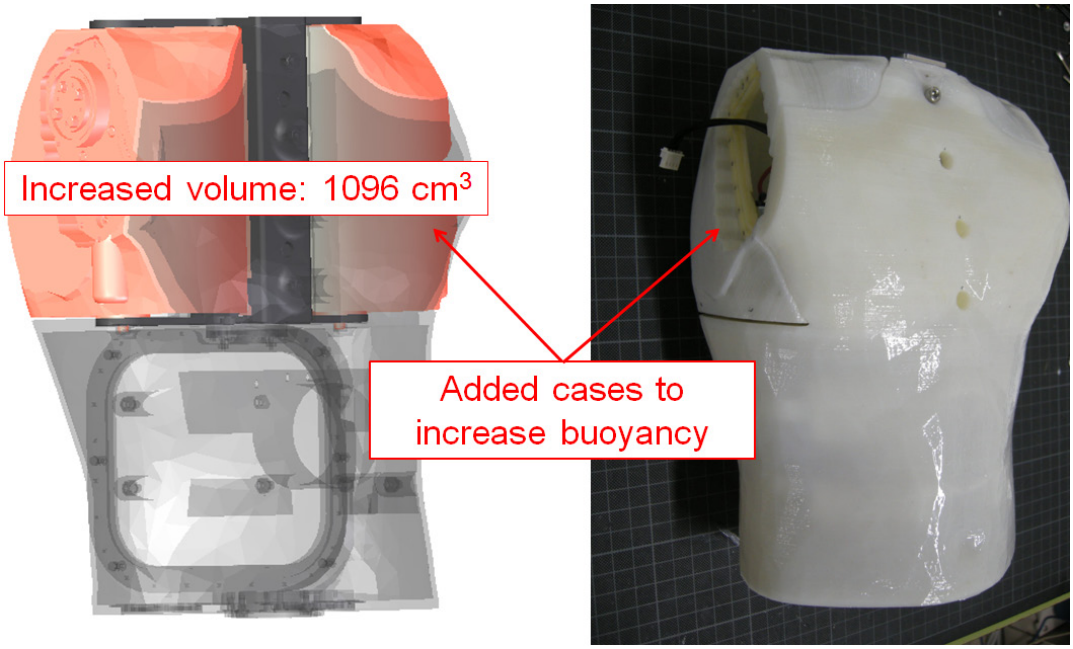

(b) CAD and actual model of the improved body case

Figure 5.1 Breast part of the swimming humanoid robot

5.2.3. Modularization of parts

In addition, larger motors were installed in the shoulder joints to generate more torque and to achieve faster stroke cycles. In chapter 4, the robot moved in quasi-steady state, that is initial velocity for the robot. However, in the free swimming experiment, the robot starts from stationary state, and moreover roll movement is not generated by external equipment. For these reasons, it needs more torque. The specifications of the changed motor are listed in Table 5.1. The upper arm and breast parts were also modularized for ease of maintenance. Figure 5.2 shows the standardized shape of motor assembly and the installation method. Wires were attached on the cover and could be detached with a cover from the motor, so motors and cases easily could be changed and repaired without concern about the reprocessing of waterproofing.

Table 5.1 Specifications of changed motors [83]

Robot Version	Ver. 1	Ver. 2	
Product Name	RX-24F	RX-28	MX-64
Weight	67g	72g	126g
Dimension	35.5mm x 50.8mm x 41.8mm	35.5mm x 50.8mm x 41.8mm	40.2mm x 61.1mm x 41mm
Gear Ratio	193 : 1	193 : 1	200 : 1
Operation Voltage (V)	9 ~ 12	12 ~ 18.5	10 ~ 14.8
Stall Torque	2.6 Nm at 12 V	2.5 Nm at 14.8 V	7.3 Nm at 14.8 V
No Load Speed	126 rpm	67 rpm	78 rpm
Position Sensor	Potentiometer	Potentiometer	Contactless Absolute Encoder
Minimum Control Angle	300°/1024	300°/1024	360°/4096
Baud Rate	7843bps ~ 1Mbps	7843bps ~ 1Mbps	8000bps ~ 4.5Mbps

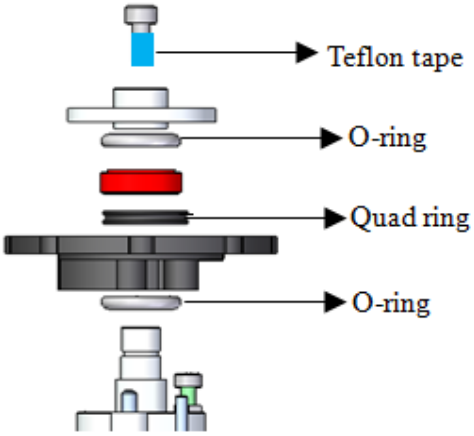

(a) Waterproofed actuator module A

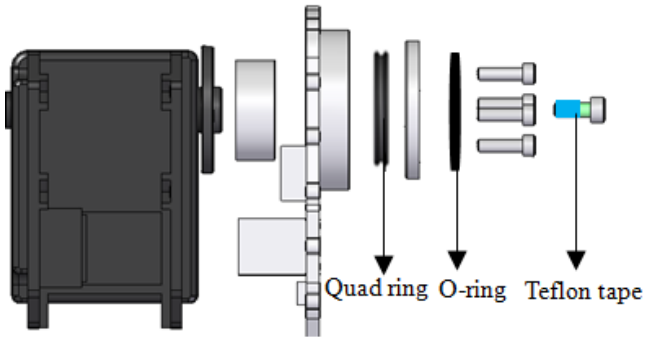

(b) Waterproofed actuator module B

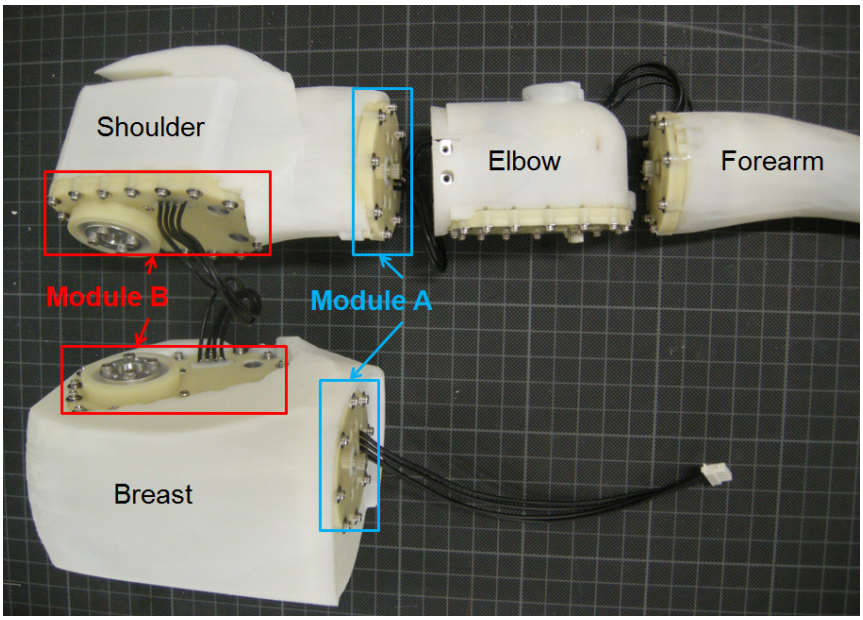

(c) Installed modules in the breast case and shoulder case

Figure 5.2 Modularized parts

5.2.4. Waterproofing

Waterproofing of the cases was reinforced by installing O-rings. In the previous model, O-rings were not used to waterproof the robot cases because space was limited. The shape of human body should be kept to measure fluid forces acting on the robot substituting a human subject. Therefore, the room could not be secured for O-rings and the covers were sealed with silicone instead. However, it caused various problems such as leakage, difficulty of maintenance, and too much assembling time. To make space on the cases for installation of O-rings, the assembly strategy of the motor was changed. Instead of inserting assembled motors into the cases, motor parts were inserted and assembled inside of the case as shown in Figure 5.3. The rotational axis of the motor was sealed by the same method of a waterproofed module 'A' in Figure 5.2 (a).

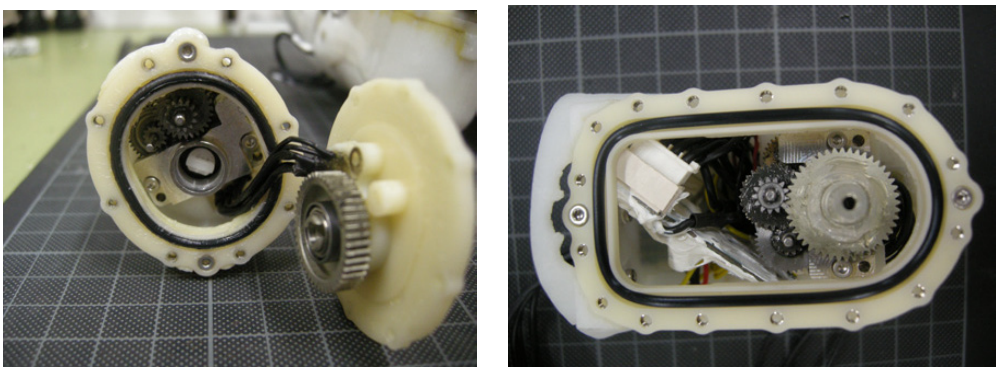

Figure 5.3 Assembled motors in the forearm and elbow part

By changing waterproofing method, testing of waterproofing performance became easier. Figure 5.4 show the schematic view of waterproofing test. We attached an injector on the test cover and inject air. If there was a hole, we can find it through the escaping air bubbles from the case.

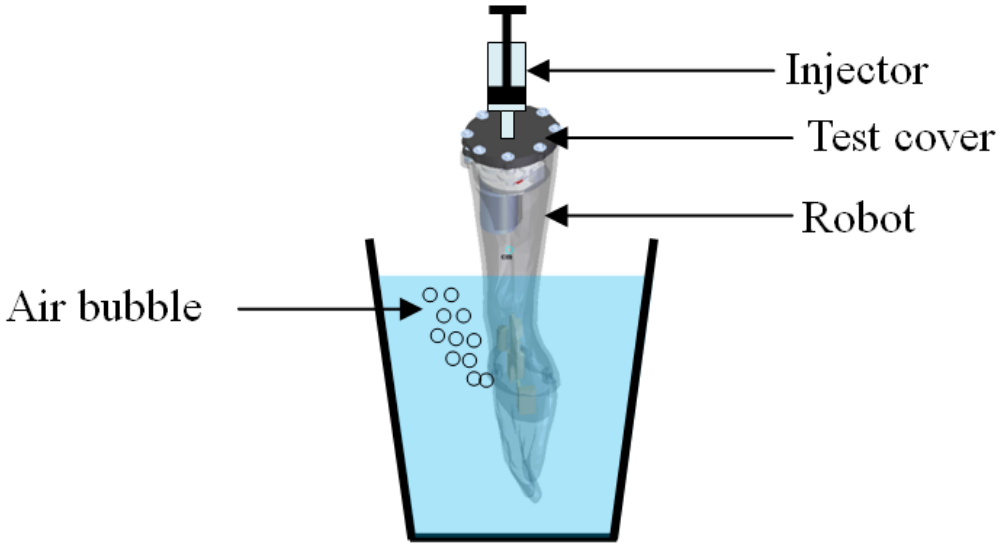

Figure 5.4 Schematic view of waterproofing test

We conducted experiment with this method as shown in Figure 5.5. This method makes it easier to find leakage points and improved the waterproofing performance. In addition, we could apply this method to every case even if electronic parts were installed inside already.

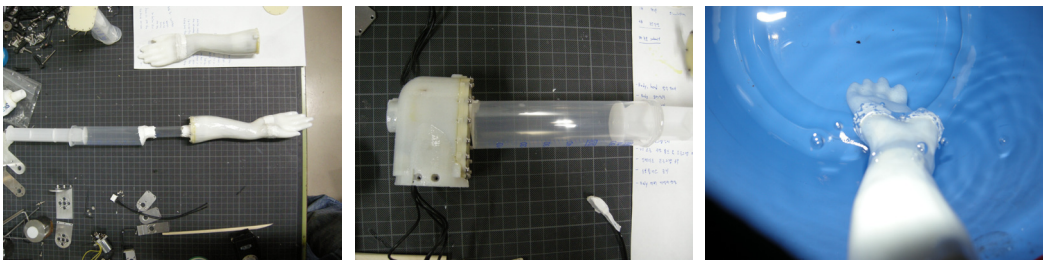

Figure 5.5 Waterproofing test by air injection

5.2.5. Body balance

Table 5.2 shows the weight and volume of each of the robot's parts. It's much more similar to real human compared to the former model. The breast part was adjusted to about 0.7 and the other parts were adjusted to about 1. The weight of each module was measured and the volume was calculated by CAD data and measurement. The total weight of the robot was approximately 7.12 kg and the specific gravity was

about 0.96. The weight was corresponding to 60 kg of a real human but it was slightly light considering the height. The reason was that the hip of the robot was smaller and lighter than a real human's and there was room for connection with experimental equipment in both sides of the hip.

Table 5.2 Weight and volume of a humanoid robot

Parts	Weight(g)	Added weight(g)	Volume (cm^3)	Specific gravity
Head & Neck	368	335	679	1.02
Forearm*2	300		306	0.98
Elbow*2	256		215	1.19
Upper arm*2	660		579	1.14
Breast	1039		1514	0.70
Waist	838	583	1460	0.97
Hip	364		353	1.03
Thigh*2	596	800	1400	0.97
Shank*2	715	60	700	1.04
Foot*2	88	120	200	1.01
Total	**5224**	**1898**	**7406**	**0.96**

5.2.6. Electrical parts and specifications

For the connection, electric wiring modified, as well. The lower body of ver. 1 is operated in 9~12 voltage but the upper body of ver. 2 is operated in 12~18.5 voltage. We can use 12 V in common but the upper body can't generate enough torque in the low voltage. For this reason, we used two batteries of different voltages. Also, arranging two batteries in both sides has the advantage to keep balance of the body between right and left side. Figure 5.6 shows schematic view and picture of the electrical wiring.

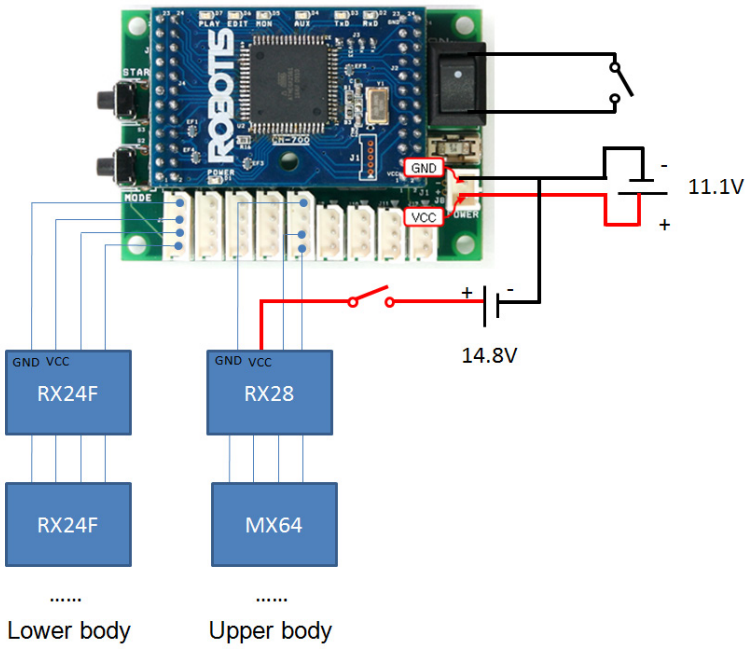

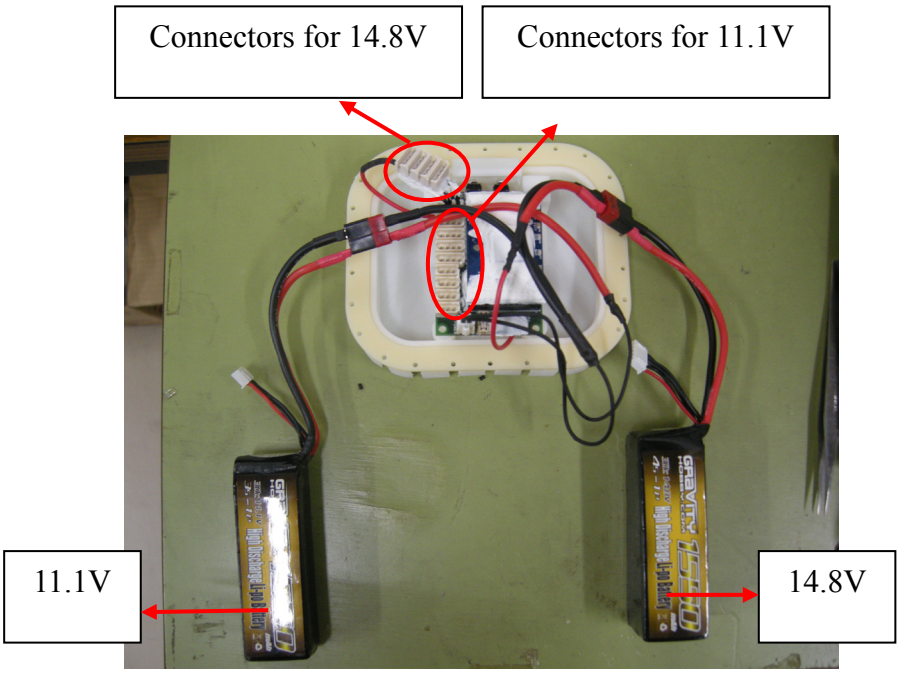

Figure 5.6 Electrical wiring for two different types of batteries

The robot is driven by 20 servo actuators called 'DYNAMIXEL' (RX and MX series, Robotis Co.). They are linked by a daisy chain, so wiring is simple and many steps are saved in waterproofing the wires compared to normal RC servo motors. The installed motors are controlled by a robot controller (CM-700, Robotis Co.). In order to measure the rolling angular velocity of the robot, a gyro sensor (GS-12, Robotis co.) is installed in the body. Figure 5.7 shows a photo of the sensor and hardware specification is followed in Table 5.3.

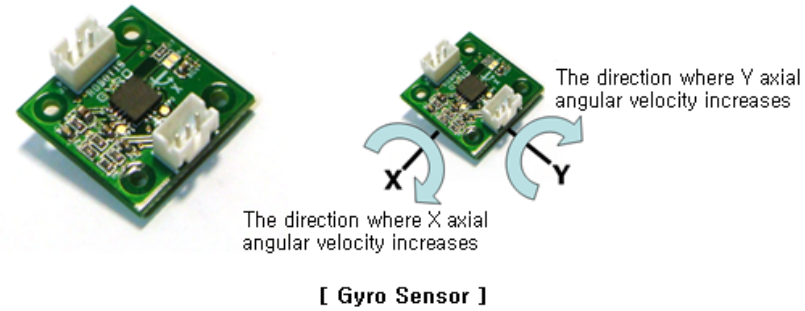

Figure 5.7 Image of gyro sensor [83]

Table 5.3 Hardware specifications of gyro sensor [83]

Product Name	GS-12
Weight	2.8g
Dimension	23mm x 23mm x 10mm
Operating Temperature	-40°c ~85°c
Angular Velocity Measurement Range	-300°/s ~ 300°/s
Recommended Voltage Supply	4.5V ~ 5.5V

To receive the sensor data and control the robot remotely, the ZigBee module (ZIG-100/100A, Robotis co.) is installed on the back of the robot and PC respectively. The Zigbee communication makes serial communication (UART) possible. The photograph and hardware specification is as shown in Figure 5.8 and Table 5.4. The ZigBee module which is installed in the back of the robot was fixed at the top of a pole not to sink under water during swimming. Figure 5.9 shows the module installed on the robot. Figure 5.10 shows the remodeled upper body for free swimming. Table 5.5 shows specifications of the improved humanoid robot.

Figure 5.8 Image of ZigBee module [83]

Table 5.4 Hardware specifications of ZigBee model [83]

Product Name	ZIG-100 / ZIG-100A
Weight	ZIG-100: 3.1g / ZIG-110A: 5.7g
Dimension	ZIG-100: 19mm x 26.7mm x 12mm (Without connector, height is 6mm) ZIG-110A: 18.1mm x 29.9mm x 9.1mm
Frequency Bandwidth	2.4 GHz ISM Band
Driving Voltage	2.7V ~ 3.6V (Recommended: 3.3V)
Consumed Current	30mA (at 3.3V)
Default Baud rate	ZIG-100: 57600bps ZIG-110A: 57600bps

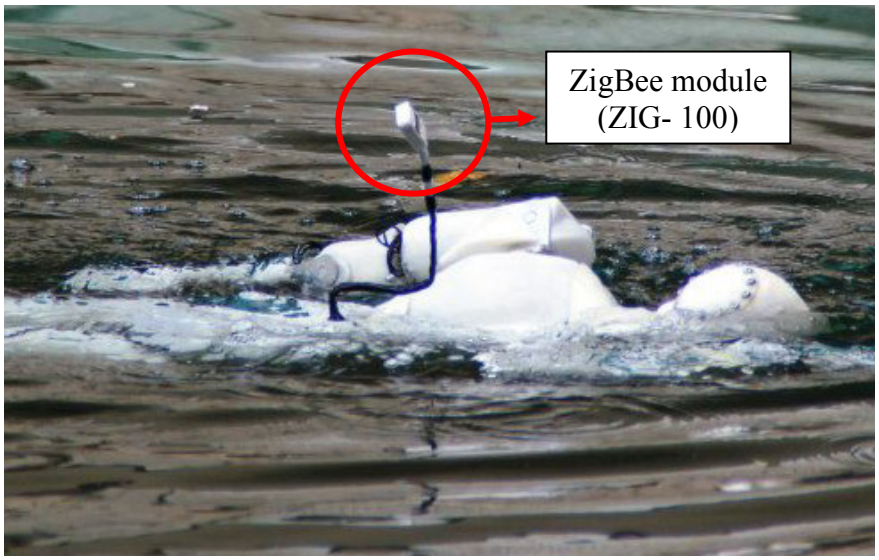

Figure 5.9 Installed ZigBee module on the back of the robot

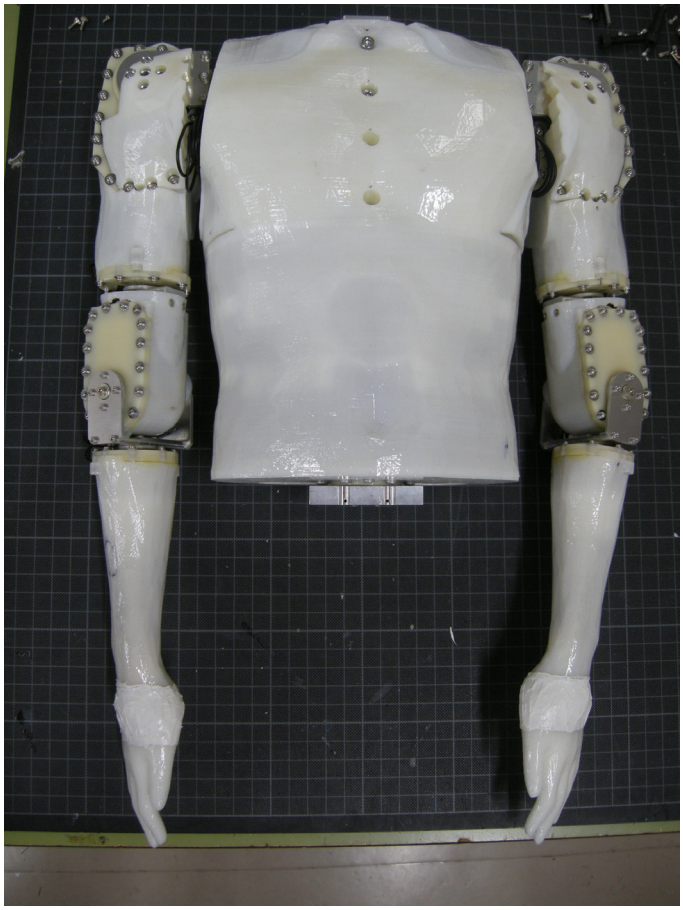

Figure 5.10 Remodeled upper body for free swimming

Table 5.5 Specifications of the improved model

Items	Specifications
Size	(H) 890mm (W) 270mm (D) 100mm
Weight	7.4 kg
Actuators (Dynamixel: ROBOTIS Corp.)	RX-24F: 2.6 Nm at 12 V RX-28 : 2.5 Nm at 14.8 V MX-64: 7.3Nm at 14.8 V
DOF	Total: 20 DOFs Arm: 2 Arms x 6 DOF Waist: 2 DOF Leg: 2 Legs x 3 DOF
Controller	CM-700 (ROBOTIS Corp.)
Microprocessor	ATmega 2561 (Atmel Corp.)
Battery	Li-Po 11.1V 1550 mhA , 14.8 V 1550 mhA
Communication	ZigBee Module

5.3. Simulation Study for Free Swimming

5.3.1. Overview of simulation model

To reduce the process of trial and error during the experiment, the crawl stroke of SWUMANOID was simulated first. As the implementing method of the fluid force model, the swimming human simulation model 'SWUM', which was developed by Nakashima et al. [39], is employed. The present simulation model computes the absolute movement of the swimmer's whole body as one rigid body, by solving the equations of motion for the rigid body with the given relative body motion as joint angles. The swimming speed, floating degree of the body, motions of roll, pitch, yaw, and so on are obtained as the calculated results. As external forces act on the human body, unsteady fluid forces, including buoyancy and gravitational force, are taken into account. The unsteady fluid force is assumed to be computable from the local motion of each body part, that is, position, velocity, acceleration, direction, angular velocity, and angular acceleration, without solving the flow field. Their details are described in Appendix C. The recent progress related to SWUM was reviewed in the reference [40]. Some of the analysis data and animation movies are open to the public at the SWUM website [41].

5.3.2. Modeling of the robot

Figure 5.11 shows the constructed simulation model and CAD model of SWUMANOID. In the simulation each body segment of the robot was represented as a truncated elliptical cone and its dimension was determined by feature points of the body and the position of the joints. Details of body parts were readjusted by the volume of each segment because the major role of the body parts during swimming is to make buoyant force. The robot had covers on the hip and water can flow inside the covers so, the shape of covers was ignored and only volume was considered and calculated. Density of each part of the robot was measured and entered into the simulation. Therefore the weight of the simulation model was almost the same as the actual model.

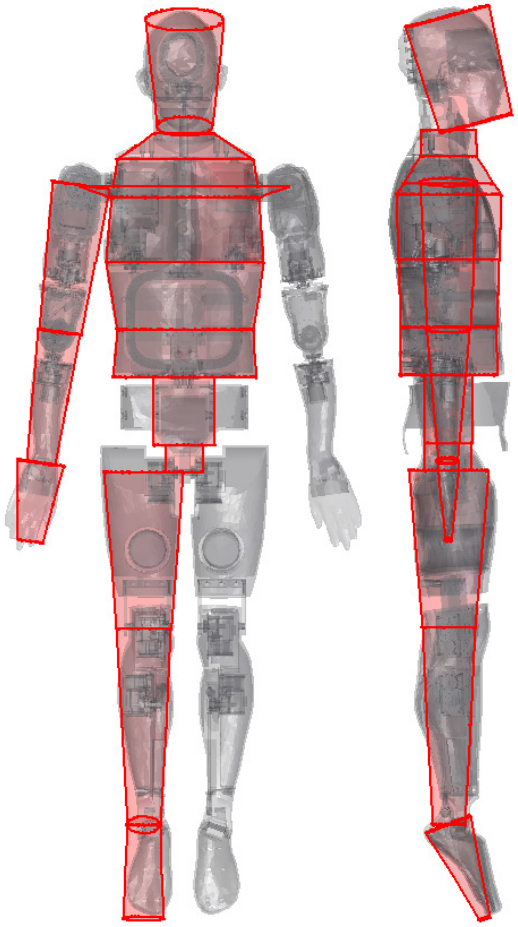

Figure 5.11 Constructed simulation model and CAD model of SWUMANOID

5.3.3. Joint motion

The joint motion in the present study was determined based on standard six-beat crawl stroke of SWUM. With respect to the six-beat crawl, Nakashima et al. have already analyzed contributions of each fluid force component and of each body part to the thrust, effect of the flutter kick, estimation of the active drag, roll motion, and the propulsive efficiency [34]. However, some joint motions were modified to adapt to SWUMANOID. The elevation motion of the shoulder was ignored because it could not be realized with the present shoulder joints. The push motion of the crawl stroke was modified to avoid the collision of the hands to the trunk. The motions of the shoulder and ankle were slightly modified due to the limited range of the motion of the robot. The modified standard crawl stroke motion was validated experimentally in chapter 4.

5.3.4. Modified models

Through prior simulation analysis, it was found that the present model could not realize the crawl stroke properly. The primary cause was the roll movement and recovery stroke didn't occur well. These two actions have a complementary relationship. The roll movement makes the recovery of the arm easier and the recovering arm creates the roll moment by translating the center of gravity and buoyancy [34][68]. To improve this condition, two simulation models were constructed in which the roll movement and the recovery stroke were improved respectively. The modification of the model was conducted within the practical range. Figure 5.12 shows the two modified models.

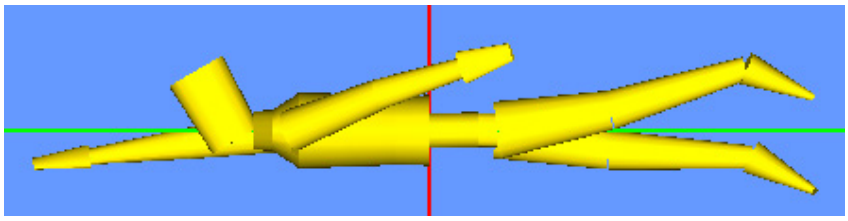

(a) Model I – Raised head model

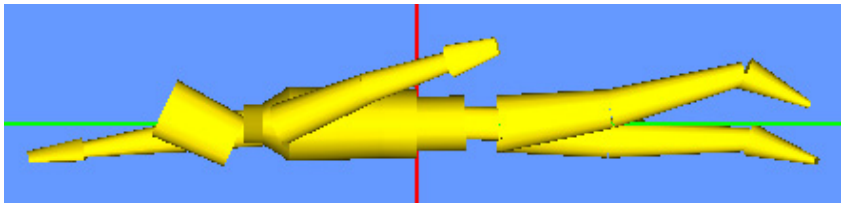

(b) Model II – Weight and buoyancy rearranged model

Figure 5.12 Improved simulation models of SWUMANOID

Model I was constructed to strengthen the roll movement by adjusting the head pitch angle. The model lifted its head up as shown in Figure 5.12 (a) to produce the larger roll angle. During the roll movement, the lifted head balanced with the recovering hand and the condition became easier to roll. Also, the rolling time was delayed by the increased rotational inertia. Therefore, it was expected that the stroke cycle would be extended. Although the standard crawl stroke of SWUM was suitable for a stroke cycle of 1.96 sec, it could be extended and a load of the actuators of the robot could be reduced.

Model II was constructed to reinforce the supporting force of the recovery arms.

While the volume of the upper limbs of SWUMANOID was larger than that of the standard simulation model, the volume of the trunk was smaller. So, the buoyancy of the trunk was regarded as not enough to support the heavy upper limb during the recovery stroke. However, in the case of Model I, the recovering hands could go out of the water by a large roll motion even though the body sank a little. Model II was made by removing some weight from the head to lighten the load of the body buoyancy and by increasing the volume of the hip as shown in Figure 5.12 (b). As a result, the specific gravity of the whole body was changed from 0.965 to 0.95.

5.3.5. Simulation results

Table 5.6 shows the simulation results. The swimming speed of each simulation model according to different stroke cycles was presented. Every trial was simulated during 20 stroke cycles and the last three strokes were averaged as shown in Table 5.6. The original model could not swim at every trial. Model I could swim at stroke a cycle of 2.0, 2.2 and 2.4 sec but the recovery was not realized well at the stroke cycle of 2.6 sec. The overall speed was slow compared to Model II because the lifted head produced drag. Model II could swim at a stroke cycle of 2.0 and 2.2 sec. However, at a stroke cycle of 2.4 and 2.6 sec, the roll movement and recovery was not realized properly and could not go forward.

Table 5.6 Swimming speeds of simulation models (m/s)

Stroke cycle [s]	Original model	Model I	Model II
2.0	X	0.37	0.48
2.2	X	0.30	0.46
2.4	X	0.24	X
2.6	X	X	X

'X' means the swimming speed is lower than 0.15 m/s

5.4. Experiment

5.4.1. Experimental setup

Figure 5.13 shows the schematic diagram of the experimental setup. The swimming speed and rolling angular velocity of the humanoid robot were measured at an outdoor pool which was 25 m length, 12 m width and 1.3 m depth. Every experiment was filmed by a camera, which followed the swimming robot from the side. The position of the robot was estimated by measuring tape located on both sides of the robot's heading direction. SWUMANOID was controlled wirelessly from a laptop computer.

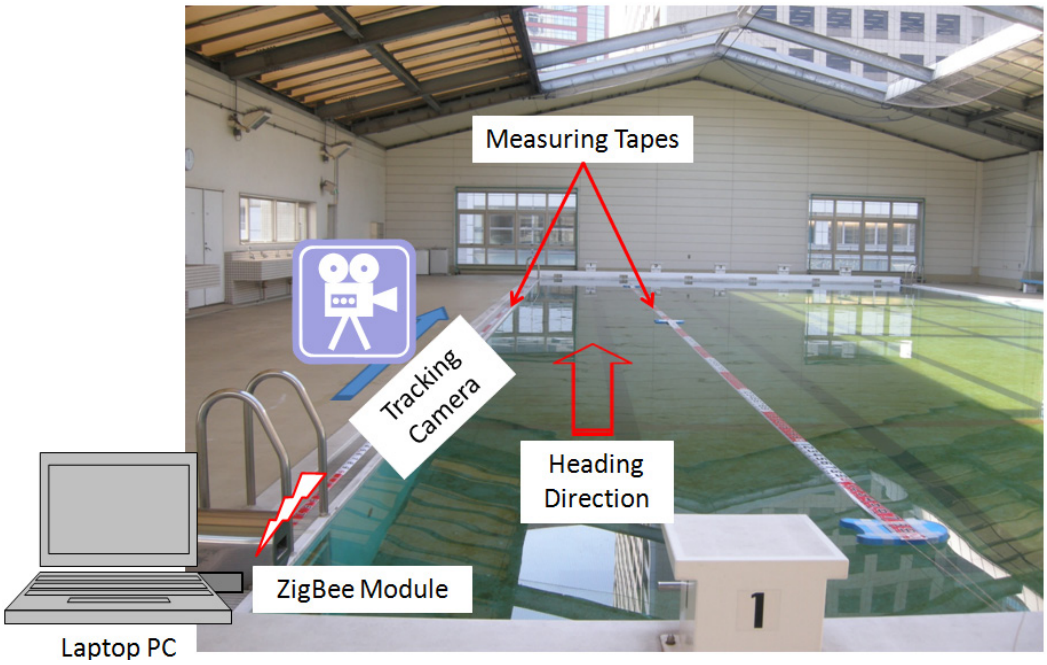

Figure 5.13 Experimental setup for the free swimming experiment

5.4.2. Experimental method

In the experiment, SWUMANOID performed the crawl stroke under two different conditions of the body. The defined joint motions in the simulation were converted to the joint angles of SWUMANOID through kinematic calculation as explain in chapter 3 [90]. Some weights and volumes were rearranged to realize the two

simulation models. To fit SWUMANOID to simulation Model I, weight was attached at the back of the head as shown in Figure 5.14 (a). SWUMANOID did not have a pitch joint on the neck, so the center of gravity was adjusted by distribution of weight inside and outside of the head. The total weight of the head was unchanged and the specific gravity of the head was maintained at about 1. To realize simulation Model II, some weight was removed from the head and Styrofoam was attached to add volume to the hip as shown in Figure 5.14 (b). The specific gravity of the head decreased to about 0.72. The volume of the hip increased about 300 cm^3 after the Styrofoam was attached. Additionally, weight was added to maintain the specific gravity of the hip. The stroke cycle was quickened gradually from 4 sec to 2.27 sec. The swimming speed was estimated from analysis of video recording and the rolling angular velocity was measured by a gyro sensor which was installed inside of the body.

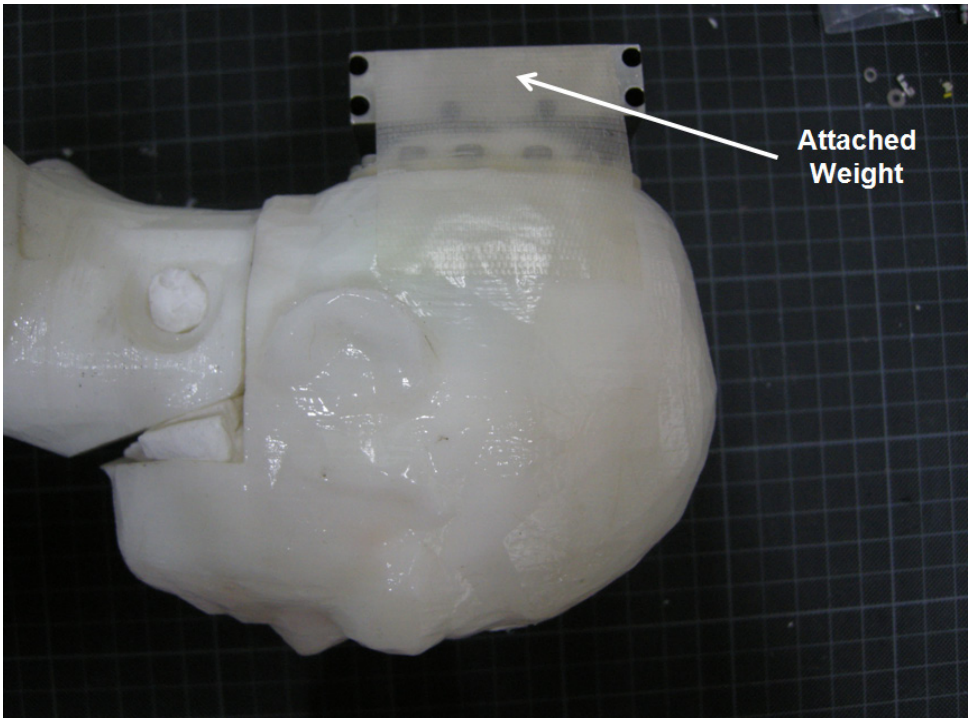

(a) Fitting to model I

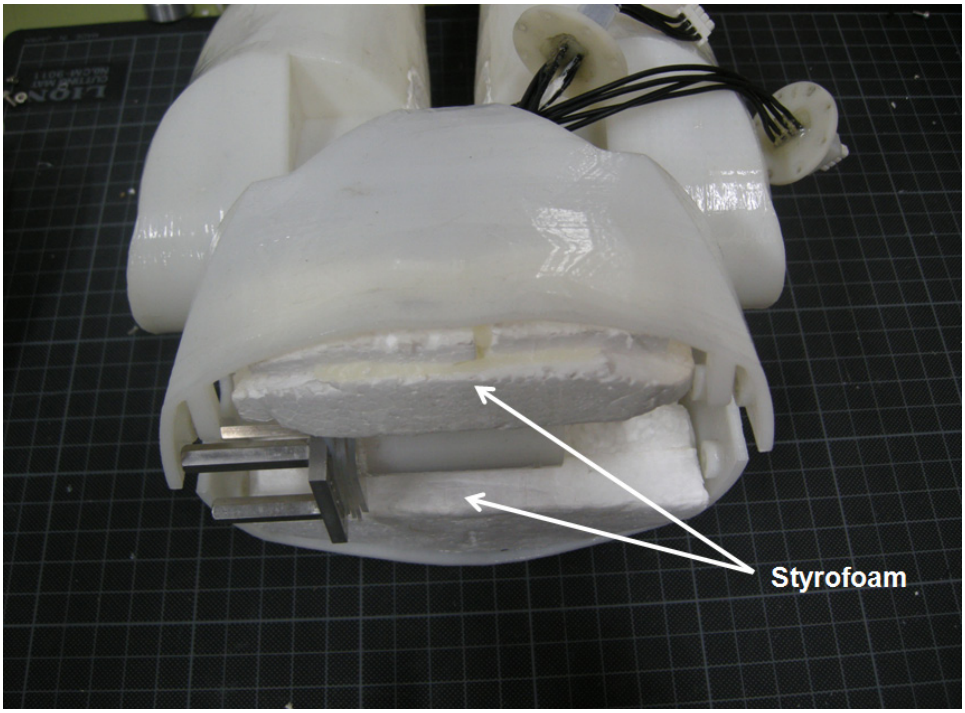

(b) Fitting to model II

Figure 5.14 Adjusted SWUMANOID to realize condition of simulation models

5.4.3. Experimental results

Model I performed the crawl stroke successfully. Figure 5.15 shows a series of images of the crawl stroke at the stroke cycle 2.39 sec. At the stroke cycle of 4, 3 and 2.7 sec, Model I could not swim forward and floundered in the water because the rolling motion was not realized properly. As a result, the recovery stroke was performed in the water not in the air. At the stroke cycle 2.39 sec the recovery stroke was performed properly and the robot went straight. From this experiment, we confirmed that the swimming stroke motion should be changed to swim at slow stroke cycle. However, it is difficult to clarify how people change their swimming form depending on their stroke cycle. Using the developed robot, bring up such a problem and clearing it up is significant for research of human swimming.

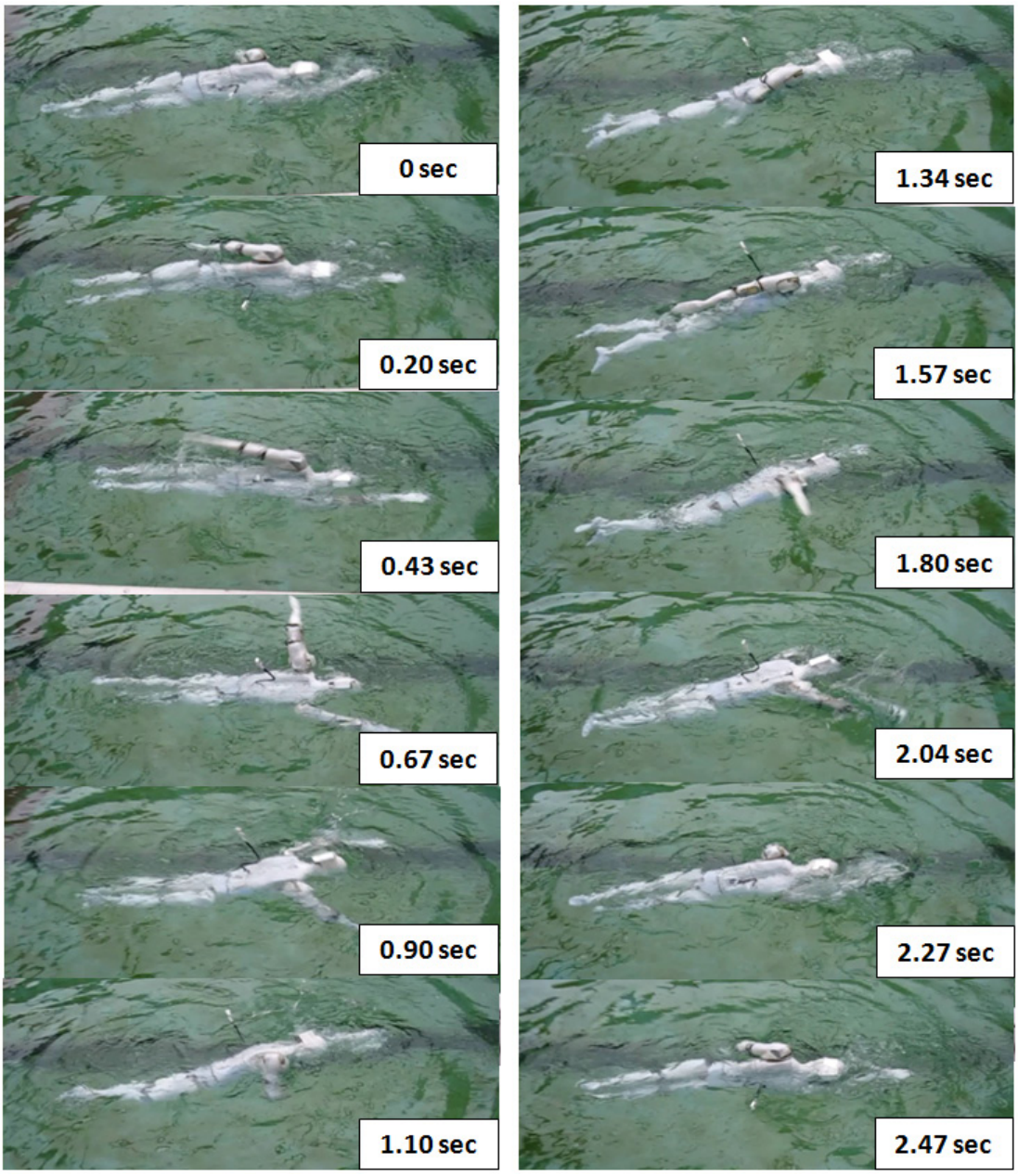

Figure 5.15 Snapshots of the crawl stroke performance of actual Model I at s stroke cycle of 2.39 sec

Figure 5.16 shows the roll angle of actual Model I and simulation Model I. In the experiment, the angular velocity was measured by a gyro sensor. The roll angle was calculated by integration of the angular velocity. In the calculation, the drift component of the angular velocity was deducted as a constant value. The amplitude of the roll angle of actual Model I was about ± 60 degrees. The good agreement between the simulation and experiment was seen with respect to the amplitude as well as the curve shape. It shows that buoyancy, which is the primary source of generating body roll in crawl swimming, and body balance are fit those of simulation model.

The average overall swimming speed of the robot model was measured about 0.23 m/s. It is correspond to under half the speed of actual swimmer model when it is calculated the model size and stroke cycle proportionally. About the swimming speed is discussed in the result of Model II.

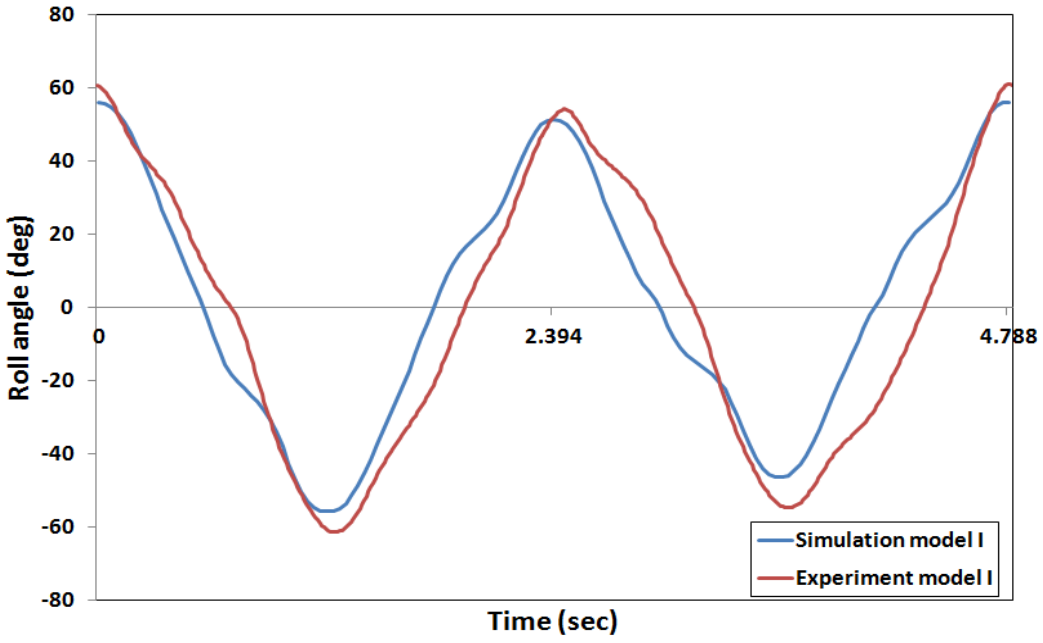

Figure 5.16 Angle of roll movement for two cycles at a stroke cycle of 2.39 sec

Model II performed the crawl stroke successfully as well. Figure 5.17 shows a series of images of the experimental result and simulation result of the crawl stroke at the stroke cycle of 2.27 sec. It was confirmed that the simultaneous motions corresponded well.

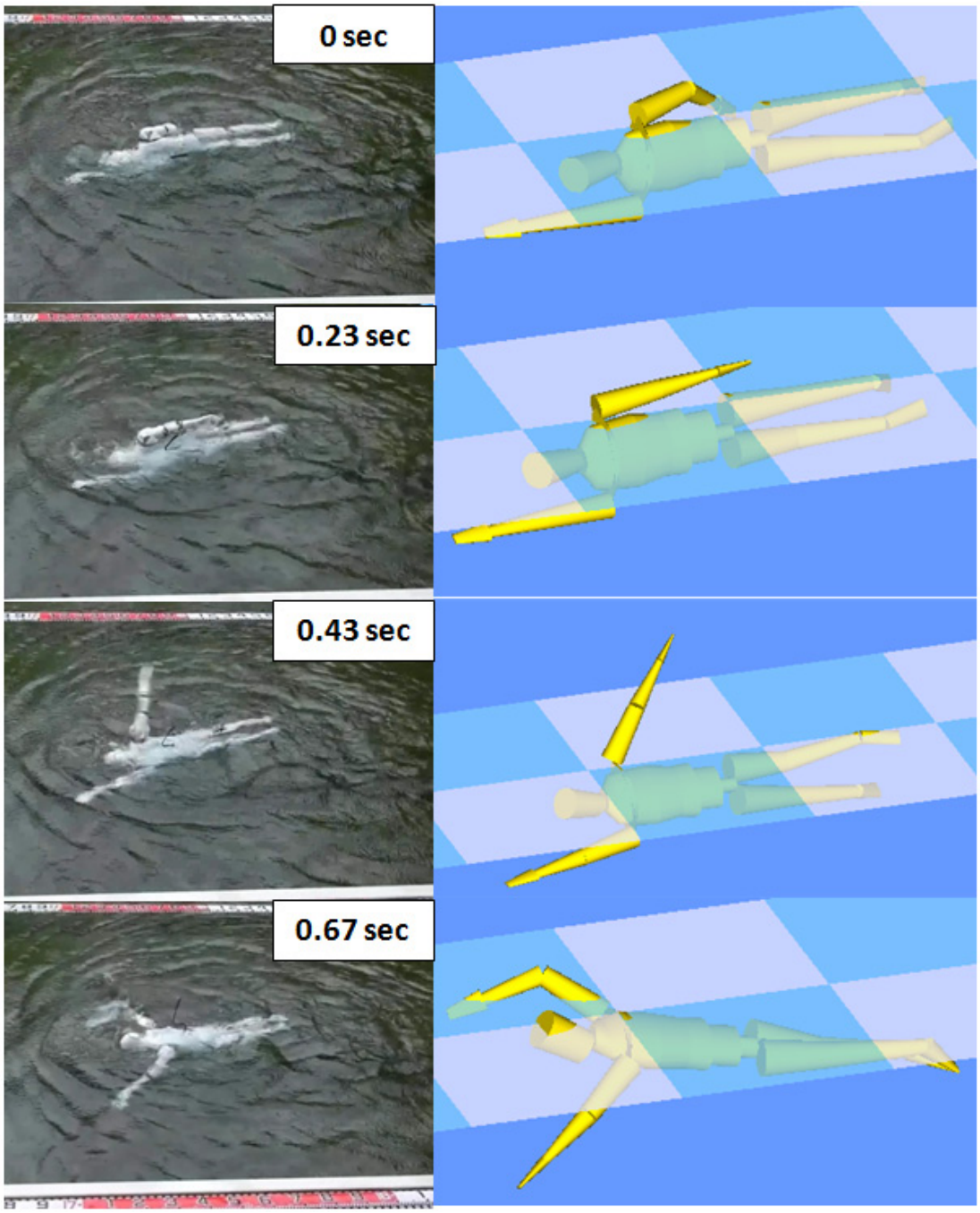
0 sec
0.23 sec
0.43 sec
0.67 sec

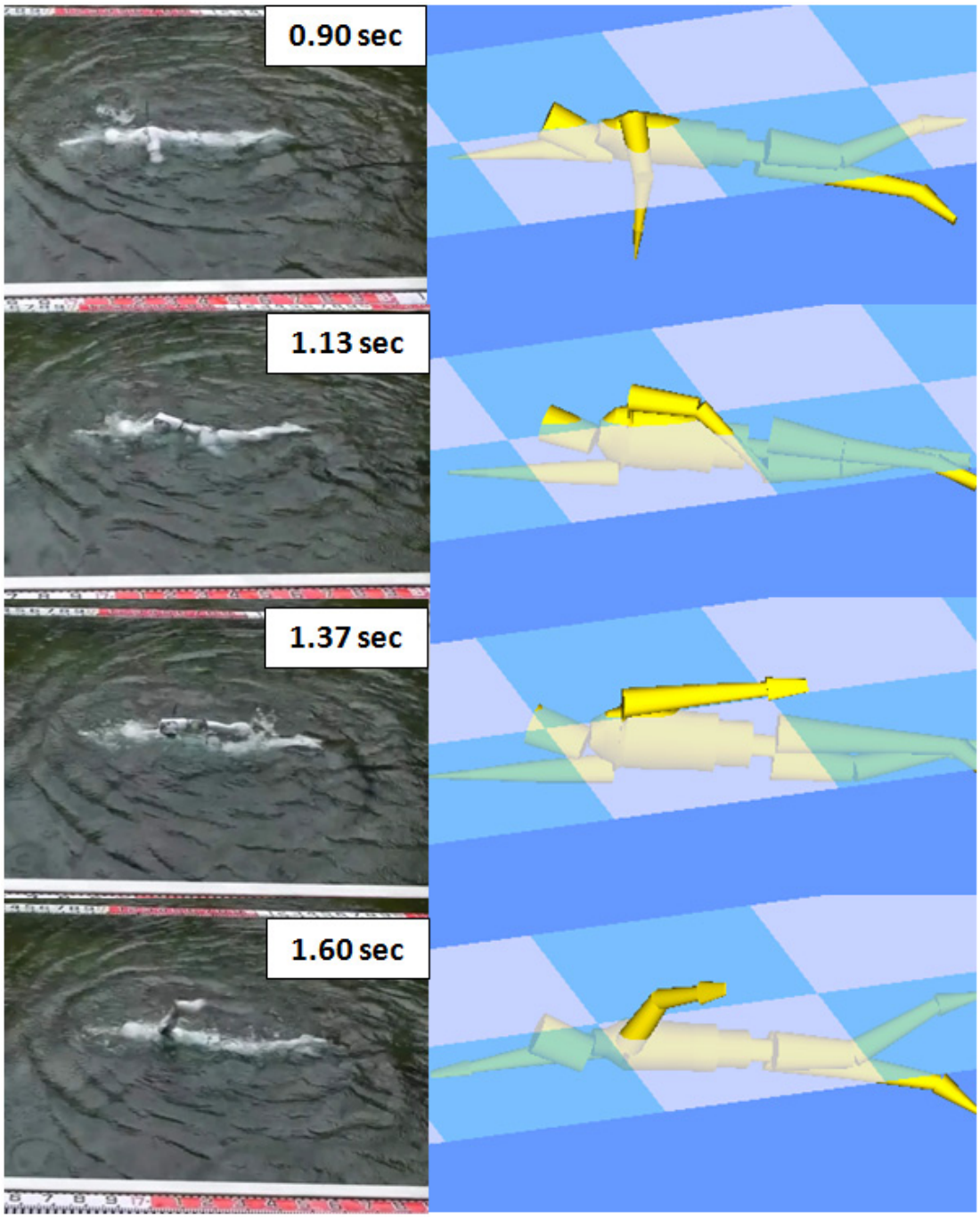
0.90 sec
1.13 sec
1.37 sec
1.60 sec

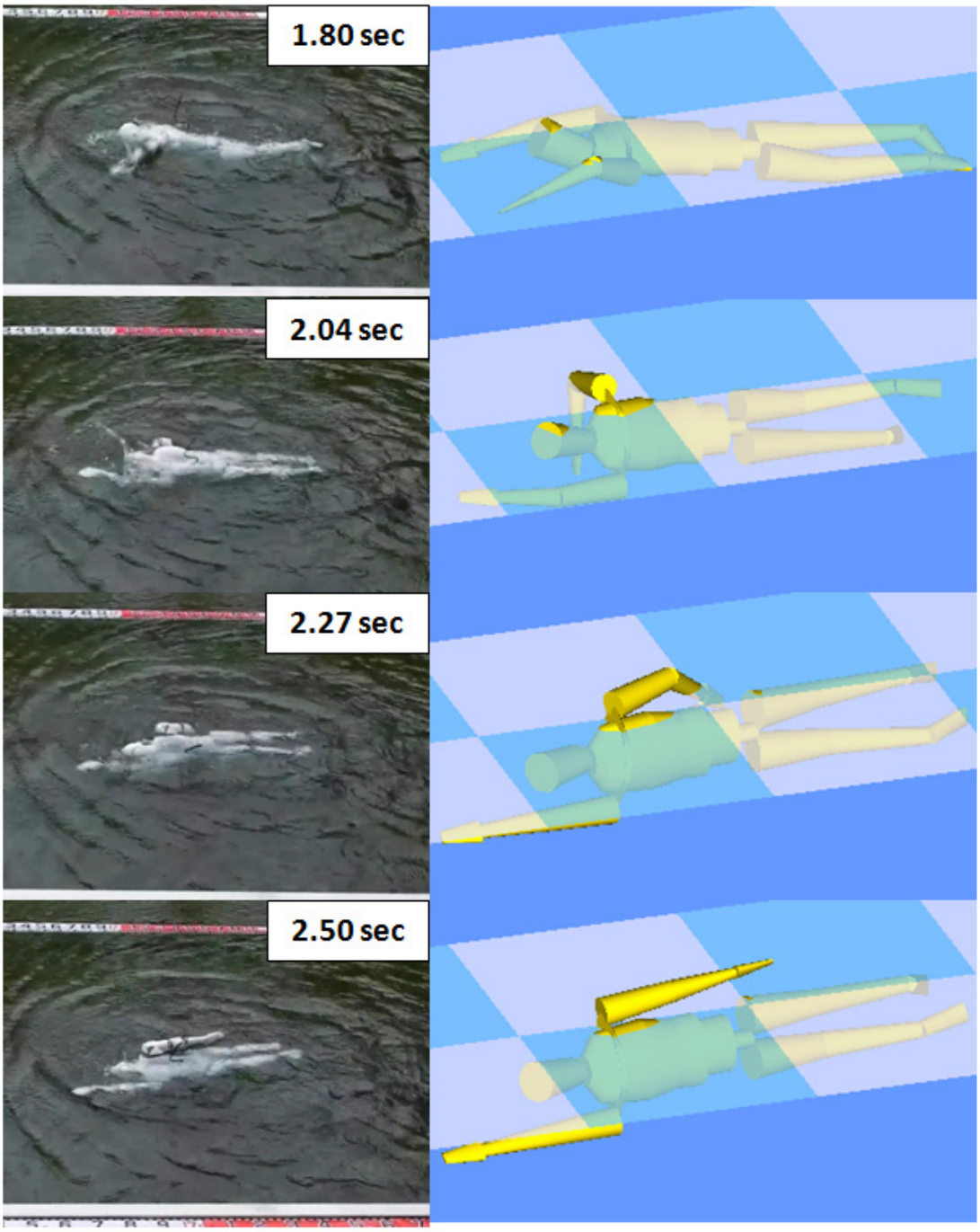

Figure 5.17 Snapshots of the crawl stroke performance of actual Model II and simulation Model II at a stroke cycle of 2.27 sec

The swimming speed was calculated at each stroke cycle. The moving distance by each stroke was calculated using two parallel pieces of measuring tape. The position of the head was checked at the beginning and ending of the strokes as shown in Figure 5.18. Not only the forward movement but also lateral movement was considered, though the robot went almost straight. Figure 5.19 shows the results of the calculation. Mostly, the swimming speeds were between 0.2 m/s and 0.24 m/s. However, sometimes the recovery was not performed properly as shown in Figure 5.20 and the swimming speed was slowed down to under 0.2 m/s.

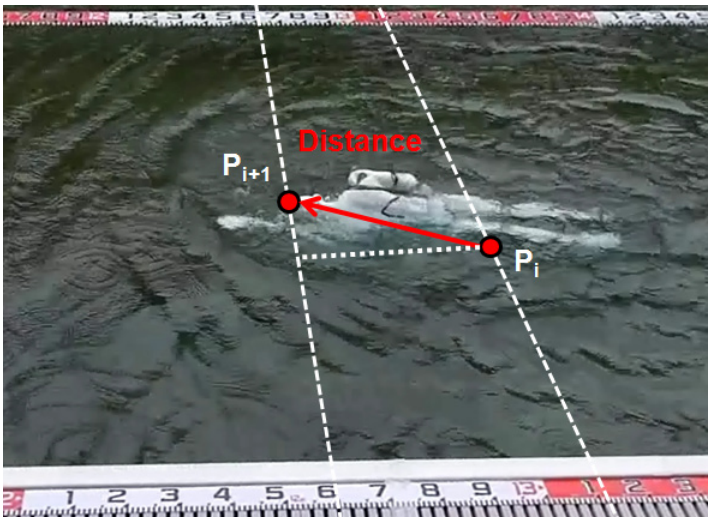

Figure 5.18 Calculation of moving distance

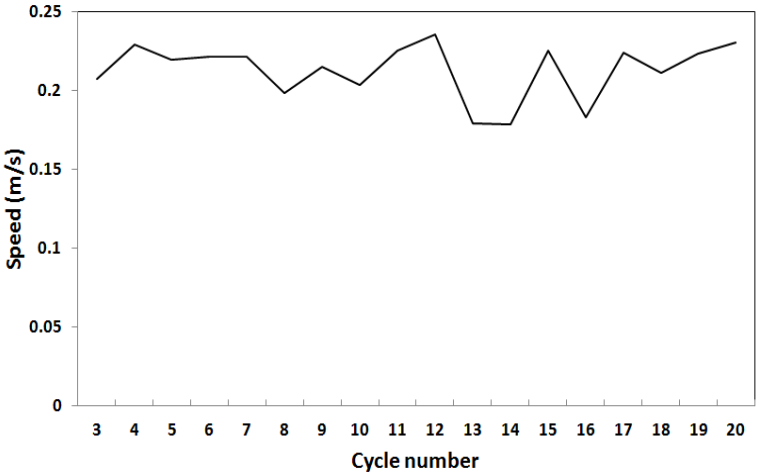

Figure 5.19 Swimming speed of actual Model II at a stroke cycle of 2.27 sec

Figure 5.20 Abnormal recovery stroke during the experiment

Even though the abnormal recovery strokes were considered, the swimming speed was slower compared to the simulation result. In the simulation, the swimming speed of Model II was about 0.43 m/s at the stroke cycle of 2.27 sec. It was supposed that this was caused by differences between the actual model and simulation model, such as the difference of surface area of limbs including hands and attack angle of hands. Unidentified fluid coefficients with the present robot model in SWUM may be one of the reasons. Therefore, more research is needed to reduce the gap between the actual model and the simulation model.

5.5. Conclusion

In this chapter, the upper body of SWUMANOID was remodeled to fit the free swimming experiment in the crawl stroke. Using a human swimming simulation model SWUM, a feasibility study was conducted and two different models were proposed to perform the free swimming in the crawl stroke. Model I was constructed to produce larger roll movement and Model II was constructed to improve buoyancy for the stable recovery stroke. The two simulation models were realized in actual models with SWUMANOID. The crawl stroke was performed successfully by the two models respectively. The roll movement of Model I was calculated to be about ± 60 degrees. The crawl stroke motions of Model II matched very well with the simulation model. Meanwhile, there was some difference in the swimming speed.

Chapter 6

Conclusion

6.1. Conclusion of Each Chapter

In “Chapter 1 Introduction,” background and objectivity of this research were discussed and followed by thesis organization.

In “Chapter 2 Design of the Robot,” a swimming humanoid robot, named SWUMANOID, was developed. In order to use it as an experimental platform for research of human swimming, the appearance and body properties were fitted to those of human. To preserve the shape of human body, compact waterproofing motor which can be installed inside of body was developed.

In “Chapter 3 Methodology to Realize Swimming Motions,” in order to realize swimming motion, inverse kinematics was analyzed and joint angles of the robot were determined by the kinematics. The continuous shoulder movement of the swimming stroke motion was realized using the scapular joint. The joint angle of the scapular joint was determined by proposed methodology. The efficiency of the scapular joint, which was moved by the methodology, was validated by simulation of the crawl, back and butterfly strokes. In the simulation, it was confirmed that the robot can rotate its shoulder continuously in all simulated swimming strokes.

In “Chapter 4 Stroke Motion Experiment in Fixed State,” the developed humanoid robot realized the crawl stroke successfully in the circulating water tank supported by four struts. The constructed measurement system involving the developed experimental platform was validated as well. The humanoid robot generated

propulsive force in the circulating water tank and it was measured by the system. However, the results were not sustained and left room for improvement.

In "Chapter 5 Free Swimming Experiment," the upper body of SWUMANOID was remodeled to fit the free swimming in the crawl stroke. Using a human swimming simulation model SWUM, a feasibility study was conducted and two different models were proposed to perform the free swimming in the crawl stroke. Model I was constructed to produce larger roll movement and Model II was constructed to improve buoyancy for the stable recovery stroke. The two simulation models were realized in actual models with SWUMANOID. The crawl stroke was performed successfully by the two models respectively. The roll movement and stroke motions matched well with the simulation model. However, there was a difference in the swimming speed. The swimming speed of robot model was slower than that of simulation model.

6.2. Contributions

From the conclusions described above, it is possible to summarize the main contributions of this thesis as follows:

1. The developed full-body experimental platform reflects body properties of a human faithfully. The similarity between the body properties of human and robot were validated by quantified data of each segment such as dimension, volume, and weight. Overall balance was also confirmed through experiments. It is expected that the mechanics of human swimming, which could not be clarified by the previous experimental methods, will be investigated through various experiments using this experimental platform.

2. The complex shoulder motion in human swimming was realized efficiently using the scapular joint of the robot and validated by simulation. Although it was difficult to imitate human's shoulder movement perfectly, the swimming stroke motion was realized about the same using the scapular joint. Due to the simple structure of the robot shoulder, kinematics of the robot arm was

analyzed clearly and the methodology to use the joint was established. Also, it enable to convert easily the joint motions of the robot to the motions of the simulation model in SWUM, which has been validated by various studies. Research using both experimental model and simulation model together has the advantage of the reliability in hydrodynamics field including human swimming.

3. Through the stroke motion experiment in fixed state, the effectiveness of the scapular joint was reconfirmed practically. The constructed measurement system was useful to measure fluid forces in conventional experimental conditions of quasi-steady state. Even though, the measured data was not consistent but it was confirmed that the measurement system can record propulsive force during swimming and it is sensitive to setup conditions. In this experiment, the experimental conditions could be controlled. The different experimental condition with actual condition might cause spurious results of the experiment, while the limited experiment environment makes it possible to reduce variables and focus on interest part. If experiment in real environment is combined, it might possible to strengthen the strength and make up for the weakness of the experiment in quasi-steady state.

4. Through free swimming experiment which was conducted in the actual conditions of human swimming, the usefulness of the developed humanoid robot as an experimental platform was reconfirmed. When the robot swam with standard crawl motion of SWUM, the rolling movement was seriously affected by the stroke cycle. At the slow stroke cycle, the robot could not swim forward because the rolling motion was not realized properly. On the other hand, an actual swimmer can adjust his/her stroke cycle keeping the rolling movement. This implies human changes his/her stroke motion according to the stroke cycle. Bring up such a problem and clearing it up is significant in research of human swimming and the developed robot can play an important role.

   In this experiment, the roll angle and swimming speed was measured during

the swimming. The roll angle was corresponded well with the simulation result but the swimming speed was slower than the simulation result. It shows that buoyancy, which is the primary source of generating body roll in crawl swimming, and body balance are fit those of simulation model but there are still differences between the robot model and simulation model in drag or propulsive force. To reduce the gap between the actual model and the simulation model is also meaningful research not only for human swimming but also for control of the humanoid robot for underwater use.

6.3. Future Work

What follows are the main improvements in the next version of the developed experimental platform to obtain stable swimming performance and additional abilities:

1. Improving the simulation model.

   In this research, simulation model and fluid force model were constructed using the swimming human simulation software SWUM but there was a difference between the simulation model and the actual robot model. Especially, there was a distinct difference in the swimming speed. The cause of difference could be clarified by measuring drag and propulsive force of the actual model. Analysis of the difference will be useful to understand human swimming, as well.

2. Deriving control parameters in the swimming.

   To control the robot we should find control parameters which have influence on the swimming performance. However, the motion of human swimming is complex to clarify and there are few researches related with controlling human swimming. In order to get control parameters, the influence of parameters should be clarified through experiment and simulation first. It will be useful particularly for the research of human swimming related to control strategy of the body motion during swimming,

as well.

3. Increase degrees of freedom of the lower body to realize the breaststroke kick.

The lower body of present model has insufficient degree of freedom to perform breaststroke kick. Unlike the other formal swimming strokes, the breaststroke kick is responsible for a considerable portion of the forward propulsion [91]. Therefore, realization of the leg motion is important for research of the breaststroke. In addition, the increased degree of freedom in the lower body enables to perform various motions such as eggbeater kick. It might extend research field using the robot.

Appendix A

Link transformations of the robot arm

To simplify the notation, s_i, c_i, s_{i-90} and c_{i-90} are $\sin\theta_i$, $\cos\theta_i$, $\sin(\theta_i\text{-}90°)$, and $\cos(\theta_i\text{-}90°)$ respectively.

$$ {}^{b}_{0}T = \begin{bmatrix} c_0 & -s_0 & 0 & 0 \\ s_0 & c_0 & 0 & 0 \\ 0 & 0 & 1 & 0 \\ 0 & 0 & 0 & 1 \end{bmatrix} $$

$$ {}^{0}_{1}T = \begin{bmatrix} c_{1-90} & -s_{1-90} & 0 & a \\ 0 & 0 & 1 & \mathrm{b} \\ -s_{1-90} & -c_{1-90} & 0 & 0 \\ 0 & 0 & 0 & 1 \end{bmatrix} $$

$$ {}^{1}_{2}T = \begin{bmatrix} c_{2-90} & -s_{2-90} & 0 & 0 \\ 0 & 0 & 1 & 0 \\ -s_{2-90} & -c_{2-90} & 0 & -b-c \\ 0 & 0 & 0 & 1 \end{bmatrix} $$

$$ {}^{2}_{3}T = \begin{bmatrix} c_3 & -s_3 & 0 & 0 \\ 0 & 0 & 0 & l_1 \\ -s_3 & -c_3 & 0 & 0 \\ 0 & 0 & 0 & 1 \end{bmatrix} $$

$$ {}^{3}_{4}T = \begin{bmatrix} c_4 & -s_4 & 0 & 0 \\ 0 & 0 & 1 & 0 \\ -s_4 & -c_4 & 0 & l_2 \\ 0 & 0 & 0 & 1 \end{bmatrix} $$

$$ {}^{4}_{5}T = \begin{bmatrix} c_5 & -s_5 & 0 & 0 \\ 0 & 0 & -1 & 0 \\ s_5 & c_5 & 0 & 0 \\ 0 & 0 & 0 & 1 \end{bmatrix} $$

$$ {}^{5}_{w}T = \begin{bmatrix} 1 & 0 & 0 & 0 \\ 0 & 1 & 0 & 0 \\ 0 & 0 & 1 & l_3 \\ 0 & 0 & 0 & 1 \end{bmatrix} $$

Appendix B

Target matrixes of the wrist and elbow from SWUM

The target matrix of the robot arm, T_{elbow_SWUM} and T_{wrist_SWUM} are obtained from swimming motion data of SWUM. In SWUM, one stroke cycle of swimming consists of 18 motion frames. So, 18 target matrixes to generate one stroke cycle.

In SWUM, the joint motions are represented as rotation of each body segment about joint. The axes of rotations are one of the body base coordinate xb, yb and zb. The rotation angle is not relative but absolute. That is, even if you rotate the upper arm for certain angle, the rotation does not affect the forearm. In order to rotate the forearm for same angle, you have to give same rotation angle for the forearm. The rotation is IN ORDER. Therefore, in the case of rotation for a certain body segment, the results become DIFFERENT between the rotation of xb-yb and of yb-xb [41].

Figure A shows the coordinate system. Table A shows standard crawl stoke data of the right arm in SWUM. In order to rotate the forearm for same angle, the rotation angles of the upper arm are repeated for the forearm but they are omitted in this table. The rotation starts from left side in order.

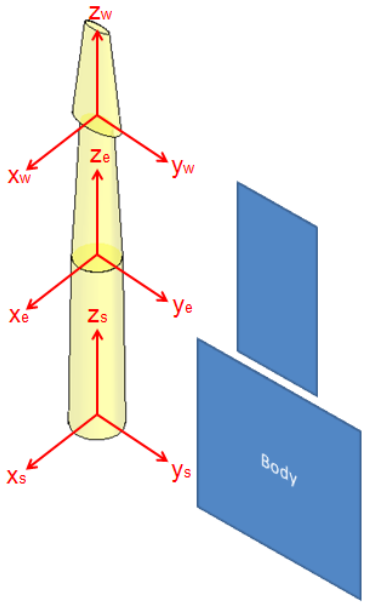

Figure A Coordinate system of simulation model in SWUM

Table A Standard crawl stroke motion data in SWUM

Frame No.(R)	Upper arm				Forearm	
	zb	xb	zb	yb	zb	yb
0	-180	160	80	7	-125	-50
1	-195	177	10	7	-97	-10
2	-205	177	-15	7	-90	-1
3	-212	150	-28	7	-85	-4
4	-200	110	-37.6	7	-81	-31.2
5	-130	63	-40.8	7	-77	-59.7
6	-110	30	-42.4	7	-73	-50.2
7	-110	10	-36	7	-70	-25.8
8	-110	0	-4.8	7	-75	-7.9
9	-110	-10	0	7	-106	-1
10	-110	-10	0	7	-111	0
11	-110	-7	0	7	-109	0
12	-114	2	4	7	-107	-1
13	-129	16	20	7	-106	-3
14	-145	32	32	7	-105	-6
15	-165	50	47	7	-104	-19
16	-180	70	62	7	-102	-60
17	-182	115	83	7	-106	-75

The rotational operators that rotate about the x, y and z by θ are

$$R_X = \begin{bmatrix} 1 & 0 & 0 & 0 \\ 0 & \cos\theta & -\sin\theta & 0 \\ 0 & \sin\theta & \cos\theta & 0 \\ 0 & 0 & 0 & 1 \end{bmatrix} \qquad R_Y = \begin{bmatrix} \cos\theta & 0 & \sin\theta & 0 \\ 0 & 1 & 0 & 0 \\ -\sin\theta & 0 & \cos\theta & 0 \\ 0 & 0 & 0 & 1 \end{bmatrix}$$

$$R_Z = \begin{bmatrix} \cos\theta & -\sin\theta & 0 & 0 \\ \sin\theta & \cos\theta & 0 & 0 \\ 0 & 0 & 1 & 0 \\ 0 & 0 & 0 & 1 \end{bmatrix}$$

$$ {}^{S}_{E}T = \begin{bmatrix} 1 & 0 & 0 & 0 \\ 0 & 1 & 0 & 0 \\ 0 & 0 & 1 & \ell_1 \\ 0 & 0 & 0 & 1 \end{bmatrix} $$

$$ T_{elbow\_SWUM} = R_Y(R_Z(R_X(R_Z\,{}^{S}_{E}T))) $$

$$ {}^{E}_{W}T = \begin{bmatrix} 1 & 0 & 0 & 0 \\ 0 & 1 & 0 & 0 \\ 0 & 0 & 1 & \ell_2 \\ 0 & 0 & 0 & 1 \end{bmatrix} $$

$$ T_{wrist\_SWUM} = R_Y(R_Z(R_X(R_Z(R_Y(R_Z\,{}^{E}_{W}T))))) + \begin{bmatrix} 0 & 0 & 0 & P_{elbow\_X} \\ 0 & 0 & 0 & P_{elbow\_Y} \\ 0 & 0 & 0 & P_{elbow\_Z} \\ 0 & 0 & 0 & 0 \end{bmatrix} $$

Table B Target matrixes of the crawl stroke

No.	T_{elbow_SWUM}				T_{wrist_SWUM}			
0	-0.1724	-0.9602	0.2198	39.5629	0.7535	0.5979	0.2733	74.82
	-0.9848	0.1632	-0.0594	-10.6904	0.2555	-0.6494	0.7162	81.7033
	0.0212	-0.2267	-0.9737	-175.2726	0.6057	-0.4699	-0.6421	-258.1058
	0	0	0	1	0	0	0	1
1	-0.898	-0.4254	-0.1127	-20.2828	0.5324	-0.8453	0.045	-14.483
	-0.4223	0.905	-0.0515	-9.2774	-0.847	-0.5319	0.0226	-6.366
	0.1239	0.0013	-0.9923	-178.6128	0.0048	-0.0501	-0.9987	-307.4495
	0	0	0	1	0	0	0	1
2	-0.9746	-0.1785	-0.1351	-24.3264	0.1785	-0.9768	-0.1181	-39.5635
	-0.1731	0.9836	-0.0506	-9.0995	-0.984	-0.1739	-0.0475	-15.2301
	0.142	-0.0259	-0.9895	-178.1163	0.0259	0.1247	-0.9919	-306.0665
	0	0	0	1	0	0	0	1
3	-0.9248	-0.1739	-0.3385	-60.935	0.0907	-0.9577	-0.2732	-96.1773
	-0.0071	0.8972	-0.4415	-79.4653	-0.897	0.0405	-0.4399	-136.213
	0.3805	-0.4059	-0.831	-149.5734	0.4323	0.285	-0.8555	-259.9304
	0	0	0	1	0	0	0	1
4	-0.7706	-0.1819	-0.6108	-109.9363	0.0271	-0.992	-0.1232	-125.8305
	0.4807	0.4633	-0.7445	-134.0116	-0.454	0.0976	-0.8858	-248.2831
	0.4184	-0.8673	-0.2696	-48.5275	0.8908	0.0799	-0.4474	-106.2371
	0	0	0	1	0	0	0	1

5	-0.7917	0.3165	-0.5225	-94.0563	-0.5	-0.7576	0.4199	-39.8878
	0.1567	-0.7215	-0.6745	-121.4078	0.5898	-0.6527	-0.4756	-182.7641
	-0.5905	-0.6159	0.5216	93.8806	0.6344	0.01	0.7729	193.5911
	0	0	0	1	0	0	0	1
6	-0.8526	0.4697	-0.2291	-41.2373	-0.66	-0.5529	0.5084	24.3452
	-0.3703	-0.8524	-0.3692	-66.461	0.6629	-0.7472	0.0482	-60.2469
	-0.3687	-0.23	0.9007	162.1185	0.3532	0.3688	0.8598	273.0299
	0	0	0	1	0	0	0	1
7	-0.8344	0.5508	0.0187	3.368	-0.772	-0.5099	0.38	52.3891
	-0.5476	-0.8248	-0.1405	-25.2872	0.5855	-0.8029	0.1119	-10.8559
	-0.0619	-0.1275	0.9899	178.1831	0.2481	0.3088	0.9182	296.63
	0	0	0	1	0	0	0	1
8	-0.4163	0.901	0.1219	21.9365	-0.973	-0.1489	0.1779	44.89
	-0.9078	-0.4195	0	0	0.1724	-0.9771	0.1248	16.0952
	0.0511	-0.1106	0.9925	178.6583	0.1553	0.152	0.9761	304.5753
	0	0	0	1	0	0	0	1
9	-0.3196	0.9399	0.12	21.6032	-0.816	-0.5642	0.1256	37.8027
	-0.9254	-0.3368	0.1736	31.2567	0.578	-0.7937	0.1898	55.7373
	0.2036	-0.0556	0.9775	175.9441	-0.007	0.2274	0.9738	301.5597
	0	0	0	1	0	0	0	1
10	-0.3196	0.9399	0.12	21.6032	-0.763	-0.6352	0.12	37.0855
	-0.9254	-0.3368	0.1736	31.2567	0.6461	-0.7432	0.1736	53.6573
	0.2036	-0.0556	0.9775	175.9441	-0.021	0.21	0.9775	302.0373
	0	0	0	1	0	0	0	1
11	-0.3255	0.9378	0.121	21.773	-0.781	-0.6131	0.121	37.3769
	-0.9327	-0.3395	0.1219	21.9365	0.6246	-0.7714	0.1219	37.6576
	0.1553	-0.0731	0.9851	177.3266	0.0186	0.1707	0.9851	304.4107
	0	0	0	1	0	0	0	1
12	-0.3434	0.9309	0.1242	22.3581	-0.791	-0.5984	0.1302	39.152
	-0.9391	-0.3418	-0.0348	-6.2666	0.6016	-0.7986	-0.0184	-8.6427
	0.01	-0.1286	0.9916	178.4961	0.115	0.0638	0.9913	306.3762
	0	0	0	1	0	0	0	1
13	-0.3595	0.9091	0.2107	37.9294	-0.778	-0.585	0.2292	67.5019
	-0.9172	-0.3027	-0.259	-46.6226	0.5471	-0.8101	-0.2107	-73.7971
	-0.1717	-0.2864	0.9426	169.6694	0.309	-0.0384	0.9503	292.2582
	0	0	0	1	0	0	0	1
14	-0.4707	0.7953	0.3821	68.773	-0.657	-0.6194	0.4292	124.1374
	-0.8466	-0.2852	-0.4494	-80.8915	0.5055	-0.7848	-0.3584	-127.1305
	-0.2484	-0.535	0.8075	145.3508	0.5589	-0.0187	0.829	252.2981
	0	0	0	1	0	0	0	1

15	-0.5572	0.5357	0.6344	114.1937	-0.442	-0.4404	0.7813	214.9773
	-0.8199	-0.2342	-0.5224	-94.0394	0.4559	-0.8606	-0.227	-123.3283
	-0.1313	-0.8113	0.5697	102.5494	0.7723	0.2557	0.5814	177.555
	0	0	0	1	0	0	0	1
16	-0.466	0.1852	0.8652	155.7354	-0.289	0.4665	0.8361	263.5977
	-0.8829	-0.1606	-0.4412	-79.4086	0.3283	-0.7721	0.5441	-9.2229
	0.0572	-0.9695	0.2384	42.9041	0.8994	0.4315	0.0696	51.8862
	0	0	0	1	0	0	0	1
17	-0.1025	-0.5307	0.8413	151.4417	0.2934	0.902	0.3168	192.3045
	-0.9937	0.0168	-0.1105	-19.8812	0.0841	-0.3544	0.9313	100.2554
	0.0445	-0.8474	-0.5291	-95.2373	0.9523	-0.2466	-0.1799	-118.4416
	0	0	0	1	0	0	0	1

Table C Standard backstroke motion data in SWUM

Frame No.(R)	Upper arm			Forearm	
	zb	xb	zb	zb	yb
0	-140	10	0	40	0
1	-120	25	-10	20	0
2	-140	40	-25	45	-10
3	-160	55	-38	64	-25
4	-180	70	-40	65	-55
5	-175	120	-30	40	-80
6	-240	150	-80	10	-60
7	-250	160	-80	0	-20
8	-260	160	-80	-60	0
9	-200	180	0	-100	0
10	-140	155	80	0	0
11	-190	135	100	80	0
12	-210	115	105	100	0
13	-210	95	85	90	0
14	-210	75	85	90	0
15	-210	45	75	100	0
16	-210	15	90	60	0
17	-210	0	90	40	0

Table D Target matrixes of the backstroke

No.	T_{elbow_SWUM}				T_{wrist_SWUM}			
0	-0.766	0.6428	0	0	-0.1736	0.9848	0	0
	-0.633	-0.7544	-0.1736	-31.2567	-0.9698	-0.171	-0.1736	-53.6573
	-0.1116	-0.133	0.9848	177.2654	-0.171	-0.0302	0.9848	304.3056
	0	0	0	1	0	0	0	1
1	-0.6287	0.7742	-0.0734	-13.2096	-0.326	0.9425	-0.0734	-22.6765
	-0.6861	-0.5967	-0.4162	-74.9156	-0.8488	-0.326	-0.4162	-128.605
	-0.366	-0.2113	0.9063	163.1354	-0.4162	-0.0734	0.9063	280.0491
	0	0	0	1	0	0	0	1
2	-0.9024	0.3346	-0.2717	-48.8977	-0.4252	0.8983	-0.1108	-63.195
	-0.1225	-0.8035	-0.5826	-104.861	-0.725	-0.4113	-0.5524	-176.126
	-0.4132	-0.4924	0.766	137.888	-0.5418	-0.1545	0.8262	244.4618
	0	0	0	1	0	0	0	1
3	-0.8613	-0.0623	-0.5043	-90.7777	-0.4916	0.8658	-0.0931	-102.785
	0.4239	-0.6353	-0.6455	-116.19	-0.5222	-0.3786	-0.7642	-214.771
	-0.2802	-0.7698	0.5736	103.2438	-0.6969	-0.3271	0.6382	185.5768
	0	0	0	1	0	0	0	1
4	-0.766	-0.2198	-0.604	-108.724	-0.594	0.7537	0.2811	-72.4682
	0.6428	-0.262	-0.7198	-129.572	-0.3308	0.0895	-0.9394	-250.759
	0	-0.9397	0.342	61.5636	-0.7332	-0.651	0.1962	86.8702
	0	0	0	1	0	0	0	1
5	-0.8409	0.3245	-0.433	-77.9423	-0.2299	0.6166	0.753	19.1913
	0.5358	0.3878	-0.75	-135	-0.2453	0.712	-0.6579	-219.873
	-0.0755	-0.8627	-0.5	-90	-0.9418	-0.336	-0.0125	-91.6114
	0	0	0	1	0	0	0	1
6	-0.8254	0.2761	-0.4924	-88.6327	-0.7785	0.4176	0.4686	-28.178
	0.3622	0.9281	-0.0868	-15.6283	0.2654	0.8956	-0.3571	-61.6889
	0.433	-0.25	-0.866	-155.885	-0.5688	-0.1536	-0.808	-260.118
	0	0	0	1	0	0	0	1
7	-0.929	0.1533	-0.3368	-60.6283	-0.9882	0.1533	0.0012	-60.4703
	0.1835	0.9812	-0.0594	-10.6904	0.1521	0.9812	-0.1186	-25.9855
	0.3214	-0.117	-0.9397	-169.145	-0.0194	-0.117	-0.9929	-297.235
	0	0	0	1	0	0	0	1
8	-0.9415	-0.0103	-0.3368	-60.6283	-0.4618	-0.8205	-0.3368	-104.079
	0.0103	0.9982	-0.0594	-10.6904	-0.8593	0.508	-0.0594	-18.3519
	0.3368	-0.0594	-0.9397	-169.145	0.2198	0.262	-0.9397	-290.365
	0	0	0	1	0	0	0	1

9	-0.9397	-0.342	0	0	0.5	-0.866	0	0
	-0.342	0.9397	0	0	-0.866	-0.5	0	0
	0	0	-1	-180	0	0	-1	-309
	0	0	0	1	0	0	0	1
10	-0.7067	-0.5721	0.4162	74.9156	-0.7067	-0.5721	0.4162	128.6051
	-0.6532	0.7536	-0.0734	-13.2096	-0.6532	0.7536	-0.0734	-22.6765
	-0.2717	-0.3237	-0.9063	-163.135	-0.2717	-0.3237	-0.9063	-280.049
	0	0	0	1	0	0	0	1
11	0.2919	-0.6556	0.6964	125.3456	-0.595	-0.4013	0.6964	215.1766
	-0.9485	-0.2919	0.1228	22.1018	-0.4522	0.8834	0.1228	37.9414
	0.1228	-0.6964	-0.7071	-127.279	-0.6645	-0.2418	-0.7071	-218.496
	0	0	0	1	0	0	0	1
12	0.4283	-0.2241	0.8754	157.5767	-0.2951	-0.3828	0.8754	270.5067
	-0.7818	-0.5777	0.2346	42.2225	-0.4332	0.8703	0.2346	72.482
	0.4532	-0.7849	-0.4226	-76.0713	-0.8517	-0.31	-0.4226	-130.589
	0	0	0	1	0	0	0	1
13	-0.0321	-0.1188	0.9924	178.6327	-0.1188	0.0321	0.9924	306.6528
	-0.8665	-0.4915	-0.0868	-15.6283	-0.4915	0.8665	-0.0868	-26.8286
	0.4981	-0.8627	-0.0872	-15.688	-0.8627	-0.4981	-0.0872	-26.9311
	0	0	0	1	0	0	0	1
14	-0.2044	0.1797	0.9623	173.205	0.1797	0.2044	0.9623	297.3353
	-0.8515	-0.5176	-0.0842	-15.1535	-0.5176	0.8515	-0.0842	-26.0135
	0.483	-0.8365	0.2588	46.5874	-0.8365	-0.483	0.2588	79.9751
	0	0	0	1	0	0	0	1
15	-0.5657	0.4621	0.683	122.9423	0.5533	0.4768	0.683	211.0509
	-0.745	-0.6415	-0.183	-32.9423	-0.5023	0.8451	-0.183	-56.5509
	0.3536	-0.6124	0.7071	127.2792	-0.6645	-0.2418	0.7071	218.496
	0	0	0	1	0	0	0	1
16	-0.483	0.8365	0.2588	46.5874	0.483	0.8365	0.2588	79.9751
	-0.866	-0.5	0	0	-0.866	0.5	0	0
	0.1294	-0.2241	0.9659	173.8666	-0.1294	-0.2241	0.9659	298.4711
	0	0	0	1	0	0	0	1
17	-0.5	0.866	0	0	0.1736	0.9848	0	0
	-0.866	-0.5	0	0	-0.9848	0.1736	0	0
	0	0	1	180	0	0	1	309
	0	0	0	1	0	0	0	1

Table E Standard butterfly motion data in SWUM

SWUM Data_Butterfly						
Frame No.(R)	Upper arm				Forearm	
	zb	xb	zb	yb	zb	yb
0	-35	22	-74	7	-106	-1
1	-50	34	-71	7	-111	0
2	-80	41	-61	7	-110	-7
3	-80	54	-47	7	-109	-20
4	-100	58	-23	7	-104	-50
5	-110	65	4	7	-90	-60
6	-120	80	26	7	-83	-72
7	-135	90	49	7	-110	-85
8	-130	119	65	7	-140	-75
9	-120	136	76	7	-150	-50
10	-115	145	80	7	-120	-15
11	-115	160	70	7	-45	-5
12	-115	150	-10	7	-110	0
13	-180	130	-19	7	-77	0
14	-180	100	-26	7	-20	0
15	-110	25	-33	7	-62	0
16	-110	5	-39	7	-75	0
17	-95	8	-52	7	-83	0

Table D Target matrixes of the butterfly

No.	base_elbow				base_wrist			
0	-0.3095	0.919	-0.2444	-43.9948	-0.7969	-0.5548	-0.239	-74.8229
	-0.934	-0.342	-0.1033	-18.586	0.5867	-0.8051	-0.0869	-29.8012
	-0.1785	0.1963	0.9642	173.5483	-0.1442	-0.2095	0.9671	298.3075
	0	0	0	1	0	0	0	1
1	-0.4405	0.7915	-0.4238	-76.2754	-0.581	-0.6949	-0.4238	-130.939
	-0.8145	-0.5508	-0.1821	-32.77	0.8061	-0.563	-0.1821	-56.2551
	-0.3775	0.265	0.8873	159.7129	-0.1121	-0.4474	0.8873	274.1738
	0	0	0	1	0	0	0	1
2	-0.6404	0.6015	-0.4775	-85.9588	-0.328	-0.8577	-0.3959	-137.036
	-0.5122	-0.7978	-0.3181	-57.2515	0.9368	-0.2413	-0.2533	-89.9234
	-0.5723	0.0409	0.819	147.4223	0.1217	-0.454	0.8827	261.2849
	0	0	0	1	0	0	0	1

3	-0.3997	0.7578	-0.5156	-92.8142	-0.5368	-0.7686	-0.3478	-137.683
	-0.5218	-0.6506	-0.5517	-99.3147	0.8363	-0.4302	-0.34	-143.177
	-0.7536	0.0485	0.6555	117.992	0.1117	-0.4734	0.8737	230.7038
	0	0	0	1	0	0	0	1
4	-0.4628	0.8461	-0.2643	-47.5754	-0.7	-0.6898	0.1846	-23.7556
	-0.4125	-0.4695	-0.7806	-140.5138	0.6644	-0.7239	-0.1858	-164.477
	-0.7846	-0.2523	0.5664	101.9433	0.2618	-0.0074	0.9651	226.4398
	0	0	0	1	0	0	0	1
5	-0.4149	0.9026	0.1143	20.5657	-0.9026	-0.1085	0.4165	74.2908
	-0.42	-0.0786	-0.9041	-162.738	0.0786	-0.993	-0.0883	-174.129
	-0.8071	-0.4231	0.4118	74.1174	0.4231	-0.047	0.9048	190.843
	0	0	0	1	0	0	0	1
6	-0.4846	0.7503	0.4497	80.938	-0.7109	0.3673	0.5998	158.3108
	-0.3543	0.3016	-0.8851	-159.3251	-0.4153	-0.9075	0.0635	-151.136
	-0.7998	-0.5882	0.1197	21.5535	0.5676	-0.204	0.7976	124.4485
	0	0	0	1	0	0	0	1
7	-0.5466	0.3743	0.7491	134.8351	-0.5906	0.5285	0.6098	213.5029
	-0.5337	0.5337	-0.6561	-118.0906	-0.262	-0.8404	0.4745	-56.8865
	-0.6453	-0.7584	-0.092	-16.5557	0.7632	0.1204	0.6348	65.3372
	0	0	0	1	0	0	0	1
8	-0.6854	-0.0275	0.7277	130.9829	-0.3849	0.3589	0.8503	240.6777
	-0.4256	0.826	-0.3696	-66.5334	-0.173	-0.933	0.3154	-25.8418
	-0.5909	-0.563	-0.5778	-104.0038	0.9066	-0.0257	0.4212	-49.6692
	0	0	0	1	0	0	0	1
9	-0.7933	-0.1808	0.5813	104.6402	0.1463	0.1242	0.9814	231.241
	-0.3344	0.9273	-0.1681	-30.2496	-0.166	-0.9749	0.1482	-11.1353
	-0.5087	-0.3277	-0.7961	-143.3017	0.9752	-0.1846	-0.122	-159.046
	0	0	0	1	0	0	0	1
10	-0.8619	-0.2117	0.4608	82.9481	0.54	-0.5118	0.6682	169.1443
	-0.2873	0.9527	-0.0996	-17.9281	-0.6734	-0.739	-0.0219	-20.7471
	-0.4179	-0.2182	-0.8819	-158.7394	0.505	-0.4381	-0.7437	-254.673
	0	0	0	1	0	0	0	1
11	-0.9756	-0.0804	0.2045	36.8061	-0.6178	-0.7314	0.2887	74.0519
	-0.1058	0.9875	-0.117	-21.056	-0.78	0.6165	-0.1073	-34.8986
	-0.1925	-0.1358	-0.9719	-174.9341	-0.0995	-0.2915	-0.9514	-297.662
	0	0	0	1	0	0	0	1
12	-0.333	0.9232	-0.1917	-34.5094	-0.7536	-0.6287	-0.1917	-59.2411
	0.8463	0.2031	-0.4924	-88.6327	-0.4803	0.7259	-0.4924	-152.153
	-0.4157	-0.3263	-0.849	-152.818	0.4487	-0.279	-0.849	-262.338
	0	0	0	1	0	0	0	1

13	-0.9385	0.1144	-0.3259	-58.6578	-0.3225	-0.8887	-0.3259	-100.696
	0.3256	0.6078	-0.7243	-130.3757	-0.519	0.4539	-0.7243	-223.812
	0.1152	-0.7858	-0.6076	-109.3684	0.7916	-0.0645	-0.6076	-187.749
	0	0	0	1	0	0	0	1
14	-0.8921	-0.0445	-0.4497	-80.938	-0.8231	-0.3469	-0.4497	-138.944
	0.4384	0.1561	-0.8851	-159.3251	0.3586	0.2966	-0.8851	-273.508
	0.1095	-0.9867	-0.1197	-21.5535	0.4404	-0.8898	-0.1197	-37.0001
	0	0	0	1	0	0	0	1
15	-0.7935	0.597	-0.118	-21.2414	-0.8997	-0.4203	-0.118	-36.4643
	-0.528	-0.7718	-0.3544	-63.7987	0.4336	-0.8285	-0.3544	-109.521
	-0.3027	-0.2189	0.9276	166.9686	0.0512	-0.37	0.9276	286.6295
	0	0	0	1	0	0	0	1
16	-0.8585	0.5084	0.067	12.0538	-0.7133	-0.6977	0.067	20.6924
	-0.5123	-0.8562	-0.0677	-12.1919	0.6944	-0.7164	-0.0677	-20.9294
	0.0229	-0.0925	0.9955	179.1817	0.0952	-0.0018	0.9955	307.5952
	0	0	0	1	0	0	0	1
17	-0.8417	0.5398	0.0118	2.1296	-0.6383	-0.7697	0.0118	3.6557
	-0.5387	-0.8381	-0.0857	-15.423	0.7663	-0.6368	-0.0857	-26.4762
	-0.0363	-0.0785	0.9963	179.3254	0.0735	-0.0456	0.9963	307.8419
	0	0	0	1	0	0	0	1

Appendix C

Formulation of fluid forces in SWUM

In SWUM, the swimmer's body is modeled as a series of body segments. Each body segment is represented as a truncated elliptic cone. The inertial force due to added mass of the fluid, the drag force normal and tangential to the longitudinal direction, and buoyancy are taken into account. Each truncated elliptic cone is divided into thin elliptic plates along the longitudinal axis, as shown in Figure 6.1 (a), and all fluid force components except buoyancy are assumed to act at the center of each plate. Buoyancy, on the other hand, is calculated by integrating the pressure due to the gravitational force acting on each tiny quadrangle, into which the edge of the thin elliptic plate is again divided in the circumferential direction, as shown in Figure 6.1 (b). The unit vectors in the directions of the ellipse's major and minor axes, their half-lengths, and the thickness of the plate are respectively denoted as $\boldsymbol{e}1$, $\boldsymbol{e}2$, $r1$, $r2$ and dl as shown in Figure 6.1 (c).

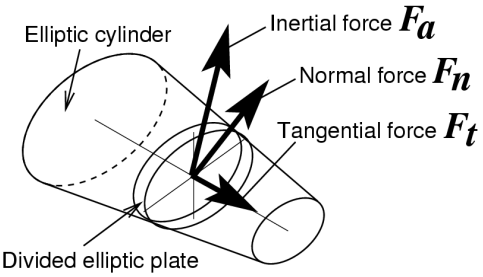

(a) Acting points of fluid forces

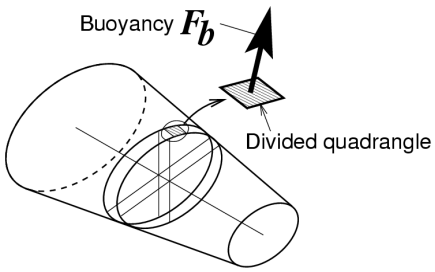

(b) Acting point and direction of buoyancy

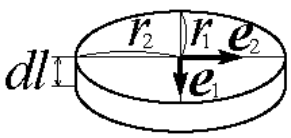

(c) Divided quadrangle

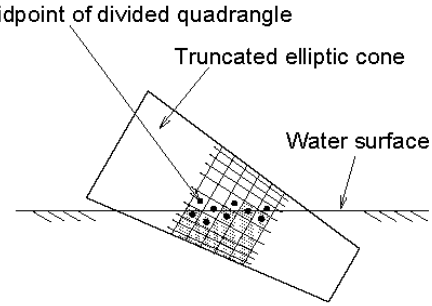

(b) Classification of submerged quadrangles

Figure 6.1 Analytical models of the fluid force in SWUM

In addition, the normal component of the acceleration vector of the center of the ellipse in inertial space, that is the component which is perpendicular to the longitudinal axis, is denoted as ***an***. Thus the inertial force, ***Fa***, due to the added mass is assumed to be given by:

$$\mathbf{F}_a = -C_a \rho \varepsilon_f dl \pi \left\{ r_2^2 (\mathbf{a}_n \cdot \mathbf{e}_1)\mathbf{e}_1 + r_1^2 (\mathbf{a}_n \cdot \mathbf{e}_2)\mathbf{e}_2 \right\} \tag{1}$$

where *Ca* is the coefficient for the added mass effect which becomes 1.0 in a two-dimensional ideal fluid. This coefficient is used to correct the fluid forces for a three-dimensional real fluid. The coefficient ε_f, defined below, represents the 'submerged fraction' of the plate. If the absolute velocity component of the elliptic plate's center normal to the longitudinal axis is denoted by $\boldsymbol{v}_n$, the drag force in the normal direction, $\boldsymbol{F}_n$, is assumed to be given by:

$$\mathbf{F}_n = -C_a \rho \varepsilon_f dl \left\{ r_2 \left(\frac{r_2}{r_1} \right)^p |\mathbf{v}_n| (\mathbf{v}_n \cdot \mathbf{e}_1)\mathbf{e}_1 + r_1 \left(\frac{r_1}{r_2} \right)^p |\mathbf{v}_n| (\mathbf{v}_n \cdot \mathbf{e}_2)\mathbf{e}_2 \right\} \tag{2}$$

where C_n is the drag coefficient for the normal direction. In Eq.(2), the normal absolute velocity component, $\boldsymbol{v}_n$, is decomposed into components along the plate's major and minor axes, respectively. The fluid forces proportional to the squares of the velocities in both directions are then computed. Therefore, the resultant fluid force corresponds to the sum of the 'lift' and 'drag' components. Note that the coefficient *p* represents the effect of ellipse flatness on the fluid forces. The coefficient *p* was determined to be 1.0 in a previous study [33].

Next, if the absolute velocity component of the elliptic plate's center tangential to the longitudinal axis is denoted by $\boldsymbol{v}_t$, and the ellipse's circumference by *c*, the drag force in the tangential direction, $\boldsymbol{F}_t$, is assumed to be given by:

$$\mathbf{F}_t = -\frac{1}{2} C_t \rho \varepsilon_f dlc |\mathbf{v}_t| \mathbf{v}_t \tag{3}$$

where Ct is the drag coefficient for the tangential direction. This equation represents the tangential force proportional to the elliptic plate's side surface area acting in the longitudinal direction.

Buoyancy is calculated by integrating the pressure, $\boldsymbol{F}_b$, due to gravity acting on the tiny quadrangles, as shown in Figure 6.1 (b). When the area of the quadrangle, the vector normal to the quadrangle, and z coordinate of the quadrangle center are respectively denoted as d_s, $\boldsymbol{e}_n$, and z_q , the pressure force, $\boldsymbol{F}_b$, is given by:

$$\mathbf{F}_b = -\rho z_q ds g \mathbf{e}_n \tag{4}$$

where g represents the gravitational acceleration. Since the pressure force $\boldsymbol{F}_b$ does not act above the water surface, each tiny quadrangle is classified as to whether it is below the water surface or not, i.e., whether $z_q < 0$ is true or not, where $z = 0$ represents the water surface. The pressure force $\boldsymbol{F}_b$ is assumed to act only on the quadrangles classified as being below the water surface, as schematically shown in Figure 6.1 (d). The black points represent the centers of the quadrangles. The shaded quadrangles are classified to be below the water surface and the nonzero force $\boldsymbol{F}_b$ on them is thus calculated. Since this classification is performed in the simulation program by dividing the elliptic plate into tiny quadrangles in the circumferential direction, the ratio (number of quadrangles where $z_q < 0$ holds)/(number of all quadrangles) can be calculated for each elliptic plate. In the present model, this ratio is called the 'submerged fraction,' ε_f . This is a factor in the inertial force of the added mass, and the drag force in the normal and tangential directions, as already shown in Eqs.(1),(2) and (3)

References

[1] Colwin, C., "Breakthrough Swimming," (2002), pp.3-18, Human Kinatics 1.

[2] Maglischo, E.W., "Swimming Fastest," (2003), pp.97, Human Kinetics.

[3] Toussaint, Huub M., Coen Van Den Berg, and Wiero J. Beek, "Pumped-up propulsion during front crawl swimming," Medicine and science in sports and exercise 34.2 (2002), pp.314-319.

[4] Brent S. Rushall, Eric J. Springings, "A Re-evaluation of Forces in Swimming," Journal of Swimming Research, Vol. 10, (1994), pp.6-30.

[5] Schleihauf, R.E., Gray, L., and De Rose, J., "Three-Dimensional Analysis of Hand Propulsion in The Sprint Front Crawl Stroke," Biomechanics and Medicine in Swimming IV, 1983, pp.173-184.

[6] Schleihauf, R.E. Higgins, J.R., Hinrichs, R., Luedtke, D., Maglischo, C., Maglischo, E.W., and Thayer, A., "Propulsive Techniques: Front Crawl Stroke, Butterfly, Backstroke, and Breaststroke," Swimming Science V, 1988, pp.53-59.

[7] Berger, M.A.M., Hollnader, A.P., and de Groot, G., "Determining propulsive force in front crawl swimming: A comparison of two methods," Journal of Sports Sciences, 17, (1999), pp.97-105.

[8] Ito, S. and Okuno, K., A Fluid Dynamical Consideration for Arm Stroke in Swimming, Biomechanics and Medicine in Swimming IX, 2003, pp.39-44.

[9] Pai, Y. and Hay, J.G., "A hydrodynamic study of the oscillation motion in swimming," International Journal of Sports Biomechanics, 4, (1988), pp.21-37.

[10] Toussaint, H.M., "An alternative fluid dynamic explanation for propulsion in front crawl swimming," Proceedings of XVIII International Symposium on Biomechanics in Sports. Applied Program: Application of Biomechanical Study in Swimming, (Ed. by R.Sanders and Y. Hong), (2000), pp.96-103. The Chinese University Press, Hong Kong.

[11] Boicev, K. and Tzvetkov, A., "Instrumentation and methods for the complex investigations of swimming," Swimming II, (Ed. By L. Lewillie and J. P. Clays), (1975), pp.80-89. University Park Press, Baltimore.

[12] Van Manen, J.D. and Rijken, H., "Dynamic measurement technique on swimming bodies at the Netherlands ship model basin," Swimming II, (Ed. By L. Lewillie and J. P. Clays), (1975), pp.70-79. University Park Press, Baltimore.

[13] Svec, O. J., "Biofeedback for pulling efficiency," Swimming technique, 19, (1982), pp.38-46.

[14] Loetz, C., Reischle, K. and Schmitt, G., "The evaluation of highly skilled swimers via quantitative and qualitative analysis," Swimming Science V, (Ed. by B.E. Ungerechts, K. Reischle and K. Wilke), (1988), pp.361-367. Human Kinetics, Champaign, IL.

[15] Thayer, A.M., "Hand pressures as predictors of resultant and propulsive hand forces in swimming," Unpublished Ph.D. dissertation, (1990), The University of Iowa, Iowa city, IA.

[16] Takagi, H. and Wilson, B., "Calculating hydrodynamic force by using pressure differences in swimming," Biomechanics and Medicine in Swimming VIII, (Ed. By K. Keshinen, P. Komi and A.P. Hollander), (1999), pp. 101-106. Gummerus Printing Hyvaskyla.

[17] Takagi, H. and Sanders, R., "Measurement of propulsion by the hand during competitive swimming," *The Engineering of Sport 4 (Eds. Ujihashi, S and Haake, S.J.)*, (2002), pp.631-637, Blackwell Publishing.

[18] Amar J. "The human motor; or, The scientific foundations of labour and industry," London:G. Routledge & Sons, Ltd, 1920.

[19] Karpovich PV, "Water resistance in swimming," Res Quart 1993;4:21-28.

[20] Pendergast DR, di Prampero PE, Craig AB, Wilson DR, Rennie DW, "Quantitative analysis of the front crawl in men and women," Journal of Applied Physiology, 1977;43: pp.475-479.

[21] Clarys JP. "Relationship of human body form to passive and active hydrodynamic drag," Biomechanics VI-B, 1978, pp.120-125.

[22] Kolmogorov SV, Rumyantseva OA, Gordon BJ, Cappaert JM, "Hydrodynamic characteristics of competitve swimmers of different genders and performance lavels," Journal of Applied Biomechanics 1997, 13, pp.88-97

[23] Toussaint, H.M., de Groot, H.H., Saveberg, C.M., Vervoorn, K., Hollander, A.P. and van Ingen Schenau, G.J. "Active Drag Related to Velocity in Male and Female Swimmers," Journal of Biomechanics, Vol. 21, No. 5, (1998), pp.435-438.

[24] Hollander AP, Groot G de, Ingen S. G.J. van, Toussaint HM, Best H de, Peeters W, Meulemans A, Schreurs AW., "Measurement of active drag forces during swimming" *Journal of Sports Sciences* Vol. 4, Issue 1, 1986, pp. 21-30

[25] Toussaint, H. M., Hollander, A. P., Berg, C. v. d., & Vorontsov, A. (2000). Biomechanics of swimming. In W. E. Garrett & D. T. Kirkendall (Eds.), Exercise and Sport Science (pp. 639-660). Philadelphia: Lippincott, Williams & Wilkins.

[26] Kolmogorov, S.V. and Duplishcheva, O.A. "Active Drag, Useful Mechanical Power Output and Hydrodynamic Force Coefficient in Different Swimming Strokes at Maximal Velocity," Journal of Biomechanics, Vol. 25, No. 3, (1992), pp.311-318.

[27] Takagi, H., Shimizu, Y. and Kodan, N. "A Hydrodynamic Study of Active Drag in Swimming," JSME Internationsl Journal, Series B, Vol. 42, No. 2, 1999, pp. 171-177.

[28] Bixler, B.S. and Riewald, S., "Analysis of Swimmer's Hand and Arm in Steady Flow Conditions Using Computational Fluid Dynamics," Journal of Biomechanics, Vol. 35 (2002), pp.713-717.

[29] Rouboa, A., Silva, A., Leal, L., Rocha, J. and Alves, F., "The Effect of Swimmer's Hand/Forearm Acceleration on Propulsive Forces Generation Using Computational Fluid dynamics, Journal of Biomechanics, Vol.39 (2006), pp.1239-1248.

[30] Sato, Y. and Hino, T., "Estimation of Thrust of Swimmer's Hand Using CFD," Proceedings of the Second International Symposium on Aqua Bio-Mechanisms (ISABMEC2003), (2003), P2-07 (CDROM)

[31] Alberto E. Minetti, Georgios Machtsiras, Jonathan C. Masters, "The optimum finger spacing in human swimming," Journal of Biomechanics, 42, (2009), pp.2188-2190.

[32] Keys, M. and Lyttle, A., "Computational Fluid Dynamics – a Toll for Future Swimming Technique Prescription," The Impact of Technology on Sport II (Eds. Fuss, F.K., Subic, A. and Ujihashi, S.), (2007), pp.587-592, Taylor & Francis.

[33] Nakashima, M., Satou, K., and Miura, Y., "Development of Swimming Human Simulation Model Considering Rigid Body Dynamics and Unsteady Fluid

Force for Whole Body," Transactions of the Japan Society of Mechanical Engineers, Series B, Vol.71, No.705 (2005), pp.1361-1369.

[34] Nakashima, M., "Mechanical Study of Standard Six Beat Front Crawl Swimming by Using Swimming Human Simulation Model," Transactions of the Japan Society of Mechanical Engineers, Series B, Vol.71, No.705 (2005), pp.1370-1376.

[35] Nakashima, M., "Analysis of Breast, Back, and Butterfly Strokes By the Swimming Human Simulation Model SWUM," Biomechanisms of Swimming and Flying – Fluid Dynamics, Biomimetic Robots, and Sports Science – (eds. Naomi Kato and Shinji Kamimura), Springer, Tokyo, (2007), pp.361-372.

[36] Nakashima, M., "Simulation Anaysis of the Effect of Trunk Undulation on Swimming Performance in Underwater Dolphin Kick of Human," Journal of Biomechanical Science and Engineering, Vol. 4, No. 1, (2009), pp.94-104.

[37] Kiuchi, H., Nakashima, M., Cheng, K.B. and Hubbard, "Modeling Fluid Forces in the Dive Start of Competitive Swimming," Journal of Biomechanical Science and Engineering, Vol. 5, No. 4, (2010), pp.314-328.

[38] Nakashima, M., Kiuchi, H. and Nakajima, K., "Multi Agent/Object Simulation in Human Swimming," Journal of Biomechanical Science and Engineering, Vol. 5, No. 4, (2010), pp.380-387.

[39] Nakashima, M., Suzuki, S. and Nakajima, K., "Development of a Simulation Model for Monofin Swimming," Journal of Biomechanical Science and Engineering, Vol. 5, No. 4, (2010), pp.408-420.

[40] Nakashima, M., "Modeling and Simulation of Human Swimming," Journal of Aero Aqua Bio-mechanisms, Vol. 1, No. 1, (2010), pp.11-17.

[41] Swum developer team, "SWUM home page," SWUM website, (online), available from http://www.swum.org/, (accessed 2013-6-05).

[42] Berger, Monique AM, Gert de Groot and A. Peter Hollander, "Hydrodynamic drag and lift forces on human hand/arm models," Journal of Biomechanics, Vol. 28, No. 2, (1995), pp.125-133.

[43] Pai, Y., "A Hydrodynamic Study of the Oscillation Motion in Swimming," Unpublished PhD thesis, (1987), The University of Iowa.

[44] Kudo, S., Wilson, B., and Takagi, H., "The Error of a Quasi-Static Approach in Predicting Fluid Forces on the Hand in Unsteady Conditions," Japanese Journal of Sciences in Swimming and Water Exercise, Vol. 10, No. 1 (2007), pp.1-11.

[45] M.A. Lauder, P. Dabnichki, "Estimating propulsive forces-sink or swim?" Journal of Biomechanics 38 (2005) 1984-1990

[46] Sidenik, N.O. and Young, B.W., "Optimising The Freestyle Swimming Stroke: The Effect of Finger Spread," Sports Engineering, Vol.9 (2006), pp.129-135.

[47] M. Nakashima and A. Takahashi, "Clarification of Unsteady Fluid Forces Acting on Limbs in Swimming Using an Underwater Robot Arm(Development of an Underwater Robot Arm and Measurement of Fluid Forces)," *Journal of Fluid Science and Technology*, Vol. 7 (2012) No. 1 pp.100-113.

[48] M. Nakashima and A. Takahashi, "Clarification of Unsteady Fluid Forces Acting on Limbs in Swimming Using an Underwater Robot Arm," *Journal of Fluid Science and Technology*, Vol. 7 (2012) No. 1 pp.114-128.

[49] M. Nakashima and Y. Ejiri, "Measurement and Modeling of Unsteady Fluid Force Acting on the Trunk of a Swimmer Using a Swimmer Mannequin Robot," *Journal of Fluid Science and Technology*, Vol. 7 (2012) No. 1 pp.11-24.

[50] Coundsilman, J.E., "Science of swimming," Englewood Cliffs, NJ: Prentice-Hall, 1968

[51] Hay, J. G., Q., and Andrews, J. G., "Body roll and hand path in free swimming: A computer simulation study," Journal of Applied Biomechanics, 9, (1993), pp.227-237.

[52] Castro, F., Minghelli, F., Floss, J., and Guimaraes, A., "Body roll angles in front crawl swimming at different velocities," In J. C. Chatard (Ed.), Biomechanics and medicine in swimming IX , (2003), (pp.111-114). St Etinenne: University of St Etienne Publications.

[53] Ciullo, J. V., and Stevens, G. G., "The prevention and treatment of injuries to the shoulder in swimming," Sports Medicine, (1989), 7, pp.182-204.

[54] Penny, J. N., and Smith, C., "The prevention and treatment of swimmer's shoulder," Canadian Journal of Applied Sport Sciences, (1980), 5, pp.195-202.

[55] Weldon, E. J., III, and Richardson, A. B., "Upper extremity overuse injuries in swimming: A discussion of swimmer's shoulder," Clinics in Sports Medicine, (2001), 20, pp.423-438.

[56] Hay, J. G., Liu, Q., and Andrews, J. G., "Body roll and handpath in freestyle swimming: A computer simulatin study," Journal of Applied Biomechanics, (1993), 9, pp.227-237.

[57] Payton, C. J., Hay, J. G., and Mullineaux, D. R., "The effect of body roll on had speed and hand path in front crawl swimming- a simulation study," Journal of Applied Biomechanics, (1997), 13, pp.300-315.

[58] Beekman, K. M., and Hay, J. G., "Characteristics of the front crawl techniques of swimmers with shoulder impingement syndrome," Journal of Swimming Research, (1988), 4 (3), pp.15-21.

[59] Castro, F. A. S., Vilas-Boas, J. P., and Guimaraes, A. C. S., "Effect of swimming intensity and breathing in front crawl body roll angles for swimmers and triathletes," Brazilian Journal of Biomechanics, (2006), 7, pp.85-90.

[60] Liu, Q., Hay, J. G., and Andrews, J. G., "Body roll and handpath in freestyle swimming: An experimental study," Journal of Applied Biomechanics, (1993), 9, pp.238-253.

[61] Paytone, C. J., Baltzopoulos, V., and Bartlett, R. M., "Contributions of rotations of the trunk and upper extemity to hand velocity during front crawl swimming," Journal of Applied Biomechanics, (2002), 18, pp.243-256.

[62] Payton, C. J., Bartlett, R. M., Baltzopoulos, V., and Coombs, R., "Upper extremity kinematics and body roll during preferred-side breating and breath-holding front crawl swimming," Journal of Sports Science, (1999), 17, pp.689-696.

[63] Cappaert, J. M., Pease, D. L., and Troup, J. P., "Three dimensional analysis of the men's 100-m freestyle during the 1992 Olymic Games," Journal of Applied Biomechanics, (1995), 11, pp.103-112.

[64] Psycharakis, S. G., and Sanders, R. H., "Shoulder and hip roll changes during 200-m front crawl swimming," Medicine and Science in Sports and Exercise, (2008), 40, pp.2129-2136.

[65] Sanders, R. H., and Psycharakis, S. G, "Rolling rhythms in front crawl swimming with six-beat kick," Journal of Biomechanics, (2009), 42, pp.273-279.

[66] Yanai, T., “What causes the body to roll in front-crawl swimming?” Journal of Applied Biomechanics, (2001), 17, pp.28-42.

[67] Yanai, T., “Stroke frequency in front crawl: Its mechanical link to the fluid forces required in non-propulsive directions,” Journal of Biomechanics, (2003), 36, pp.53-62.

[68] Yanai, T., “Buoyancy is the primary source of generating bodyroll in front-crawl swimming,” Journal of Biomechanics, (2004), 37, pp.605-612.

[69] Yanai, T. and Hay, J. G., “Shoulder impingement in front crawl swimming: II. Analysis of stroking technique,” Medicine and Science in Sports and Exercise, (2000), 32, pp.30-40.

[70] Lee, J., Mellifont, R., Winstanley, J., and Burkett, B., “Body roll in simulate freestyle swimming,” International Journal of Sports Medicine, (2008), 29, pp.569-573.

[71] Li, Q., Takanishi, A., Kato, I., “Learning of robot biped walking with the cooperation of a human,” Robot and Human Communication, Proceedings., 2nd IEEE International Workshop on, 1993, pp.393-397.

[72] Atkeson, C.G., Hale, J.G., Polick, F., Riley, M., Kotosaka, S., Schaul, S.,Shibata, T., Tevatia, G., Ude, A., Vijayakumar, S., Kawato, E., Kawato, M., “Using humanoid robots to study human behavior,” Intelligent Systems and their Applications, IEEE, Vol. 15, 4, (2000), pp.46-56.

[73] Nomura, T., Kanda, T., Suzuki, T., Kato, K., “Prediction of human behavior in human-robot interaction using psychological scales for anxiety and negative attitutdes toward robots,” Robotics, IEEE transactions, Vol. 24, 2, (2008), pp.442-451.

[74] K. Hirai, M. Hirose, Y. Haikawa, T. Takenaka, “The Development of Honda Humanoid Robot,” Proceedings of the 1988 IEEE International Conference on Robotics & Automation, Leuven, Belgium, May 1998, pp. 1321-1326.

[75] R. Tajima, D. Honda, and K. Suga, “Fast Running Experiments Involving a Humanoid Robot,” 2009 IEEE International Conference on Robotics and Automation, Kobe International Conference Center, Kobe, Japan, May 12-17, 2009, pp. 1571-1576.

[76] S. Nakaoka, A. Nakazawa, K. Yokoi, H. Hirukawa, and K. Ikeuchi, “Generating Whole Body Motions for a Biped Humanoid Robot from Captured

Human Dances," Proceedings of the 2013 IEEE International Conference on Robotics & Automation, Taipei, Taiwan, September 14-19, 2003, pp. 3905-3910.

[77] K. Akachi et al. "Development of Humanoid Robot HRP-3P," Proceedings of 2005 5th IEEE-RAS International Conference on Humanoid Robots, pp. 50-55.

[78] M.A. Diftler et al. "Robonaut 2-The First Humanoid Robot in Space," 2011 IEEE International Conference on Robotics and Automation, Shanghai International Conference Center, May 9-13, Shanghai, China, pp. 2178-2183.

[79] H. Oya and K. Suzuki, "Behavior Based Water Depth Estimation for Diver Type Small Humanoid Robot," *Proceedings of the 4th International Conference on Autonomous Robots and Agents*, Feb. 10-12, 2009, Wellington, New Zealand.

[80] Y. Li, E. Shimizu and M. Ito, "Development of a humanoid robot for underwater use," *Journal of Artificial Life and Robotics*, Vol. 15, Issue 4, December 2010.

[81] M. Nakashima and H. Kobayashi, "Development of small-sized swimming humanoids," in *The Engineering of Sport 7 (Eds. M. Estivalet and P. Brisson)*, Vol. 2. Paris: Springer-Verlag, 2008, pp. 303-309.

[82] Hoerner, S.F., Fluid-Dynamics Drag, (1965), Chapter 3, pp.1-28, Hoerner Fluid Dynamics.

[83] http://support.robotis.com/en/ , (accessed 2013-6-5)

[84] M. Okada and Y. Nakamura, "Development of a Cybernetic Shoulder-A 3-DOF Mechanism That Imitates Biological Shoulder Motion," *IEEE Transactions on robotics*, Vol. 21, No. 3, June 2005

[85] N. S. Pollard, J.K. Hodgins, M.J. Riley, and C.G. Atkeson, "Adapting human motion for the control of a humanoid robot," *Proceedings of International Conference on Robotics and Automation*, 2002

[86] S. Nakaoka, A. Nakazawa, K. Yokoi, H. Hirukawa and K. Ikeuchi, "Generating Whole Body Motions for a Biped Humanoid Robot from Captured Human Dances," *Proceedings of the 2003 IEEE International Conference on Robotics & Automation Taipei*, Taiwan, September 14-19, 2003

[87] IPA(Information-technology Promotion Agency, Japan. “Physical Education (Swimming)” (in Japanese). Picture Materials for Education (in Japanese). (online), available from < http://www2.edu.ipa.go.jp/gz2/list.html#suiei>, (accessed 2013-6-5)

[88] C. Chung and M. Nakashima, “Development of an underwater humanoid for the research of unsteady fluid forces acting on swimmer,” 日本機械学会 ROBOMEC2012, 日本機械学会 ROBOMEC2012 講演論文集, 1A2-R07 (CDROM), May. 2012.

[89] C. Chung and M. Nakashima, “ Measurement System of Fluid Force in Human Swimming Using a Swimming Humanoid Robot,” Fifth International Symposium on Aero Aqua Bio-mechanisms, Proceedings of the fifth International Symposium on Aero Bio-mechanisms, pp. 174-179, Aug. 2012.

[90] C. Chung and M. Nakashima, “Development of the Upper Body of an Underwater Humanoid Robot for Research of Unsteady Fluid Forces Acting on a Swimmer,” Proceedings of Fourth IEEE RAS/EMBS International Conference on Biomedical Robotics and Biomechatronics, pp. 701-706, Jun. 2012.

[91] Strzata, Marek, et al., “Swimming Speed of the breaststroke kick,” Journal of Human Kinetics, Vol. 35, 1, (2012), pp. 133-139.

Acknowledgments

First of all, I would like to warmly thank my supervisor, associate professor Motomu Nakashima, for supporting me over all these years. It was a pleasure to work with him as my advisor. His intereseting idea motivated me to start study in Japan and I have learned a lot during the last few years. I also would like to thank professor Koji Kimura, professor Norio Inou, associate professor Hideyuki Tsukagosi, associate professor E. Fumihiko Fukushima and associate professor Yusuke Miyazaki for being my examiner and taking time from busy schedule to give me valuable advice.

I would like to thank all my friends and members of Nakashima lab. and Yamaura lab. for the pleasant atmosphere. Beomsuk, Dongjin, Hyunjin and many other Korean students helped me and became dependable friends, when I first came here and could not speak Japanese at all. Hadi-san, Yu-san and Sisay-san also became supportive friends, when I was unfamilar with daily life in the laboatory. I cannot write all the names in here, but I would like to thank every student I have met in Nakashima lab. and Yamaura lab. including old members and exchange students.

Also, I would like to thank all those who have believed in and supported me in Korea. Especially, I thank professor Ryuh for his practical advice and support.

Above all, I wish to thank my wife who has always supported me for always being at my side, for cooking marvelous meals, and for enjoying life with our lovely daughter and son and me in an unfamiliar place away from home.

Research Achievements

<Journal>

1. Changhyun Chung and Motomu Nakashima, “Development of the Swimming Humanoid Robot SWUMANOID for Research of Human Swimming”, *Journal of Aero Aqua Bio-mechanisms*, Vol.3, No.1, (2013), pp.109-117.

2. Changhyun Chung and Motomu Nakashima, “Free Swimming of the Swimming Humanoid Robot for the Crawl Stroke”, *Journal of Aero Aqua Bio-mechanisms*, Vol.3, No.1, (2013), pp.118-125.

<International Conference>

1. Changhyun Chung and Motomu Nakashima, “Development of the Upper Body of an Underwater Humanoid Robot for Research of Unsteady Fluid Forces Acting on a Swimmer”, *Proceedings of Fourth IEEE RAS/EMBS International Conference on Biomedical Robotics and Biomechatronics*, pp. 701-706, Jun. 2012.

2. Changhyun Chung and Motomu Nakashima, “Measurement System of Fluid Force in Human Swimming Using an Underwater Humanoid Robot”, *Proceedings of the Fifth International Symposium on Aero Aqua Bio-mechanisms*, pp. 174-179, Aug. 2012.

<Domestic Conference>

1. Changhyun Chung and Motomu Nakashima, “Development of an underwater humanoid for the research of unsteady fluid forces acting on swimmer”, 日本機械学会ROBOMEC2012, 日本機械学会ROBOMEC2012講演論文集, 1A2-R07 (CDROM), May. 2012.

2. Changhyun Chung and Motomu Nakashima, “Realization of Free Swimming in the Crawl Stroke by a Humanoid Robot”, 日本機械学会 ROBOMEC2013, 日本機械学会 ROBOMEC2013 講演論文集, 1A2-B05 (CDROM), May. 2013..